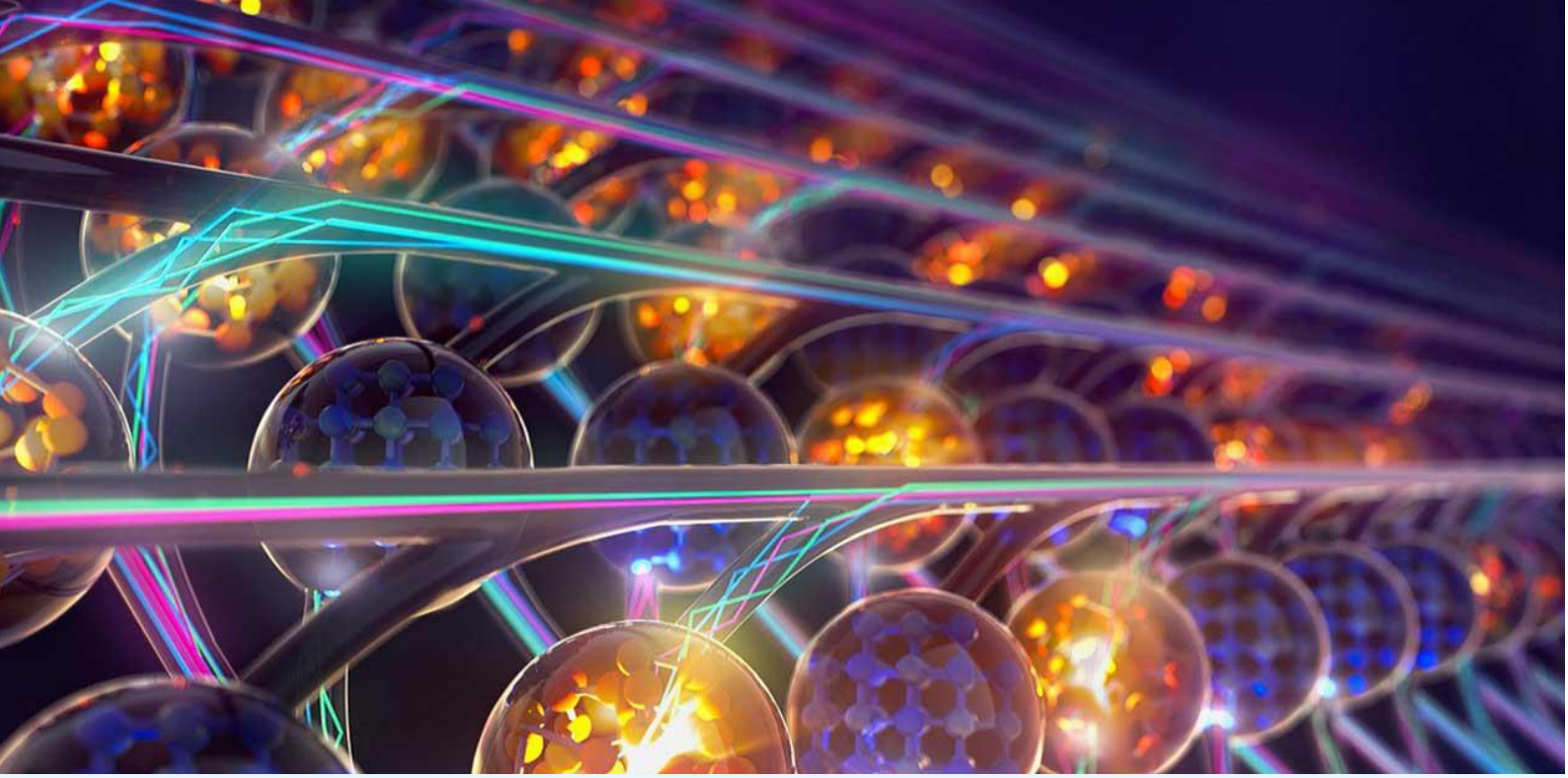

ICLLT-2022

25 – 27 MAY
ANKARA-TURKEY

3rd INTERNATIONAL CONFERENCE ON LIGHT AND LIGHT-BASED TECHNOLOGIES

Abstract and Proceeding Book

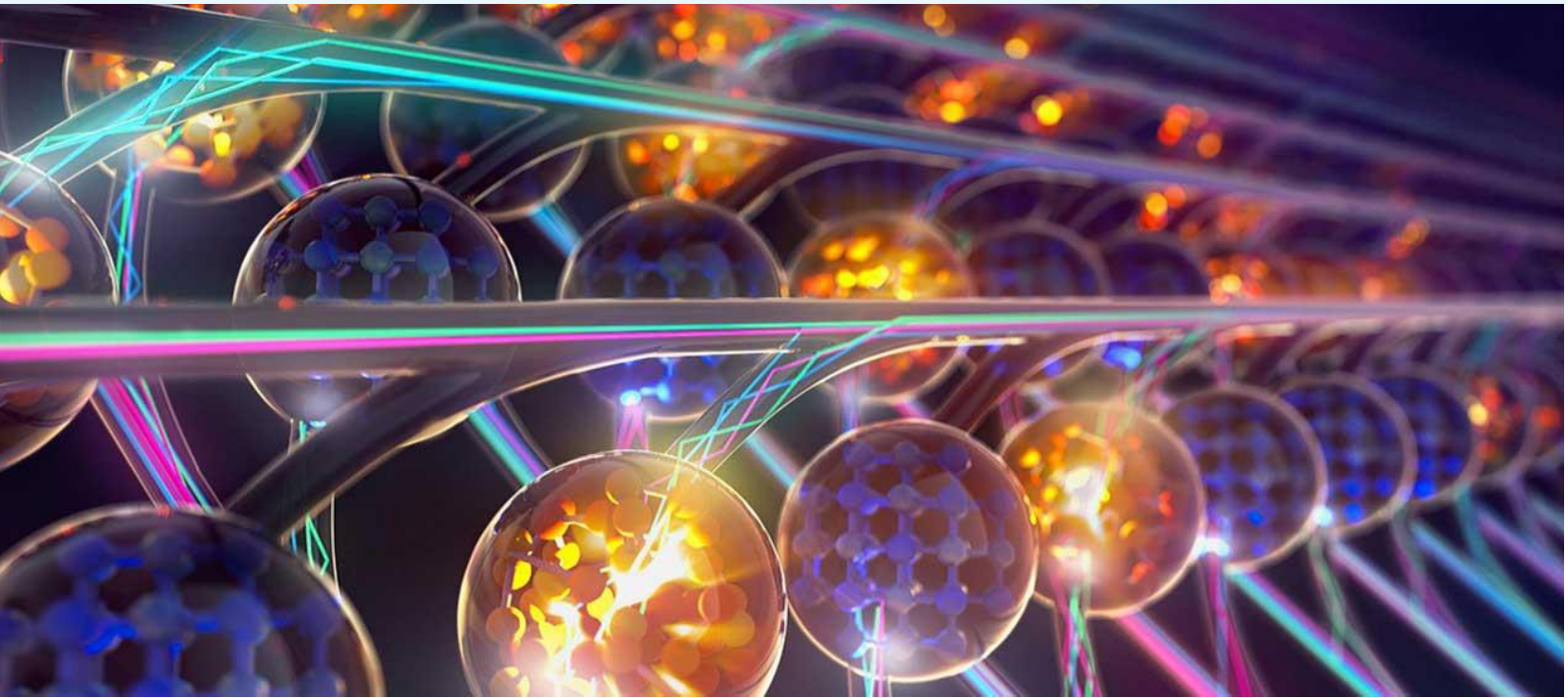

ABSTRACT AND PROCEEDING BOOK

3rd International Conference on Light and Light-Based Technologies (3rd ICLLT 2022)

25th-27th May, 2021, Gazi University, Ankara, Turkey

Edited by

Prof. Dr. Süleyman ÖZÇELİK

First Published, July 1, 2022

This book is available on the ICLLT website: *https://icllt-3.gazi.edu.tr/*

ORGANISERS

- Photonics Application & Research Center (Gazi Photonics), Gazi University
- Photonics Department of Applied Science Faculty, Gazi University

Welcome to the 3rd ICLLT-2022

Dear Distinguished Participants and Colleagues

"International Day of Light" has been declared on 16 May at UNESCO 39th General Conference held in Paris between 30 October and 14 November 2017. UNESCO aims with this precious day to raise awareness of people in all United Nations countries in light and light-based technologies. The goal of sharing knowledge and increasing cooperation from R&D studies on photonics, nanotechnology, microtechnology and semiconductor technology of Gazi University Photonics Application and Research Center is in line with UNESCO's goal of creating Light Science awareness. With this aim, "3rd International Conference on Light and Light-based Technologies (3rd ICLLT-2022)" was held at the Gazi University (Ankara, Turkey), from 25 to 27 May 2022 as virtually due to Covid-19 pandemic.

The 3rd ICLLT-2022 conference targets guests from various branches and disciplines related to Optics and Photonics Technologies**.** Its interdisciplinary approach is the key to maximizing the potential and development of light-based technologies and tools for various applications. The purpose of the conference is to explore new ideas, effective solutions and collaborative partnerships for business growth by catalyzing the creation of a beneficial synergy between researchers, engineers, manufacturers, suppliers, and end-users of all sectors and making full use of this potential. At this event, the world's leading scientists in Optical and Photonic technologies discussed the latest developments in related technologies. 74 oral presentations were made, including 7 keynote speakers, 16 invited speakers and 51 oral presentations from 13 different countries. While 44 of the presented papers were presented by researchers from abroad, 30 papers were presented by researchers from Turkey. The event was held with 190 registered participants.

On behalf of the organizing committee, we would like to thank all participated academics, research institutions and organizations and especially young students from around the world for exchange of ideas and experiences at ICLLT-2022.

We are honored to invite you to the 4th ICLLT conference will be held face to face in May 2023!

Prof. Dr. Süleyman ÖZÇELİK
Conference Chair

COMMITTEES

International Organizing Committee

Prof. Süleyman Özçelik *Gazi Univ., Turkey*
Assoc. Prof. Yashar Azizian-Kalandaragh *Gazi Univ., Turkey*
Prof. Andrew Forbes *Witsatersrand Univ., South Africa*

Local Organizing Committee

Prof. Musa Yıldız *Gazi Univ., Turkey*
Prof. Süleyman Özçelik, *Gazi Univ., Turkey*
Assoc. Prof. Nihan Akın Sönmez, *Gazi Univ., Turkey*
Assoc. Prof. Yashar Azizian Kalandaragh, *Gazi Univ., Turkey*
Dr. Tuğçe Ataşer, *Gazi Univ., Turkey*
Dr. Meltem Dönmez Kaya, *Gazi Univ., Turkey*
Dr. Buse Cömert Sertel, *Gazi Univ., Turkey*
Gökhan Gözlekçi, *Gazi Univ., Turkey*

Scientific Committee

Prof. Şemsettin Altındal, *Gazi Univ., Turkey*
Prof. Aytunç Ateş, *Yıldırım Beyazit Univ., Turkey*
Prof. Bülent Çakmak, *Erzurum Technical Univ., Turkey*
Prof. Mehmet Çakmak, *Gazi Univ., Turkey*
Prof. Sezai Elagöz, *Vice President of R&D at ASELSAN, Turkey*
Prof. Andrew Forbes, *Witsatersrand Univ, South Africa*
Prof. Leonid Golovan, *Moscow State Univ., Russia*
Prof. Valery Gremenok, *National Academy of Science of Belarus*
Prof. Rasim Jabbarov, *Azerbaijan National Academy of Sciences, Azerbaijan*
Prof. Victor Kotlyar, *Samara Univ., Russia*
Prof. Oliver Martin, *EPFL, Lausanne, Switzerland*
Prof. Mohammed Missous, *University of Manchester, UK*
Prof. Nahida Musayeva, *Azerbaijan National Academy of Sciences, Azerbaijan*
Prof. Sermin Onaygil, *İstanbul Tecnicak Univ., Turkey*
Prof. Ekmel Özbay, *Bilkent Univ., Turkey*
Prof. Süleyman Özçelik, *Gazi Univ., Turkey*
Prof. Raşit Turan, *Middle East Technical Univ., Turkey*
Prof. Canan Varlıklı, *İzmir Institute of Technology, Turkey*
Prof. Jian Wang, *Huazhong University of Science and Technology, China*
Prof. Halime Gül Yağlıoğlu, *Ankara Univ., Turkey*
Prof. Fahrettin Yakuphanoğlu, *Elazığ Fırat Univ., Turkey*
Prof. Ellen Petrovna Zaretskaya, *Belarus Bilimler Akademisi, Belarus*
Prof. Hamidreza Khalesifard, *Institute for Advanced Studies in Basic Sciences, Iran*

Prof. Alper Kiraz, *Koç Univ., Turkey*
Assoc. Prof. Yashar Azizian Kalandaragh, *Gazi Univ., Turkey*
Assoc. Prof. Barış Kınacı, *İstanbul Univ., Turkey*
Assoc. Prof. Viktor Kisel, *Belarusian National Technical University, Belarus*
Assoc. Prof. Nihan Akın Sönmez, *Gazi Univ., Turkey*
Dr. Raul Arenal, *University of Zaragoza, Spain*
Dr. Matteo Bosi, *IMEM-The National Research Council (CNR), Italy*
Dr. Benedetta Marmiroli, *Graz University of Technology, Austria*

PARTNERS & SPONSORS

The Best Presentation Awards for top three presenter were supported by Optical Society of America (OSA) and ASENTEK Company.

PROGRAM

Wednesday 25th May

09:00 – 09:30	**Opening Ceremony** (Zoom webinar and Youtube-Stream) Prof. Süleyman Özçelik *Chair of Photonics Department, Faculty of Applied Sciences, Gazi University, Ankara, Turkey* *Director of Photonics Application and Research Center, Gazi University, Ankara, Turkey* Prof. M. Öcal Oğuz *President of Turkish National Commission for UNESCO* Prof. Musa Yıldız *Rector of Gazi University, Ankara, Turkey*
Session I	**Chair:** Assoc. Prof. Yashar Azizian-Kalandaragh *Department of Photonics, Faculty of Applied Sciences, Gazi University, Ankara, Turkey*
09:30 – 10:10	Plenary Speaker / Prof. Gerd Leuchs *Max Planck Institute, Germany* **What are the limits to focusing light tightly**
10:10 – 10:50	Plenary Speaker / Prof. Andrew Forbes *School of Physics, University of the Witwatersrand, Johannesburg, South Africa* **1,2,3 … Infinity: quantum mechanics with structured light**
10:50 – 11:00	**Coffee Break**
11:00 – 11:30	Invited Speaker / Prof. Martin J. Booth *Department of Engineering Science, University of Oxford, UK* **Building a universal framework for wavefront sensorless adaptive optics microscopy**
11:30 – 12:00	Invited Speaker / Prof. Hamidreza Khalesifard *Department of Physics, Institute for Advanced Studies in Basic Sciences (IASBS), Zanjan, Iran* **Optical remote sensing of atmospheric aerosols, a focus on the Iran Plateau**
13:15 – 14:00	**Lunch Break**
Session II	**Chair:** Prof. Mehmet Çakmak *Department of Photonics, Faculty of Applied Sciences, Gazi University, Ankara, Turkey*
13:00 – 13:30	Invited Speaker / Prof. Benedetta Marmiroli *Institute of Inorganic Chemistry, Graz University of Technology, Graz, Austria* **X-ray radiation assisted nanomaterials patterning by Deep X-ray lithography and investigation by Small Ange X-ray Scattering**
13:30 – 13:45	Speaker / Dr. Zeynep Demircioğlu *TÜBİTAK SAGE, TURKEY* **Laser texturing of AZO layer on ultra-thin glass substrate for flexible solar cells**
13:45 – 14:00	Speaker / Mehmet Berke Işık *Turkish Aerospace, Ankara, TÜRKİYE* **A Special catadioptric optical system design**
14:00 – 14:15	Speaker / Lehloa Peter Mohapi *Physics, University of the Witwatersrand, Johannesburg, South Africa* **Modelling a deformable mirror with a liquid crystal display**
14:15 – 14:30	Speaker / Assoc. Prof. Maryam Zoghi *University of Tehran, School of Engineering Science, Tehran, Iran* **Reflection shift characterization of plasmonic core/shell metasurfaces**
14:30 – 14:45	Speaker / Sevinj Mammadyarova *Nanoresearch Laboratory, Baku State University, Baku, Azerbaijan* **Effect of Ag doping on structural and optical properties of Co_3O_4 nanoparticles**

14:45 – 15:00	Speaker / Dr. Atilla Eren Mamuk *Mugla Sitki Kocman University, Department of Physics, Liquid Crystal Laboratory, Mugla, Turkey* **Presenting the optical properties of liquid crystal/polymer fibers for potential use as a light modulator**
15:00 – 15:10	**Coffee Break**
Session III	**Chair:** Prof. Halime Gül Yağlıoğlu *Physics Eng. Department, Ankara University, Ankara, Turkey*
15:10 – 15:40	Invited Speaker / Dr. Luis L. Sánchez-Soto *Faculty of Physics, Complutense University of Madrid, Spain* **Achieving the ultimate optical resolution**
15:40 – 15:55	Speaker / Dr. Frank Somhorst *Faculty of Science and Technology, University of Twente, Netherland* **Integrated photonic quantum information processing**
15:55 – 16:10	Speaker / Bereneice Sephton *School of Physics, University of the Witwatersrand, South Africa* **Teleporting scalably in high dimensions with nonlinear optics**
16:10 – 16:25	Speaker / Cade Peters *School of Physics, University of the Witwatersrand, South Africa* **Structuring light for robust optical communication through atmospheric turbulence**
16:25 – 16:40	Speaker / Chane Moodley *School of Physics, University of the Witwatersrand, Johannesburg, South Africa* **Resolution enhanced ghost imaging using machine learning**
16:40 – 17:05	**Coffee Break**
Session IV	**Chair:** Prof. Canan Varlıklı *Department of Photonics, İYTE, İzmir, Turkey*
17:05 – 17:55	Plenary Speaker / Prof. Manijeh Razeghi *Director, Center for Quantum Devices, Department of Electrical and Computer Engineering, Northwestern University, USA* **UV Quantum semiconductor materials and devices; for virus/bacteria detection and disinfection**
17:55 – 18:35	Plenary Speaker / Prof. Federico Capasso Robert *Wallace Professor of Applied Physics, Vinton Hayes Senior Research Fellow in Electrical Engineering, Harvard University, USA* **Flat Optics: arbitrary wavefront control with passive and active metasurfaces**
18:35 – 18:50	Speaker / Ashley M. Phala *Department of physics, University of the Witwatersrand, Johannesburg, South Africa* **Spatial mode generation for use in optical fiber**
18:50 – 19:00	**Coffee Break**
19:00 – 19:15	Speaker / Dhouha Baghdedi *Department of Physics, Sivas Cumhuriyet University, Sivas, Turkey* **Reflectance properties of GeO_2 films grown on p-Si substrate deposited by magnetron sputtering**
19:15 – 19:30	Speaker / Pedro Ornelas *Physics, University of the Witwatersrand, Johannesburg, South Africa* **Embedding the skyrmionic topology into the stokes field**
19:30 – 19:45	Speaker / Dr. Wagner Tavares Buono *School of Physics, University of the Witwatersrand, Johannesburg, South Africa* **Nonlinear optics with structured light: modal selection rules**

Thursday 26th May

Session I	**Chair:** Dr. Benedetta Marmiroli *Graz University of Technology, Austria*
09:00 – 09:40	Plenary Speaker / Prof. Hilmi Volkan Demir *Bilkent University Department of Electrical and Electronics Engineering, Department of Physics, UNAM– Institute of Materials Science and Nanotechnology, Ankara, Turkey* **Emerging semiconductor nanocrystal optoelectronics: from colloidal quantum dots to wells**
09:40 – 10:10	Invited Speaker / Dr. Angela Dudley *School of Physics, University of the Witwatersrand, Johannesburg, South Africa* **The generation and control of the structured polarisation**
10:10 – 10:40	Invited Speaker / Prof. Alexander Vladimirovich Volyar *Head of General Physics at VI Vernadsky Crimean Federal Univ.* **Structurally stable transitions in combined vortex beams upon excitation of each of its degrees of freedom**
10:40 – 10:50	**Coffee Break**
Session II	**Chair:** Süleyman Umut Eker *ASELSAN, Ankara, Turkey*
10:50 – 11:20	Invited Speaker / Dr. Luca Seravalli *Institute of Materials for Electronics and Magnetism, IMEM-CNR, Parma, Italy* **2-dimensional MoS_2 for photonic applications: CVD growth and properties**
11:20 – 11:35	Speaker / Dr. Amardeep Bharti *Elettra Sincrotrone Trieste, Italy* **Time-Resolved SAXS study on nucleation and growth kinetics of PVP stabilized Ag nanoparticles**
11:35 – 11:50	Speaker / Dr. Zeynep Baz *TÜBİTAK Defense Industries Research and Development Institute, Ankara, Turkey* **Surface-Enhanced raman scattering (SERS) properties of DLC films on Au nanoparticles**
11:50 – 12:05	Speaker / Bahareh Khaksar Jalali *Department of physics, Kharazmi University, University Sq., Shahid Beheshti Street, Karaj, Iran* **Differential evaluation of normal and cancer breast cell lines by optical methods**
12:05 – 13:00	**Lunch Break**
Session III	**Chair:** Dr. Zeynep Demircioğlu *TÜBİTAK SAGE, Ankara, Turkey*
13:00 – 13:30	Invited Speaker / Assoc. Prof. Alpan Bek *Department of Physics, Middle East Technical University (METU), Ankara, Turkey* **LIPSS for SERS: metal coated direct laser written periodic nanostructures for surface enhanced raman spectroscopy**
13:30 – 13:45	Speaker / Berkcan Erenler *Gazi University Photonics Application and Research Center, Ankara, Turkey* **Growth and laser properties of Tm^{3+}:$KY(WO_4)_2$ crystals**
13:45 – 14:00	Speaker / Kazım Canyurt *Department of Physics, Graduate School of Natural and Applied Sciences, Gazi University, Ankara, Turkey* **A new three-dimensional PCB design**
14:00 – 15:10	**Coffee Break**
Session IV	**Chair:** Prof. Dr. Bülent Çakmak *Department of Electrical and Electronic Engineering, Erzurum Technical University, Turkey*
15:10 – 15:40	Invited Speaker / Dr. Ehsan Ahadi-Akhlaghi *Department of Physics, Institute for Advanced Studies in Basic Sciences (IASBS), Zanjan, Iran* **Fresnel diffraction from phase steps: Theory and Applications**

15:40 – 15:55	Speaker / Navid Farezi *Research Institute for Applied Physics and Astronomy, University of Tabriz, Tabriz, Iran* **The effect of temperature on refractive indices in two high birefringence liquid crystals using the wedge-cell technique**
15:55 – 16:10	Speaker / Nader Safarinia *Department of Physics, Institute for Advanced Studies in Basic Sciences (IASBS), Zanjan, Iran* **Studying the effects of indistinguishable photonic sases on dynamics of multimodal quantum optomechanical systems**
16:10 – 16:25	Speaker / Kamal Heidary *Department of Physics, Institute for Advanced Studies in Basic Sciences, Zanjan, Iran* **Simulation of optical coherence tomography in MATLAB by using angular spectrum propagation and Fresnel equations for multilayer samples**
16:25 – 16:40	Speaker / Mohammad Khanjani *Department of Physics, Institute for Advanced Studies in Basic Sciences (IASBS), Zanjan, Iran* **Using Mirau microscope to nanoscale calibrate piezoelectric actuators**
16:40 – 16:55	Speaker / Ali Ebrahimzadeh *Department of Physics, Institute for Advanced Studies in Basic Sciences (IASBS), Zanjan, Iran* **Simultaneous thickness and group index measurement of multilayer thin films with spectral-domain optical coherence tomography**
16:55 – 17:10	Speaker / Mahdi Rameh *Department of Physics, Institute for Advanced Studies in Basic Sciences (IASBS), Zanjan, Iran,* **Acoustic trapping of large micro-particles**
17:10 – 17:20	**Coffee Break**
Session V	**Chair:** Prof. Alpan BEK *Department of Physics, Middle East Technical University (METU), Ankara, Turkey*
17:20 – 18:00	Plenary Speaker / Prof. Halina Rubinsztein-Dunlop *Australian Institute for Bioengineering and Nanotechnology* **Structured light in nano and microsystems**
18:00 – 18:30	Invited Speaker / Prof. Mirfaez Miri *Department of Physics, University of Tehran, Tehran, Iran* **Mie scattering: Optical signature of magnetoelectric polarizability of topological insulators**
18:30 – 18:45	Speaker / Merhan Kılıç *Cukurova University Department of Physics, Adana, Turkey* **Fabrication and characterization of ZnO p-n homojunction by spin coating method**
18:45 – 19:00	Speaker / Berkcan Erenler *Gazi University Photonics Application and Research Center, Ankara, Turkey* **PbSe quantum-dot doped borosilicate glasses as saturable absorbers**
19:00 – 19:10	**Coffee Break**
19:10 – 19:25	Speaker / Berk Serbest *Gazi University Photonics Application and Research Center, Ankara, Turkey* **Developing interdigital electrodes for electro-optical applications with aerosol jet printing technique**
19:25 – 19:40	Speaker / Mehmet Ziya Keskin *Department of Electrical and Electronics Engineering, TOBB University of Economics and Technology, Söğütözü, Ankara, Turkey* **Acousto-optic control of a laser beam profile in a DIRCM laser laboratory setup**
19:40 – 19:55	Speaker / Burak Korkmaz *Gazi University Photonics Application and Research Center, Ankara, Turkey* **Sapphire single crystal growth with kyropoulos technique**

19:55 – 20:10	Speaker / Sevdiye Başak Turgut *Solar Energy Institute, Ege University, Izmir, Turkey* **Improving power conversion efficiency by Light-Assisted annealing of triple cation perovskite layer in solar cell applications**

Friday 27th May

Session I	**Chair:** Dr. Angela Dudley *School of Physics, University of the Witwatersrand, Johannesburg, South Africa*
09:00 – 09:40	Plenary Speaker / Prof. Alper Kiraz *Department of Physics, Department of Electrical and Electronics Engineering Koç University, Turkey* **Deep learning enhanced digital microscopy and bioimage analysis**
09:40 – 10:10	Invited Speaker / Dr. Zakhar Kudrynskyi *Research Fellow, The University of Nottingham, United Kingdom* **2D Indium Selenide: from physical phenomena to emerging technologies**
10:10 – 10:40	Invited Speaker / Prof. Valeri V. Tuchin *Science Medical Center, Saratov State University, Saratov, Russia* **Optical clearing of tissues fort he improvement of laser medical technologies**
10:40 – 10:50	**Coffee Break**
Session II	**Chair:** Prof. Ebru Şenadım Tüzemen *Sivas Cumhuriyet University, Sivas, Turkey*
10:50 – 11:20	Invited Speaker / Prof. Mustafa Muradov *Nano Research Center, Baku State University, Baku, Azerbaijan* **Nanowires on base of Ag-Ag_2S: Synthesis and Optical Properties**
11:20 – 11:35	Speaker / Muhammed Baghir Baghirov *Nanoresearch Laboratory, Baku State University, Baku, Azerbaijan* **Dependence of the optical properties of composites based on GO/PVA on the annealing temperature and filler concentration**
11:35 – 11:50	Speaker / Keshaan Singh *School of Physics, University of the Witwatersrand, Johannesburg, South Africa* **Encoding information into the classical non-separability of light**
11:50 – 13:00	**Lunch Break**
Session III	**Chair:** Assoc. Prof. İlkay Demir *Sivas Cumhuriyet University, Sivas, Turkey*
13:00 – 13:30	Invited Speaker / Prof. Sinan Balcı *Photonics Department of Izmir Institute of Technology, Turkey* **Colloidal Plexcitonic Nanoparticles**
13:30 – 13:45	Speaker / Hasan Oğuz *Department of Physics, Pamukkale University, Denizli, Turkey* **Low Symmetry Photonic Crystal Cavity Phase Properties**
13:45 – 14:00	Speaker / Parisa Soleimani *Department of Chemistry, Faculty of Science, University of Guilan, Iran* **The study of diffraction polarization of fork grating printed on dye-doped liquid crystal cell**
14:00 – 14:15	Speaker / Dr. Pınar Özden *Mugla Sitki Kocman University, Department of Physics, Mugla, Turkey* **Wavelength depending measurements of the optical anisotropic properties of 5CB liquid crystal**
14:15 – 14:30	Speaker / Prof. Nikolai Staskov *A.A. Kuleshov Mogilev State University, Mogilev, Republic of Belarus* **Investigation of Optical Characteristics of In_2S_3 Thin Films by Spectroscopic Ellipsometry and Spectrophotometry Methods**
14:30 – 14:45	Speaker / Ömer Akpınar *Gazi University Photonics Application and Research Center, Ankara, Turkey* **Ti Doped Sapphire Crystal Growth**
14:45 – 15:15	**Coffee Break**

Session IV	**Chair:** Assoc. Prof. Dr. Güven Turgut *Science Faculty of Erzurum Technical University, Erzurum, Turkey*
15:15 – 15:45	Invited Speaker / Dr. Siamak Golshahi *Department of Physics, Islamic Azad University, Rasht Branch* **Photocatalytic properties of Graphene-based nanocomposites**
15:45 – 16:00	Speaker / Zekeriya Mehmet Yüksel *Department of Physics, Pamukkale University, Denizli, Turkey* **Evaluation of Optical Properties of Hexagonal and Circular Solid Core Photonic Crystal Fibers for Various Structural Design Parameters**
16:00 – 16:15	Speaker / Göktuğ Gencehan Artan *Teops, Arp Kule Business Center, Ankara, Turkey* **Future Trends of EO/IR Systems for Airborne ISR Systems**
16:15 – 16:30	Speaker / Dr. Ali Emre Gümrükçü *Gazi University Photonics Application and Research Center, Ankara, Turkey* **Effect of sputtering conditions on the physical quality of sub-10 nm Ag films prepared by DC magnetron sputtering**
16:30 – 16:45	Speaker / Büşra Güloğlu Bülbül *Gazi University Photonics Application and Research Center, Ankara, Turkey* **Development of the Near Infrared Absorbing LaB_6 Optical Filter**
16:45 – 17:00	Speaker / Mahsa Seyedmohammadzadeh *Department of Physics, Bilkent University, Ankara, Turkey* **2D heterostructures formed by graphene-like ZnO and MgO for novel optoelectronic applications**
17:00 – 17:15	Speaker / Dr. Halil İbrahim Efkere *Gazi University Photonics Application and Research Center, Ankara, Turkey* **Investigation of the effect of annealing on the structural and optical properties of RF sputtered WO_3 nanostructure for memristor applications**
17:15 – 17:25	**Coffee Break**
Session V	**Chair:** Assoc. Prof. Nihan Akin Sonmez *Gazi University Department of Photonics, Photonics Application and Research Center, Ankara, Turkey*
17:25 – 17:55	Invited Speaker / Assoc. Prof. Dr. Güven Turgut *Science Faculty of Erzurum Technical University, Erzurum, Turkey* **Optimizing CVD Growth Parameters of InSe Monolayers**
17:55 – 18:10	Speaker / Malika Tuzelbay *Physics and Astronomy, Al-Farabi Kazakh National University, Almatı, Kazakistan* **About statistical patterns of exoplanets**
18:10 – 18:25	Speaker / Dr. Meltem Dönmez Kaya *Gazi University Photonics Application and Research Center, Ankara, Turkey* **Fabrication and Characterization of MoS_2/Si Heterojunction Structure**
18:25 – 18:40	Speaker / Zhila Alipanah *Faculty of Physics, University of Tabriz, Tabriz, Iran* **Role of UV absorbers on the IR-LD spectra of liquid crystal network polymer**
18:40 – 18:50	**Coffee Break**
18:50 – 19:05	Speaker / Hicret Hopoğlu *Department of Physics, Sivas Cumhuriyet University, Sivas, Turkey* **Dependence of film thicknesses on the XRD, AFM and Transmittance Properties of NiO_x**
19:05 – 19:20	Speaker / Yeliz Özkök *Gazi University Photonics Application and Research Center, Ankara, Turkey* **Production and characterisation of TiO_xN_y thin films for stent applications by co-sputtering system with confocal geometry**

19:20 – 19:35	Speaker / Volkan Bozkuş *Department of Photonics, Izmir Institute of Technology, Urla, Izmir, Turkey* **Tunning and enhancing the electroluminescence properties of blue polymer light emitting diode by incorporation of perylene diimide derivatives**
19:35 – 19:50	Speaker / Lala Gahramanli *Baku State University, Baku, Azerbaijan* **Influence of environment to optical properties of CdS nanoparticles**
21:30 – 21:45	**Closing Ceremony and Best Presentation Awards** (Zoom webinar and Youtube-Stream)

TABLE OF CONTENTS

PLENARY SPEAKERS

PS1

What are the limits to focusing light tightly

Gerd Leuchs

Max Planck Institute, Germany

PS2

1,2,3 … Infinity: quantum mechanics with structured light

Andrew Forbes

School of Physics, University of the Witwatersrand, Johannesburg, South Africa

Photons can be described in terms of their spatial modes – the “patterns” of light. As there are an infinite number of spatial modes, entanglement in this degree of freedom offers the opportunity to realise high-dimensional quantum states: quantum mechanics with pictures. In this talk I will review the recent progress in quantum entanglement of photons in their spatial degree of freedom. I will explain how to create high-dimensional quantum states in the laboratory, how to measure them, and what the present state of the art is in terms of applications. In particular, I will outline the advantages and disadvantages of using such entangled states as a means to encode information for secure quantum communication channels, and will consider the use of non-linear optics as novel detectors.

PS3

UV Quantum Semiconductor materials and devices; for virus/bacteria detection and disinfection

Manijeh Razeghi

Director, Center for Quantum Devices, Department of Electrical and Computer Engineering, Northwestern University, USA

PS4

Flat Optics: arbitrary wavefront control with passive and active metasurfaces

Federico Capasso Robert

John A. Paulson School of Engineering and Applied Sciences Harvard University, Cambridge, MA 02138
capasso@seas.harvard.edu

Metaoptics offer fresh opportunities for structuring light as well as dark as well as for active control. I will discuss metasurfaces that enable light's spin and OAM to evolve, simultaneously, from one state to another along the propagation direction[1,2], along with nonlocal supercell designs that demonstrate multiple independent optical functions at arbitrary large deflection angles with high efficiency[3]. In one implementation the incident laser is simultaneously diffracted into Gaussian, helical and Bessel beams over a large angular range and in another one a compact wavelength-tunable external cavity laser with arbitrary beam control capabilities including hologram lasing was demonstrated[3]. 2D phase and polarization singularities ("structured dark") have been realized, which open up new opportunities for the detection of point defects in transparent materials for failure mode detection[4].

Transparent materials do not absorb light but have profound influence on the phase evolution of transmitted radiation. One consequence is chromatic dispersion causing ultrashort laser pulses to elongate in time while propagating. We experimentally demonstrated ultrathin nanostructured coatings that resolve this challenge: we tailored the dispersion of silicon nanopillar arrays such that they temporally reshape pulses upon transmission using slow light effects and act as ultrashort laser pulse compressors[5]. The coatings induce anomalous group delay dispersion in the visible to near-infrared spectral region around 800 nm wavelength over an 80 nm bandwidth. We characterized the arrays' performance in the spectral domain via white light interferometry and directly demonstrate the temporal compression of femtosecond laser pulses. Applying these coatings to conventional optics renders them ultrashort pulse compatible and suitable for a wide range of applications.

Tailored nanostructures also provide at-will control over the properties of light using nonlinear optics, with applications in imaging and spectroscopy. Nanomaterials with $\chi(2)$ nonlinearities achieve highest switching speeds. We have shown that a thin film of organic electro-optic molecules JRD1 in polymethylmethacrylate combined with nanograting provides excellent performance for free-space optics: broadband record-high nonlinearity (10-100 times higher than traditional materials at wavelengths 1100-1600 nm), a custom-tailored nonlinear tensor at the nanoscale, and engineered optical and electronic responses[6]. We demonstrated a tuning of optical resonances by $\Delta\lambda = 11$ nm at DC voltages and a modulation of the transmitted intensity up to 40%. We realize 2×2 single- and 1×5 multi-color spatial light modulators and showed their potential for imaging and remote sensing[6].

We have also employed a metasurface from sub-wavelength Mie resonators that support quasi bound states in the continuum (BIC) as a key mechanism to demonstrate electro-optic modulation of free-space light with high efficiency at GHz speeds[7]. Our geometry relies on hybrid silicon-organic 35 nanostructures that feature low loss (Q = 550 at λ=1594 nm) while being integrated with GHz compatible coplanar waveguides. We maximized the electro-optic response by using the high-performance electro-optic molecules of Ref. 6 and by nanoscale optimization of the optical modes. We demonstrated both DC tuning and high -speed modulation up to 5 GHz[7].

Reference:

[1] Ahmed H. Dorrah, Noah A. Rubin, Aun Zaidi, Michele Tamagnone & Federico Capasso Nature Photonics 15, 287 (2021)
[2] Ahmed H Dorrah, Noah A Rubin, Michele Tamagnone, Aun Zaidi, & Federico Capasso Nature Communications, 12, 6249 (2021)
[3] Christina Spägele, Michele Tamagnone, Dmitry Kazakov, Marcus Ossiander, Marco Piccardo, and Federico Capasso Nature Communications, 12, 3787 (2021).
[4] Soon Wei Daniel Lim, Joon-Suh Park, Maryna L. Meretska, Ahmed H. Dorrah, & Federico Capasso Nature Communications, 12, 4190 (2021)
[5] M. Ossiander, Y.-W. Huang, W. T. Chen, Z Wang, X Yin, YA Ibrahim, M Schultze, and F. Capasso Nature Communications, 12, 6518 (2021)
[6] Ileana-Cristina Benea-Chelmus, M. L Meretska, D. L Elder, M. Tamagnone, L. R Dalton, and F. Capasso Nature Communications, 12, 5928 (2021)
[7] Ileana-Cristina Benea-Chelmus, Sydney Mason, Maryna L Meretska, Delwin L Elder, Dmitry Kazakov, Amirhassan Shams-Ansari, Larry R Dalton, and Federico Capasso. Nature Communications, 13, 3170 (2022)

PS5

Emerging semiconductor nanocrystal optoelectronics: *from colloidal quantum dots to wells*

Hilmi Volkan Demir

Bilkent University Department of Electrical and Electronics Engineering, Department of Physics, UNAM– Institute of Materials Science and Nanotechnology, Ankara, Turkey
NTU Singapore – Nanyang Technological University School of Electrical and Electronic Engineering, School of Physical and Mathematical Sciences, School of Materials Science and Engineering, Singapore
volkan@bilkent.edu.tr, hvdemir@ntu.edu.sg, volkan@stanfordalumni.org

Semiconductor nanocrystals have attracted great interest for color conversion and enrichment in quality lighting and displays. Optical properties of these solution-processed nanostructures are conveniently controlled by tailoring their size, shape and composition in an effort to realize high-performance light generation and lasing. These colloids span different types and heterostructures of semiconductors in the forms of quantum dots and rods, most recently extending to the latest sub-family of nanocrystals, the colloidal quantum wells (CQWs). In this talk, we will introduce the emerging field of semiconductor nanocrystal optoelectronics, with most recent examples of their photonic structures and optoelectronic devices employing such atomically-flat, tightly-confined, quasi-2-dimensional CQWs, also popularly nick-named 'nanoplatelets'. Among various extraordinary features of theirs, we will show that these CQWs enable record high optical gain coefficients [1] and can achieve gain thresholds at the level of sub-single exciton population per CQW on the average [2], empowered by carefully engineering their heterostructures [3,4]. Next, we will present a powerful, large-area self-assembly technique for orienting these nanoplatelets (either all face-down or all edge-up) [5], which provides us with a tool to help engineering their interfaces. Using three-dimensional constructs of all-face-down self-assemblies of CQWs with monolayer precision, we will demonstrate ultrathin optical gain media and lasers of these oriented-CQW slabs [6]. Finally, we will show record high-efficiency colloidal LEDs using CQWs employed as the electrically-driven active emitter layer [7] and record low-threshold solution lasers using the same CQWs employed as the optically-pumped fluidic gain medium [8]. Given their current accelerating progress, these solution-processed quantum well materials hold great promise to challenge their epitaxial thin-film counterparts in semiconductor optoelectronics in the near future.

References:

[1] B. Guzelturk et al., HVD, Nano Letters 19, 277 (2019)
[2] N. Taghipour et al., HVD, Nature Comm 11, 3305 (2020)
[3] Y. Altıntas et al., HVD, ACS Nano 13, 10662 (2019)
[4] F. Shabani et al., HVD, Small (2022) (*in press*)
[5] O. Erdem et al., HVD, Nano Letters 19, 4297 (2019)
[6] O. Erdem et al., HVD, Nano Letters 20, 6459 (2020)
[7] B. Liu et al., HVD, Advanced Materials 32, 1905824 (2020)
[8] J. Maskoun et al., HVD, Advanced Materials 33, 2007131 (2021)

PS6

Structured light in nano and microsystems

Halina Rubinsztein-Dunlop

Australian Institute for Bioengineering and Nanotechnology

PS7

Deep learning enhanced digital microscopy and bioimage analysis

Alper Kiraz

Department of Physics, Department of Electrical and Electronics Engineering Koç University, Turkey
akiraz@ku.edu.tr

Deep learning has triggered a revolutionary transformation in digital optical microscopy. Studies at the intersection of machine learning, optics and life sciences have shown that the performance of digital microscopes can be enhanced, and very large datasets can be automatically analyzed with high accuracy. Deep learning approaches that employ problem specific deep neural network models have largely replaced standard image processing techniques such as thresholding and watershed transformation for processing optical microscopy images. In addition to data analysis, deep learning can also be used exquisitely to improve the overall performance of an optical microscope. Deep learning enhanced approaches can be used to increase the signal-to-noise ratio, to obtain super-resolution images above the diffraction limit, or to create virtually stained images from images that do not contain any staining. This enables developing more compact and low-cost devices with similar performance parameters as compared to expensive alternatives such as confocal microscopes. In this presentation I discuss our recent works on novel deep learning-based solutions for automated cell counting and viability analysis, brain vasculature analysis, and improving the contrast and resolution of fluorescence microscopes.

INVITED SPEAKERS

IS1

Building a universal framework for wavefront sensorless adaptive optics microscopy

Qi Hu, Martin Hailstone, Jingyu Wang, Matthew Wincott, and Martin J Booth

Department of Engineering Science, University of Oxford, United Kingdom
martin.booth@eng.ox.ac.uk, http://www.eng.ox.ac.uk/dop/

Adaptive optics is widely used in high resolution microscopy to overcome the problems caused by specimen induced aberrations. This is particularly useful when focussing deep into biological specimens, due the the variations in refractive index throughout the volume of cells and tissues. Wavefront sensorless adaptive optics (AO) methods (or “sensorless” AO methods, for short) are common as their simple implementation does not include the extra hardware required for a wavefront sensor path. Furthermore, these methods are necessary in microscopes where wavefront sensing is not practical. These sensorless methods perform aberration correction through efficient optimisation of image quality. The wide range of such approaches that have been developed are tailored for different microscopes and applications. We have previously shown that all such methods can be fitted into the same framework, permitting side-by-side evaluation of effectiveness in different imaging scenarios. The parts of this framework include the aberration representation, the optimisation metric (or cost function), and the estimation algorithm. This approach to understanding sensorless AO shows that the seemingly differing methods have many common features. We use this framework to define new approaches that are applicable across a wide range of microscopes. In particular, we examine machine learning approaches to estimation that are independent of the wide range of specimen structures that might be encountered in general application of microscopes. We show how appropriate algorithms can be chosen to enhance the correction range of aberration magnitudes, processing efficiency or accuracy of the sensorless AO microscopes. Furthermore, we show how the methods can be translated across different microscopes. These tools will have broad application across a range of microscope modalities.

IS2

Optical remote sensing of atmospheric aerosols, a focus on the Iran Plateau

Hamidreza Khalesifard

Department of Physics, Institute for Advanced Studies in Basic Sciences (IASBS), Zanjan, Iran
khalesi@iasbs.ac.ir

Atmospheric aerosols are small particles that depending on their size, type and elevation may suspend in the atmosphere from few minutes to few months. Such particles not only influencing the earth radiation budget, but have impacts on social health, agriculture, aviation, industry and economy. Awareness about the existence conditions and prediction of transportation and evolution of such particles, reduces their negative impacts on the human life. Optical remote sensing techniques including lidars and radiometry are quite robust, powerful and accurate for this purpose. In this talk, after introducing principles of these techniques we will discuss how our team has used them to monitor atmospheric aerosols over the Iran Plateau. It is quite important to note political borders aren't barriers to such atmospheric phenomena and international collaborations are very important in these types of investigations.

IS3

X-ray radiation assisted nanomaterials patterning by Deep X-ray lithography and investigation by Small Ange X-ray Scattering

Marmiroli B.*[1], Sartori B. [1], Turchet A. [2], Bharti A. [2], Amenitsch H.[1]

[1]*Institute of Inorganic Chemistry, Graz University of Technology, 8010 Graz, Austria*
[2]*Elettra-Sincrotrone Trieste, 34149 Trieste, Italy*
benedetta.marmiroli@tugraz.at

The integration of micro/nano fabrication techniques for top-down processing with novel materials prepared with bottom-up approaches is an important goal whose potential still remains widely unexploited. In fact, this would open the possibility to fabricate micro/nanodevices with improved performance presenting functional materials in desired areas. To reach the objective, the control of materials and structures using suitable investigation techniques is required, leading to an interdisciplinary approach. In this communication, we want to present what we recently obtained combining Deep X-ray Lithography (DXRL) for microfabrication and Small Angle X-ray Scattering (SAXS) for investigation. DXRL is a lithographic technique that induces changes in materials due to the effect of high energy X-rays which allow producing structures with high aspect ratio and high resolution. SAXS is a standard method for structural characterization at the nanoscale and has excellent in situ and time resolved capabilities. The research has been performed at the Austrian SAXS beamline and at the DXRL beamline of Elettra- Sincrotrone Trieste (Italy). We will first describe the structural changes induced by X-rays on the precursor of cellulose TMSC (Trimethylsilyl cellulose). These lead to its application as double tone resist for the fabrication of (bio)microfluidic devices [1]. We will then report on the effect of irradiation on mechanical properties of mesoporous silica thin films [2]. Moreover we will discuss the possibility to employ such films to keep the hydration of biological substances deposited upon them, opening the possibility for their use as next generation sample holders [3]. Finally, we will show the patterning of metal xerogels that are subsequently thermally converted into the corresponding noble metals strongly reducing the waste of the expensive metal precursor [4].

References:

[1] Andreev M. et al., Microelectronic Engineering. 2022, 256, 111720
[2] P. Y. Steinberg et al., Frontiers in Materials. 2021, 8, 628245.
[3] B. Marmiroli et al., Frontiers in Materials. 2021, 8, 686353.
[4] Gayrard M. et al., Nanoscale. 2022, 14, 1706-1712

IS4

Achieving the ultimate optical resolution

Luis L. Sánchez-Soto

Faculty of Physics, Complutense University of Madrid, Spain

The measurement of the separation between two clocks is of paramount importance for many applications. With optical pulses emitted from coherent or partially coherent sources, the timing information can be measured through established interferometric methods and conventional photodetection and distance information can be extracted from timing information using the time-of-flight principle. In these cases and others, the main goal of a timing measurement is to estimate specific properties of a received signal consisting of multiple pulses, such as relative time delays, centroids, and relative intensities, and not necessarily full temporal profile reconstruction.

In many settings, the optical pulses being measured share little or no coherence. In that case, interferometric methods cannot be exploited, and the estimation precision of tools that directly measure temporal intensity, is reduced dramatically. In the spatial domain, this problem has been dubbed as Rayleigh's curse. For intensity-only direct-detection schemes in the instructive case of two mutually incoherent pulses with equal intensities, the information gained per photon detected (quantified by the Fisher information) decreases quadratically with τ. This implies that the variance of the any estimator diverges as the pulse separation approaches zero, as can be formalized through the Cramér-Rao lower bound (CRLB).

However, Rayleigh's curse is not integral to the problem, but rather an artifact of only considering the intensity of the field. By optimizing over all possible quantum measurements via the quantum Fisher information, it can be shown that the precision of an optimal measurement maintains a fairly constant value for any pulse separation. In other words, the divergence can be averted using phase-sensitive measurements, despite the incoherent nature of the sources. This information is always available, no matter how small τ becomes. We will show experiments projecting onto tailored optical field modes and exhibiting better precision than the direct-detection CRLB in both the spatial and the time domains.

IS5

The generation and control of the structured polarisation

Angela Dudley

School of Physics, University of the Witwatersrand, Johannesburg, South Africa

We will provide a brief overview to Structured Light – in particular to structured polarisation profiles, with specific attention to vector vortex modes, which possess inhomogeneous polarisation profiles. Here we will show polarisation structures that can be designed to accelerate independently from their spatial profile by encoding weighted superpositions of oppositely charged scalar Bessel beams on a Digital Micromirror Device (DMD). We experimentally reconstruct their Stokes vectors illustrating that these also accelerate. Here we make use of static polarisation optics to separate a mode into left- and right-circular states. We outline the role of DMDs in the creation, control and detection of structured light fields.

IS6

Structurally stable transitions in combined vortex beams upon excitation of each of its degrees of freedom

Alexander Vladimirovich Volyar

Head of General Physics at VI Vernadsky Crimean Federal Univ.

IS7

2-dimensional MoS_2 for photonic applications: CVD growth and properties

Luca Seravalli

Institute of Materials for Electronics and Magnetism, IMEM-CNR, Parma, Italy

Two-dimensional (2D) materials such as graphene, transition metal dichalcogenides, and boron nitride have recently emerged as promising candidates for novel applications in sensing and for new electronic and photonic devices. Their exceptional mechanical, electronic, optical, and transport properties show peculiar differences from those of their bulk counterparts and may allow for future radical innovation breakthroughs in different applications. MoS_2 is considered one of the most promising and successful transition metal dichalcogenides, in particular for light-based applications, thanks to its tunable direct gap in the 1.6 – 1.9 eV range. Control and reproducibility of the synthesis are key factors required to drive the development of 2D materials. Among various methods, chemical vapour deposition (CVD) is considered an excellent candidate for this goal thanks to its simplicity, widespread use, and compatibility with other processes used to deposit other semiconductors.

In this talk, I will present some representative novel photonic devices based on this 2D material [1-2], followed by a summary of the fundamental characterization techniques available to study its properties. Then, I will explore the CVD growth of MoS_2, by summarizing the basics of the synthesis procedure (Fig.1), discussing in depth: (i) the different substrates used for its deposition, (ii) precursors (solid, liquid, gaseous) available, and (iii) different types of promoters that favour the growth of two-dimensional layers [3]. I will conclude the talk by presenting our recent results on the study of organic promoter flux on the growth of 2D MoS_2 [4] and of the addition drop-casted Gold Nanoparticles on the surface and their effect on the nanostructure properties [5].

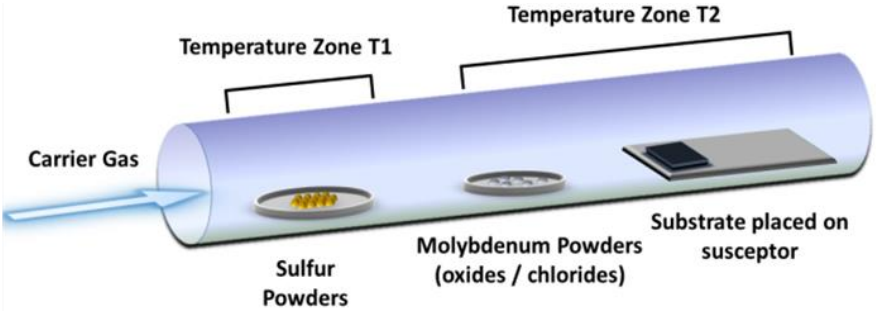

Fig.1 Schematic view of the CVD tube for MoS_2 flake growth with solid precursors

Reference:

[1] Yazyev, O. V.; Kis, A. MoS_2 and semiconductors in the flatland. Mater. Today 2015, 18, 20–30.

[2] Lee HS, Luong DH, Kim MS, et al. Reconfigurable exciton-plasmon interconversion for nanophotonic circuits. Nat. Commun. 2016, 7, 13663.
[3] Seravalli, L.; Bosi, M. A Review on Chemical Vapour Deposition of Two-Dimensional MoS2 Flakes. Materials. 2021, 14, 7590.
[4] Rotunno, E.; Bosi, M.; Seravalli, L.; Salviati, G.; Fabbri, F. Influence of organic promoter gradient on the MoS2 growth dynamics. Nanoscale Adv. 2020, 2, 2352–2362.
[5] Seravalli, L.; Bosi, M.; Fiorenza, P.; Panasci, S.E.; Orsi, D.; Rotunno, E.; Cristofolini, L.; Rossi, F.; Giannazzo, F.; Fabbri, F. Gold nanoparticle assisted synthesis of MoS2monolayers by chemical vapor deposition. Nanoscale Adv. 2021, 3, 4826–4833.

IS8

LIPSS for SERS: Metal Coated Direct Laser Written Periodic Nanostructures for Surface Enhanced Raman Spectroscopy

Alpan Bek

Department of Physics, Middle East Technical University (METU), Ankara, Turkey
bek@metu.edu.tr

In this work, a novel method of fabricating large-area, low-cost surface-enhanced Raman spectroscopy (SERS) substrates is explained which yields densely nanostructured surfaces utilizing laser-induced periodic surface structuring (LIPSS) of crystalline Si. Two different interaction regimes are utilized to yield low-spatial-frequency (LSFL) and high-spatial-frequency (HSFL) LIPSS patterns. Nanostructuring of Si surface is followed by deposition of a thin noble metal layer to complete the fabrication procedure. A 50-70 nm thick Ag layer is shown to maximize the SERS performance. The SERS effect is attributed to the electromagnetic field enhancement originating from the nanoscale surface roughness of Si that can be controlled by LSFL and HSFL nature of the structure. The SERS substrates are found to be capable ofdetecting a Raman analyte down to 10^{-11} M. SERS performance of the Ag deposited substrates are compared at 532, 660 and 785 nm excitation wavelengths. Both LSFL and HSFL Si surfaces with 70 nm thick Ag are found to exhibit strongest SERS under 660 nm excitation exhibiting Raman enhancement factors (EFs) as high as 10^9. The Raman EFs are calculated both by SERS spectra experimentally, and using finite-elements method simulation of the electric field enhancement where a good agreement is found.

Acknowledgment:
This work is supported by TÜBİTAK grant nrs.119F101 and 2211C.

IS9

Fresnel diffraction from phase steps: Theory and Applications

Ehsan Ahadi-Akhlaghi

Department of Physics, Institute for Advanced Studies in Basic Sciences (IASBS), Zanjan, Iran

When abrupt changes occur in light wave parameters such as phase, amplitude, phase gradient, and polarization the pattern of light intensity distribution and its propagation path changes, which is called diffraction. Diffraction is a fundamental phenomenon in optics that has long been studied by various scientists such as Grimaldi, Fresnel, Fraunhofer, and Maxwell. In the last two decades, Tavassoly has also paid attention to the phase step diffraction caused and has presented several articles to introduce its formulation and applications. In this presentation, the diffraction of phase objects will be introduced as a practical, accurate, and simple method for application in an optical measurement called diffractometry. Its theoretical foundations will be briefly discussed. Also, a new source for Fresnel diffraction of phase objects will be presented, and then the applications of Fresnel diffraction for simultaneous measurement of thickness and refractive index of thin films, 3D microscopic imaging, and determination of fractional topological charge of vortex beams will be reviewed.

IS10

Mie scattering: Optical signature of magnetoelectric polarizability of topological insulators

Mirfaez Miri

Department of Physics, University of Tehran, Tehran, Iran

The magnetoelectric susceptibility of a topological insulator is quantized in terms of the fine structure constant. This has been confirmed in a few experiments. It is much easier to use conventional rather than high-precision time-domain terahertz polarimetry techniques. Thus to reveal the topological magnetoelectric effect, we suggest to focus on the scattering of a linearly polarized plane wave by a cluster of topological insulator and metal spheres. We show that the topological magnetoelectric effect leaves its fingerprint on the scattered field. Indeed a giant optical activity about 20 degrees is easily measurable.

IS11

2D Indium Selenide: from physical phenomena to emerging technologies

Zakhar, Kudrynskyi[1,2,*]

[1]*School of Physics and Astronomy, University of Nottingham, United Kingdom*
[2]*Advanced Materials Research Group, Faculty of Engineering, University of Nottingham, United Kingdom*
**zakhar.kudrynskyi@nottingham.ac.uk*

Atomically thin layers of van der Waals crystals and their heterostructures, generally called as two-dimensional (2D) materials, have attracted enormous interest for nearly two decades now. Following the discovery of graphene, the first known truly 2D crystal, there has been a constant search for novel related materials to enrich the library of 2D compounds with new properties. Most attention has been focused on graphene itself, as well as semiconducting crystals of transition metal dichalcogenides and wide-gap insulator hexagonal boron nitride. However, during the recent years an exciting and rapidly growing development in the family of 2D materials involves indium selenide (InSe). This semiconducting crystal has a bandgap energy that increases markedly with decreasing layer thickness, enabling fabrication of devices with high broad-band photoresponsivity. In addition, it has a relatively low mass conduction band electrons and high electron mobility even in atomically thin films, larger than in silicon-based field effect transistors.

This talk reviews my recent research on this new 2D semiconductor. From the fundamental studies of 2D layers and heterostructures to the demonstration of prototype devices, I will discuss how this system can provide a platform for scientific investigations and new routes to ultra-thin electronics and optoelectronics, including high mobility field effect transistors and hybrid multi-layered structures for quantum metrology and photosensing [1-7].

Keywords: 2D semiconductors, InSe, van der Waals heterostructures, quantum effects.

References:

[1] Bandurin et al., Nature Nanotechnology 12, 223 (2017).
[2] Kudrynskyi et al., Physical Review Letters 119, 157701 (2017).
[3] Ubrig et al., Nature Materials, 19, 299 (2020).
[4] Kudrynskyi et al., (Nature) Communication Physics, 3, 16 (2020)
[5] Buckley et al., Advanced Functional Materials, 2008967 (2021).
[6] Zhu et al., Advanced Materials, 33, 2104658 (2021).
[7] Liang et., Advanced Electronic Materials, 2100954 (2022).

IS12

Optical clearing of tissues fort he improvement of laser medical technologies

Valeri V. Tuchin

Science Medical Center, Saratov State University, Saratov, Russia

IS13

Nanowires on base of Ag-Ag_2S: Synthesis and Optical Properties

Mustafa Muradov

Nano Research Center, Baku State University, Baku, Azerbaijan

IS14

Colloidal plexcitonic nanoparticles

Sinan BALCI

Izmir Institute of Technology, Department of Photonics, 35430 Izmir, Turkey

The understanding and control of light-matter interaction at nanoscale dimension has both provided new insights into quantum optical phenomena and led to the discovery of new functional optoelectronic devices[1]. In the strong coupling regime, plasmons supported by metal nanoparticles interact strongly with molecular excitons or excitons of semiconducting quantum dots, and hence plexcitons are formed[2]. Plexcitons show half-matter and half-light properties. In order to deeply understand plasmon–exciton interaction at the nanoscale dimension and boost the performance of nanophotonic devices made of plexcitonic nanoparticles, new types of plexcitonic nanoparticles with tunable optical properties and outstanding stability at room temperature are urgently needed[3]. We have achieved synthesis of pure colloidal nanodisk, nanoring, nanoplatelet shaped plexcitonic nanoparticles with very large Rabi splitting energies, i.e., more than 400 meV[4, 5]. In order to synthesize plexcitonic nanoparticles, we firstly synthesize silver nanoprisms by using seed mediated synthesis and then convert nanoprisms to nanodisks. The localized surface plasmon polariton resonance frequency of the silver nanodisk can be tuned by heating. Finally, self-assembly of J-aggregate dyes on plasmonic nanoparticles produces plexcitonic nanoparticles. We envision that different shaped colloidal plexcitonic nanoparticles with very large Rabi splitting energies and outstanding stability at room temperature will find critical applications in a variety of fields such as polariton laser, biosensor, plasmon laser, catalysis, light emitting diodes, solar cells, plasmon molecular nanodevices, and energy flow at nanoscale dimensions.

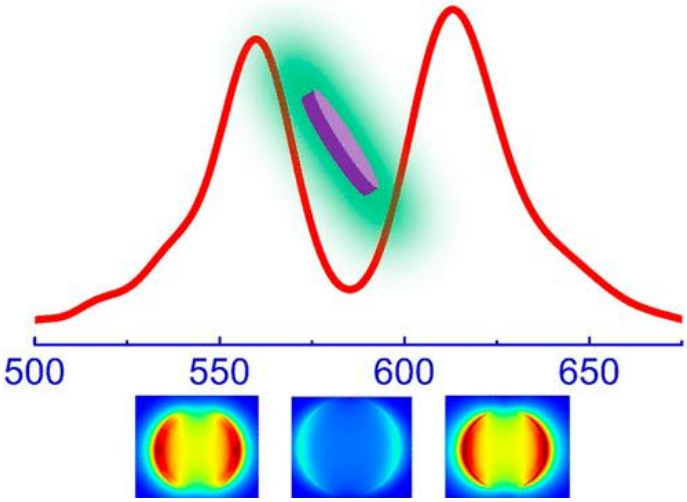

References:

[1] Ergoktas, M. S.; Soleymani, S.; Kakenov, N.; Wang, K.; Smith, T. B.; Bakan, G.; Balci, S.; Principi, A.; Novoselov, K. S.; Ozdemir, S. K.; Kocabas, C., Topological engineering of terahertz light using electrically tunable exceptional point singularities. Science 2022, 376 (6589), 184-188.

[2] Sarisozen, S.; Polat, N.; Mert Balci, F.; Guvenc, C. M.; Kocabas, C.; Yaglioglu, H. G.; Balci, S., Strong Coupling of Carbon Quantum Dots in Liquid Crystals. The Journal of Physical Chemistry Letters 2022, 3562-3570.
[3] Finkelstein-Shapiro, D.; Mante, P.-A.; Sarisozen, S.; Wittenbecher, L.; Minda, I.; Balci, S.; Pullerits, T.; Zigmantas, D., Understanding radiative transitions and relaxation pathways in plexcitons. Chem 2021.
[4] Balci, F. M.; Sarisozen, S.; Polat, N.; Balci, S., Colloidal Nanodisk Shaped Plexcitonic Nanoparticles with Large Rabi Splitting Energies. J Phys Chem C 2019, 123 (43), 26571-26576.
[5] Guvenc, C. M.; Balci, F. M.; Sarisozen, S.; Polat, N.; Balci, S., Colloidal Bimetallic Nanorings for

IS15

Photocatalytic properties of Graphene-based nanocomposites

Siamak Golshahi

Department of Physics, Rasht Branch, Islamic Azad University, Rasht, Iran

In the turn of the new century, environmental issues of wastewater have attracted lots of attentions due to its destructive effects on ecosystems and human health [1]. So, wastewater treatment plays a crucial role as a solution to this problematic issue. Employing Nanotechnology to the treatment of waste water is hot topic [2]. Enhancing the confined dimensions of materials tunes their reactivity and can be employed to the removal of water pollutants. Turning down the thickness of Graphite to a few nanometers in one hand, substantially enhances its chemical reactivity and in the other hand, boosts its electrical performance [3]. This low dimensional Graphite, called Graphene, can be found in wide various forms only by adding or removing the different functional groups on its surface. In addition, the composition of Graphene with wide band gap metal oxide semiconductors can drastically improve both its chemical reactivity and electrical properties. Non-intrinsic Metal Oxide wide band gap semiconductors (e.g.: Zinc Oxide, Tin Oxide, Indium Oxide) can absorb light to make high concentration of mono-polar carrier which can be transferred to the two-dimensional structure of graphene to improve its catalytic performance. In this work we review the photocatalytic performance of these Graphene-based nanocomposites as a function of the synthesis parameters.

References:

[1] A.D.N. Nemerow, A Dasgupta, Industrial and Hazardous Waste Treatment, Van Nostrand Reinhold, New York, 1991.
[2] Priya Kumari, Masood Alam, Weqar Ahmed Siddiqi, Usage of nanoparticles as adsorbents for waste water treatment: An emerging trend, Sustainable Materials and Technologies 22 (2019) e00128.
[3] Li, X., Yu, J., Wageh, S., Al-Ghamdi, A.A. and Xie, J. (2016), Graphene in Photocatalysis: A Review. Small, 12: 6640-6696.

IS16

Optimizing CVD Growth Parameters of InSe Monolayers

Coşkun, A.[1,2], Çelik, K.[1,2], Özerbaş, Z.E.[1,2], Baltakesmez, B.A.[1,2], Işık, M.A.[1,2], Aygün, M.[1,2,3], Çakmak, B.[1, 4], Turgut, G.[1,2,3,*]

[1]Department of Photonic, Graduate School of Science, Erzurum Technical University, 25050 Yakutiye, Erzurum, Turkey
[2]2D Research Lab., High Technology Application and Research Centre, Erzurum Technical University, 25050 Yakutiye, Erzurum, Turkey
[3]Department of Basic Sciences, Science Faculty, Erzurum Technical University, 25050 Yakutiye, Erzurum, Turkey
[4]Department of Electrical and Electronic Engineering, Engineering and Architecture Faculty, 25050 Yakutiye, Erzurum, Turkey
**guven.turgut@erzurum.edu.tr*

The layered group III-chalcogenides with the formula MX have great attention owing to their unique properties. InSe, among group-IIIA metal chalcogenides, exhibits layer dependent physical properties like direct-indirect bandgap transition going from multilayers to monolayer. InSe has high mobility due to low carrier effective mass compared to many 2D materials. These features make them suitable candidates for technological applications. In the literature, a limited number of studies have been made on single-layer InSe growth, mostly based on CVD synthesis. In the present work, InSe CVD growth parameters such as substrate type, deposition and Se temperatures, catalysts type, Ar/H_2 gas flow rate were tried to optimize the synthesis of reproductible large area monolayers. InSe monolayers were synthesized on mica substrates by using In_2O_3 and Se precursor powders under Ar and H_2 gases at low pressures. Firstly, the catalyst salts and pressure were determined to lower the melting point of In_2O_3 to react with Se. Then, the position of Se in the CVD tube and Ar/H_2 gas ratios were optimized to control In_xSe_y phase change. Finally, InSe growth was carried out in a micro-confined environment by stacking two mica substrates and the lateral area of InSe flakes increased from about 15 μm^2 to 200 μm^2. The results showed that the lateral area, thickness and phase of InSe monolayers can be controlled with CVD growth parameters.

Keywords: InSe, CVD, Controlled growth

Acknowledgement: This study has been supported by The Scientific and Technological Research Council of Turkey (TÜBİTAK), grant number 120F234.

SPEAKERS

S1

Laser texturing of AZO layer on ultra-thin glass substrate for flexible solar cells

Demircioğlu, Z.*[1], Nasser, H.[2], Turan, R.[3]

[1] *TÜBİTAK SAGE, TURKEY*
[2] *GUNAM, TURKEY*
[3] *Department of Physics, Middle East Technical University,TURKEY*
**zeynep.demircioglu@tubitak.gov.tr, hisham.nasser@odtugunam.org, turanr@metu.edu.tr*

Thin-film photovoltaic (PV) panels are promising technologies in the PV market due to their low production costs and other advantages such as temperature resistance and diffuse radiation performances. Thin-film photovoltaic panels can be produced on not only rigid substrates but also on flexible substrates. Flexible solar cells have several advantages: flexibility, lightweight, mobility, and easy transport specifications. The scope of the research presented is to study low-temperature deposition and optimization of hydrogenated amorphous silicon (a-Si:H) deposition for flexible solar cells. The aim of this study is to obtain surface texturing on transparent conductive oxide by a novel texture, which is done by direct laser writing. A novel texturing of aluminum-doped zinc oxide (AZO) films is proposed and deposited on flexible substrates for photovoltaic applications. A comparative study of the effects of different laser wavelengths on texturing/patterning of AZO is discussed. Single-junction flexible thin-film solar cell production methods and efficiency enhancements are developed and applied.

Surface texturing studies for the effective use of light in thin film solar cells are studied. A new method, direct laser processing, is developed for surface texturing of the AZO layer. As a result of this study, the texturing is optimized with the laser operated at three different wavelengths. Results of green-laser texture reach haze values as high as 64% and cover the 350nm to 1100 nm spectrum. UV laser texture reaches haze value as high as 55% at 380 nm wavelength. IR texture reaches the haze value as high as 60% at 380 nm wavelength.

S2

A special catadioptric optical system design

Işık, M.B [1,2], Asar, T.[3,4,*]

[1]Turkish Aerospace, Ankara, TÜRKİYE
[2]Gazi University, Graduate School of Natural and Applied Sciences, Advanced Technologies Department, Ankara, TÜRKİYE
[3]Gazi University, Science Faculty, Physics Department, Ankara, TÜRKİYE
[4]Gazi University, Photonics Application and Research Center, Ankara, TÜRKİYE
*trkasar@gazi.edu.tr

Meeting high-altitude surveillance needs is only possible with large-aperture optics, and direct application of optical designs often leads to unacceptably large optical systems. A catadioptric design approach is used for these large aperture requirements [1]. The optical aperture represents catadioptric systems with obstructions of between 20% to 30% of the total circular aperture [2]. In the calculations made accordingly, the chart data below was obtained, and the obscuration rate was accepted as 25%. A metric called the National Image Interpretability Rating Scale (NIIRS) has been developed so that imaging performance requirements are numeric for everyone [3]. NIIRS is a 10-level scale commonly used by intelligence and image analysts to describe image requirements, but also to investigate sensor image quality [4]. The sensors are analyzed for range requirement according to NATO standards separately in and calculated from separate analyzes. There are some parameters that limit the task systems installed on the aircraft. According to the physical limits of the aircraft, the optical design should not have too much weight by adapting.

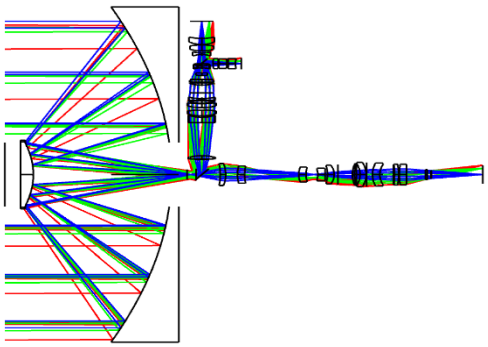

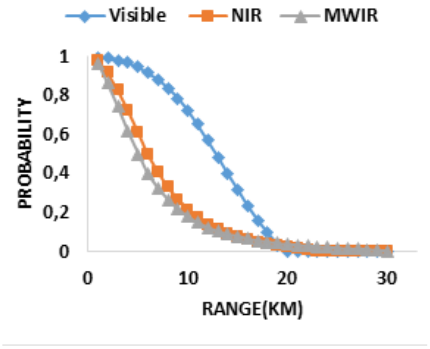

References:

[1] Coughlin, J.F. Introduction to Long Focal Length Catadioptric Systems in Long focal length, high altitude standoff reconnaissance. 1980. SPIE.
[2] Sinclair, R.L. and R.M. Hudyma, Catadioptric zoom lens assemblies. 1999, Google Patents.
[3] Driggers, R.G., M. Kelley, and P.G. Cox. National imagery interpretation rating system (NIIRS) and the probabilities of detection, recognition, and identification. in Infrared Imaging Systems: Design, Analysis, Modeling, and Testing VII. 1996. International Society for Optics and Photonics.
[4] Holst, G.C. Electro-optical imaging system performance. 2008. SPIE-International Society for Optical Engineering.

S3

Modelling a deformable mirror with a liquid crystal display

Mohapi, L.P., Dudley, A.L., Forbes, A.

Affiliation (Physics, University of the Witwatersrand, 1 Jan Smuts Ave, Braamfontein, Johannesburg, 2000, South Africa)
lehloapeter@gmail.com, angela.dudley@wits.ac.za, andrew.forbes@wits.ac.za

Deformable Mirrors are highly topical due to their ability to compensate for phase distortions caused by atmospheric turbulence. Since these devices can handle optical powers in the order of kilowatts, they are well suited for high-power applications ranging from high bandwidth optical communication to spatial profile control in additive manufacturing and other applications that involve high thermal aberration corrections. The number of mirror segments and their geometric structures are vital for beam shaping. Here we use a Liquid Crystal on Silicon Spatial Light Modulator to mimic the mechanical design of a deformable mirror and comparatively analyse the effect of mirror segments number and geometry on structured modes.

S4

Reflection shift characterization of plasmonic core/shell metasurfaces

Zoghi, M.

School of Engineering Science, University of Tehran, 16 Azar, Enqelab Square, Tehran, Iran
maryam.zoghi@ut.ac.ir

A metasurface is composed of two-dimensional subwavelength periodic array. Their functionalities and performance are dominated by the resonant optical plasmonic nanoparticles or high-refractive index dielectric nanoparticles. Metasurfaces are able to modulate the amplitude, phase and polarization of incident light. Reflected light from a surface exhibits a deviation from the rules governed by geometric optics and displaces in directions parallel and perpendicular to plane of incidence. Using generalized sheet transition conditions, we study GH reflection shift in a metasurface composed of spherical core/shell nanoparticles in a square array. A detailed analysis reveals that large reflection shifts are achievable in both visible and ultraviolet ranges due to plasmonic resonance of metallic shell. A comparison of cores with different metal oxides and shells of two noble metals is also carried out to get an inclusive characterization. The results could be useful in sensitive beam deflection measurements like in AFM or reflective UV sensors.

Keywords: Metasurface, Core-Shell Nanoparticles, Reflection Shift, Plasmonics

S5

Effect of Ag doping on structural and optical properties of Co_3O_4 nanoparticles

Muradov, M.B.[1], Mammadyarova, S.J.*[1], Eyvazova, G.M.[1], Balayeva, O.O.[2]

[1] Nanoresearch Laboratory/Baku State University/Baku, Azerbaijan
[2] Department of Chemistry/ Baku State University / Baku, Azerbaijan/
mbmuradov@gmail.com, sevinc.memmedyarova@inbox.ru, eygoncha@gmail.com, ofeliya1989@inbox.ru

Owing to its unique properties Co_3O_4 nanoparticles (NPs) created great interest at various technological applications such as gas sensor, supercapacitor, electrochromic devices, photocatalyst and etc. It is possible to enhance physicochemical properties of nanostructures by doping process with transition or noble metal. In the present work, we have synthesized pure Co_3O_4 and different concentration of silver doped Co_3O_4 NPs ($Ag_xCo_{3-x}O_4$, x=0.02, 0.04, 0.06, 0.1) by sonochemical method and subsequent calcination at 500°C for 4 h. For the synthesis, cobalt nitrate [$Co(NO_3)_2 \cdot 7H_2O$], silver nitrate ($AgNO_3$) and sodium hydroxide (NaOH) were used as precursors. Polyvinyl alcohol was used as a stabilizing agent. In order to determine the size, structure and optical properties, the synthesized nanoparticles were characterized by X-ray diffraction (XRD), ultraviolet-visible (UV–Vis) Spectroscopy. In the XRD pattern of pure Co_3O_4, the low-intensity diffraction peaks were appeared at 2θ=18.91º, 31.25º, 36.84º, 38.56º and 65.19º corresponding to (111), (220), (311), (222) and (440) crystal planes of Co_3O_4. These observed peaks are well assigned to the cubic structure, which matches well with the standard data (JCPDS-09-0418). A gradual shift towards higher angles was observed for the Ag-doped Co_3O_4 NPs and it can be due to the difference between ionic radii of Co^{2+} (0.72 Å) and Ag^+ (1.26 Å). In the XRD pattern of Ag-doped Co_3O_4 NPs, no peaks corresponding to Ag or Ag_2O were observed. The average crystallite size of pure and 2%, 4%, 6%, 10% Ag-doped Co_3O_4 NPs, determined by the Debye Scherrer's formula were 22.55 nm, 17.17 nm, 19.02 nm, 23.03 nm and 17.5 nm, respectively. The reduction in particle size for the doped nanoparticles can be attributed to the internal microstructural strain and local distortion in the Co_3O_4 lattice due to the incorporation of the Ag^+ ions. Because the ionic radii of Ag^+ is higher than the ionic radii of Co^{2+}. The values of d-spacing and lattice constant are small for Ag doped Co_3O_4 NPs compared to undoped NPs. The UV-vis absorption spectra for the undoped and Ag doped Co_3O_4 NPs were recorded in the wavelength range of 200 nm to 900 nm. Undoped Co_3O_4 exhibited two absorption peaks at 469.2 nm and 773.8 nm. The first absorption band can be attributed to the $O^{2-} \rightarrow Co^{2+}$ charge transfer process, while the second band is assigned to the $O^{2-} \rightarrow Co^{3+}$ charge transfer. 2%, 4%, 6%, 10% Ag-doped Co_3O_4 NPs showed absorption peaks 465 nm and 773.6 nm; 466 nm and 780.4 nm; 462.8 nm and 769.4 nm; 448.2 nm and 773.2 nm, respectively.

S6

Presenting the optical properties of liquid crystal/polymer Fibers for potential use as a light modulator

Mamuk, A.E.

Mugla Sitki Kocman University, Department of Physics, Liquid Crystal Laboratory, TR48050, Mugla, Turkey
aemamuk@mu.edu.tr

Liquid crystals are unique materials that possess both the rheological properties of ordinary liquids and molecular order of solid crystals. Because of anisotropy, these materials are pretty sensitive to applied fields such as electric, thermal etc., thus they can be exploited for light-based devices, especially display technology and light modulators. So as to enhance their optical properties, various researches of liquid crystals which are based on doping them with a nano-particles and polymers have been frequently carried out recently. One of effective and inexpensive method of assembling the liquid crystals and polymers is electrospinning which allows generating the phase-separated liquid crystal fibers with sub-micron thickness.

Here, by using single-needle electrospinning technique, electrospun liquid crystal-polymer core-sheath fiber structure which is composed of 4-cyano-4'-hexylbiphenyl (6CB) and polyacrylonitrile as a liquid crystal and a polymer, respectively is reported. 6CB is a room temperature nematic liquid crystal and is widely used in several mixtures for adapting it to light-based devices and is studied in fundamental researches. The polyacrylonitrile is selected as a polymer for this study since it has a mean refractive index very close to that of 6CB at room temperature and so a transparent sheath material can be obtained.

Producing steps, optical characterization, structural and morphological properties of the electrospun liquid crystal fibers are given depending on various spinning voltage. Optical properties which are essentially based on high birefringence difference between 6CB and polyacrylonitrile are presented with analyzing the fibers under polarizing optical microscopy. Moreover, owing to display change in fiber thickness according to producing parameters, and to prove to exhibiting the liquid crystal in the content of fiber, SEM and FT-IR results are shown, respectively. The results indicate that such structures can control the light modulation by adjusting the liquid crystal fibers enabling it useful material in optical devices.

Keywords: Liquid crystals, electrospinning, fiber, optical properties, birefringence

Acknowledgement: The author would like to thank The Center of Research Laboratories incorporated in Mugla Sitki Kocman University for the support on gaining the SEM pictures.

S7

Integrated photonic quantum information processing

Somhorst, F.

Faculty of Science and Technology, University of Twente, Netherland

S8

Teleporting scalably in high dimensions with nonlinear optics

Sephton, B.*[1], Vallés A.[1,2,3], Nape, I.[1], Cox, M.[4], Steinlechner, F.[5,6], Konrad, T.[7,8], Torres, J.P.[3,9], Roux, F.S[11] and Forbes, A[1].

[1]School of Physics, University of the Witwatersrand, Private Bag 3, Wits 2050, South Africa
[2]Molecular Chirality Research Center, Chiba University, 1-33 Yayoi-cho, Inage-ku, Chiba 263- 8522, Japan
[3]ICFO - Institut de Ciencies Fotoniques, The Barcelona Institute of Science and Technology, Castelldefels (Barcelona) 08860, Spain 1 School of Physics, University of the Witwatersrand, Private Bag 3, Wits 2050, South Africa
[4]School of Electrical and Information Engineering, University of the Witwatersrand, Johannesburg, South Africa
[5]Fraunhofer Institute for Applied Optics and Precision Engineering, Albert-Einstein-Str. 7, 07745 Jena, Germany
[6]Friedrich Schiller University Jena, Abbe Center of Photonics, Albert-Einstein-Str. 6, 07745 Jena, Germany
[7]School of Chemistry and Physics, University of KwaZulu-Natal, Durban, South Africa
[8]National Institute of Theoretical and Computational Sciences (NITheCS), KwaZulu-Natal, South Africa
[9]Department of Signal Theory and Communications, Universitat Politecnica de Catalunya, Campus Nord D3, 08034 Barcelona, Spain
[10]National Institute of Theoretical and Computational Sciences (NITheCS), KwaZulu-Natal, South Africa
[11]National Metrology Institute of South Africa, Meiring Naud\'e Road, Brummeria, Pretoria 0040, South Africa
**1585569@students.wits.ac.za*

By exploiting entanglement as a resource, information can be conveyed between two destinations with quantum teleportation. Here, termed the “spookiness” of quantum mechanics, non-locality between an entangled pair of entities allows one to transmit information by employing the entangled pair as a channel between two destinations. Indirect measurements, termed Bell measurements, between one of the entangled entities and a state one desires to transmit then allows the information to be conveyed to the other party, moderated by classical communication. From the fragility of the quantum-mechanical nature being exploited, the technique is largely of interest across a variety of quantum information tasks and forms a salient toolbox from quantum computing to security and quantum networks.

While being demonstrated with continuous, discrete and hybrid approaches in addition to multiple degrees of freedom in a single photon, the highest dimension achieved to date is limited to 3-dimensions. The increased dimensions, however, was achieved with the requirement of an ancillary pair of photons for each increase in dimensionality. Consequently, it comes at the cost of complex, resource intensive experiments which challenges the scalability of the scheme. Here, in lieu of the traditional linear implementation of the entangling step for teleportation, we employ a non -linear approach, allowing us to side-step the scalability issue. We implement a teleportation scheme with photons whereby quantum teleportation is achieved without ancillary

photons and demonstrate teleportation beyond this 3-dimensional mark. Furthermore, we show that on-demand teleportation of spatial states is possible with the freedom that al lows the user to choose the types of spatial modes from orbital angular momentum to the pixel states.

S9

Structuring light for robust optical communication through atmospheric turbulence

Peters, C.R., Klug, A., Forbes, A.

[1]*School of Physics, University of the Witwatersrand, Private Bag 3, Wits 2050, South Africa*
1843828@students.wits.ac.za

Long distance optical communication has long relied on the use of single mode optical fibres to transport information. This method is limited because only one mode may be used thus restricting the rate at which data can be transferred. Conversely, free space propagation can make use of multiple modes, allowing for a much greater rate of data transfer. The main obstacle to overcome in free space optical communication is atmospheric turbulence. The atmosphere undergoes many fluctuations in temperature and pressure which in turn create random fluctuations in the refractive index. This turbulent behaviour can greatly alter any shape of structured light travelling through the atmosphere thus making long range propagation of structured light very difficult for encoding information. Several methods have been put forward to compensate for this including the use of machine learning, adaptive optics for pre- and post-correction and iterative routines. In our approach, we aim to find shapes of light that will remain robust through atmospheric turbulence by treating the atmosphere as a single unitary operator and then calculating the eigenstates (also called eigenmodes) of the operator. The effectiveness of this technique was demonstrated by using a structured light modulator to simulate the effects of atmospheric turbulence. We then compare these effects on both our calculated eigenmode and an eigenmode of free space. Our results show that the calculated eigenmode remains significantly more robust through turbulence than the eigenmode of free space. These results and the ability to calculate the eigenmodes of complex media will be very useful in many fields such as imaging and free space optical communication.

S10

Resolution enhanced ghost imaging using machine learning

Moodley, C. and Forbes, A.

[1]*School of Physics, University of the Witwatersrand, Johannesburg, South Africa*
544489@students.wits.ac.za

Quantum ghost imaging is an alternative imaging technique which utilizes pairs of entangled photons to reconstruct an image. Information from either one of the photons alone does not allow for image reconstruction, rather the image is reconstructed by using the correlations that exist between the photon pair. Interestingly, these photon pairs can be either degenerate or non-degenerate in nature. Due to the scanning nature of spatially resolving detectors, necessary to detect one of the photon pair, and the inherent low light levels of quantum experiments - imaging speeds are inefficient and scale quadratically with the required resolution. To overcome these limitations, we implemented a series of deep learning and machine learning algorithms to achieve early object recognition and to super-resolve the reconstructed image. In applications where object discrimination is important, we achieved a 5x reduction in image acquisition times, recognizing the object and stopping the experiment early while maintaining all necessary object information. While in applications that require a high-resolution image, we super-resolved the images to a resolution 4x greater than the measured resolution, without the lossy aspects that occur with image resampling. This, therefore, leads to faster and more efficient image acquisition times without losing fine details of the image. Our techniques were tested on both degenerate and non-degenerate imaging systems but can extend to many systems that are of quantum nature. We believe that these intelligent algorithms, implemented in ghost imaging, will prove valuable to the community

S11

Spatial mode generation for use in optical fiber

Phala, A.M., Dudley, A. L., Forbes, A.

Affiliation (Department of physics, University of the Witwatersrand, Johannesburg 2000, South Africa.)
2529303@students.wits.ac.za, angela.dudley@wits.ac.za, andrew.forbes@wits.ac.za

Laser beams structured with a uniform flattop profile have become a topic of interest in industrial fields such high-power beam delivery directly to the point of contact for laser cutting, welding and additive manufacturing. These applications require fiber delivery of the optical mode to the point of contact. Here, we generate and tailor a flattop profile using a spatial light modulator. We propagate the flattop into a few mode fiber and compare the Stokes polarimetry measurements before and after the fiber, as well as the modal decomposition of the initial and emerging flattop modes to determine their modal content.

S12

Reflectance properties of GeO_2 films grown on p-Si substrate deposited by magnetron sputtering

Baghdedi, D.[*1,2], Hopoğlu, H.[2,3], Sarıtaş, S.[4], Demir, İ.[3,5], Altuntaş, İ.[3,5], Abdelmoula, N.[1], Gür, E.[6], Şenadım Tüzemen, E.[2,3]

[1]*Laboratory of Multifunctional Materials and Applications (LaMMA), Faculty of Sciences of Sfax, University of Sfax, Tunisia*
[2]*Department of Physics, Sivas Cumhuriyet University, 58140 Sivas, Turkey*
[3]*Nanophotonics Research and Application Center, Sivas Cumhuriyet University, 58140 Sivas, Turkey*
[4]*İspir Hamza Polat Vocatioanal School, Ataturk University, Erzurum, Turkey*
[5]*Department of Nanotechnology Engineering, Sivas Cumhuriyet University, 58140 Sivas, Turkey*
[6]*Department of Physics, Faculty of Science, Ataturk University, 25240 Erzurum, Turkey*
[*]*baghdedidhouha@gmail.com*

GeO_2 thin films were grown by using reactive RF magnetron sputtering method varying thickness and substrate temperature on p-Si substrate. Deposition parameters of the films grown are 8 % O_2, 60 W, rotation 10 rpm. Optical properties of the grown samples were examined by optical spectrophotometer. Reflectance spectra were obtained by spectrophotometer measurements and the effect of thickness and substrate temperature was investigated. It has been observed that as the thickness increases, the total reflectance changes. By using the diffuse reflectance curve, the absorption coefficient and then the energy band gap has been calculated with Kubelka Munk method. It has been observed that the energy band gap varies between 4.0 eV and 4.5 eV. It has been observed that the energy band gap has decreased as the substrate temperature and thickness increase.

Keywords: GeO_2, magnetron sputtering, optical properties

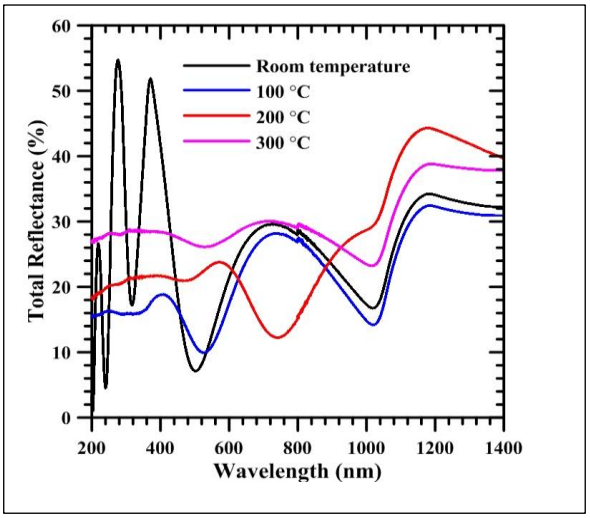

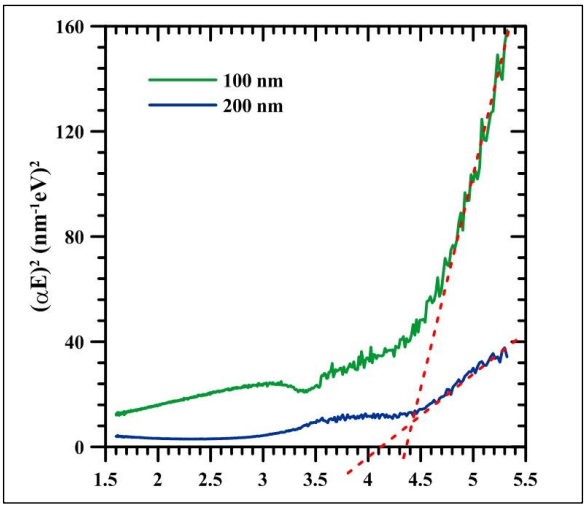

S13

Embedding the skyrmionic topology into the stokes field

Ornelas, P., Singh, K., de Mello Koch, R., Forbes, A.

Affiliation (Physics, University of the Witwatersrand, 1 Jan Smuts Ave, Braamfontein, Johannesburg, 2000, South Africa)
1836488@students.wits.ac.za, 1106433@students.wits.ac.za, robert.demellokoch@gmail.com, andrew.forbes@wits.ac.za

Skyrmions are a class of stable quasi-particles with non-trivial topological structures categorized by integer invariants called skyrme numbers. In terms of field configurations, a skyrmion is formed by the twisting of field lines into links between said field lines where the stability originates from the energy requirement to form or break any of these linkages. It is this topological stability which has made the study of skyrmions appealing in many fields such as condensed matter physics where the stability of so called magnetic skyrmions created on the surface of meta-materials has allowed for the development of new memory storage devices. Although originally formulated in the language of particle physics, the generality of the skyrmion definition allows for the creation of analogous structures in different fields. Here we present a formalism to create the Optical Skyrmion within the Stokes Field. This Optical Skyrmion exists in the plane perpindicular to the direction of propagation, with a characteristic polarization layout which achieves every possible polarization state and where the skyrme number indicates the number of times this structure repeats itself. We employ the use of structured light techniques to create and categorize skyrmions with different skyrme numbers and textures. Furthermore, we show the advantages of using non-diffracting spatial modes to create optical skyrmions. The categorization of these topological vector beams as skyrmion beams allows for a new degree of freedom in vector mode creation which may have intriguing applications in areas such as optical communication and cryptography.

S14

Nonlinear Optics with Structured Light: Modal Selection Rules

Buono, W. T., Forbes, A.

School of Physics, University of the Witwatersrand, Jan Smuts Avenue, Johannesburg, 2000, South Africa.
tavaresbuono@wits.ac.za

Structured light has been a topic of much interest in recent years [1]. The creation and manipulation of these structures are generally wavelength dependent and based on interference (superposition principle). Since very shortly after the invention of the laser, we know it is also possible to do frequency conversion of light via parametric processes. Recently, the focus has been shifted from the efficiency to the spatial structure of this converted light and the rules regarding their spatial modes. In this presentation we revisit recent works that unveil the unintuitive consequences of the superposition principle in wave mixing processes. The selection rules regarding Laguerre-Gaussian, Hermite- Gaussian, Ince-Gaussian and Bessel-Gaussian modes will be presented in processes such as second harmonic generation, sum frequency generation and stimulated parametric down conversion. These rules, however, can be extended to wave mixing processes of higher orders and be simulated using only linear optics [2]. We hope the introduction to these works, including the current gaps and horizons, can inspire new forms of light engineering, especially in exotic wavelengths.

Reference:

[1] Forbes, A., de Oliveira, M. & Dennis, M.R. Structured light. *Nat. Photonics 15*, 253–262 (2021).
[2] Buono W. T., Santos A., Maia M. R., Pereira L. J., Tasca D. S., Dechoum K., Ruchon T., and Khoury A. Z. Chiral relations and radial-angular coupling in nonlinear interactions of optical vortices. Phys. Rev. A 101, 043821 (2020).

S15

Time-resolved SAXS study on nucleation and growth kinetics of PVP stabilized Ag nanoparticles

Bharti, A.*[1], Amenitsch, H.[2], Marmiroli, B.[2], Bernstorff, S.[1]

[1]*Elettra Sincrotrone Trieste, Italy*
[2]*Graz University of Technology, Austria email: amardeep.bharti@elettra.eu,*
**abharti_phy@yahoo.com*

Metal nanoparticles remain the interest of research due to their remarkable applications in photonics, microelectronics, and biotechnology, because of their size and shape dependent localized properties [1,2]. Methods have been developed to precisely tune the morphology of the nanoparticles [3-6]. In the last decade, numerous research activities have been made to understand the nucleation and growth of the nanoparticles [7-9], however, a comprehensive understanding of the effect of surfactant on the nanoparticle's core growth and its relative interaction is still a challenge. Therefore, we investigate the reaction dynamics to better understand the growth kinetics of Ag nanoparticles using variable chain-length surfactant polymers by time-resolved small-angle X-ray scattering at the Austrian-SAXS beamline of Elettra-Sincrotrone Trieste, Italy. In order to probe the pure interaction between the metal-core and the polymer-surfactant, we adopt an external chemical reducing agent free radiation-induced synthesis via water radiolysis [4-6]. In this presentation, we will describe in-depth the step-by-step reaction dynamics and kinetics of the metal nanoparticles. The insight into the mechanism of the reaction of the polymer stabilized Ag nanoparticles will be demonstrated.

Reference:

[1] Wang L., Kafshgari M. H., Meunier M. Optical Properties and Applications of Plasmonic-Metal Nanoparticles, *Adv. Funct. Mater.* 30, 2005400 (2020).
[2] Singh S., Bharti A., Meena V. K. Green synthesis of multi-shaped silver nanoparticles: optical, morphological and antibacterial properties, *J. Mater. Sci.: Mater. Electron.* 26, 3638-3648 (2015).
[3] Bharti A., Bhardwaj R., Goyal N. Anisotropic Plasmonic Effect on Ag Nanoparticles under Microwave- Induced Plasma-in-Liquid: Insight into Growth Mechanism, *Part. Part. Syst. Charact.* 39, 2100220 (2022).
[4] Bharti, A., Agrawal, A. K., Singh, B., Gautam, S. & Goyal, N. Surface plasmon band tailoring of plasmonic nanostructure under the effect of water radiolysis by synchrotron radiation. *J. Synchrotron Rad.* 24, 1209–1217 (2017).
[5] Bharti, A., Bhardwaj, R., Agrawal, A. K., Goyal, N. & Gautam, S. Monochromatic X-ray induced novel synthesis of plasmonic nanostructure for photovoltaic application. *Sci. Rep.* 6, 22394 (2016).
[6] Bharti, A., Chae, K.H. & Goyal, N. Real-time synthesis and detection of plasmonic metal (Au, Ag) nanoparticles under monochromatic X-ray nano-tomography. *Sci Rep* 10, 20877 (2020).

[7] Paulo G. et al., An in situ SAXS investigation of the formation of silver nanoparticles and bimetallic silver– gold nanoparticles in controlled wet-chemical reduction synthesis, *Nanoscale Adv.,* 2, 225 (2020).
[8] Chen X. et al., Simultaneous SAXS/WAXS/UV−Vis Study of the Nucleation and Growth of Nanoparticles: A Test of Classical Nucleation Theory, *Langmuir,* 31, 11678−11691 (2015).
[9] Christopher B. et al., Nanoparticle Formation Kinetics, Mechanisms, and Accurate Rate Constants: Examination of a Second-Generation Ir(0)n Particle Formation System by Five Monitoring Methods Plus Initial Mechanism-Enabled Population Balance Modeling, *J. Phys. Chem. C*, 125, 13449−13476 (2021).

S16

Surface-Enhanced Raman Scattering (SERS) Properties of DLC Films on Au Nanoparticles

Zeynep BAZ

TÜBİTAK Defense Industries Research and Development Institute, Ankara, Turkey
zeynep.baz@tubitak.gov.tr

In this study, DLC (Diamond-Like Carbon) thin films were deposited on glass, Au (gold) Nanoparticles coated substrates by MW ECR (MicroWave Electron Cyclotron Resonance) plasma deposition system at room temperature. The methane (CH_4) gas was used for producing the plasma. Ultraviolet–visible (Uv-Vis) spectroscopy, XRD analysis, Raman spectroscopy, Atomic Force Microscopy (AFM) were performed to characterize films. Au NPs with a size of about 60 nm were obtained in the form of nanospheres and the size is suitable for SERS experiments [1]. SERS properties and EF (Enchancement Factor) of DLC thin films produced on Au coated substrates were calculated.

Keywords: DLC (Diamond-Like Carbon), Surface-Enhanced Raman scattering (SERS)

References:

[1] Campion, A., Kambhampati, P.,1998. Surface-enhanced Raman scattering. Chemical Society Reviews, 27(4): 241-250.

S17

Differential evaluation of normal and cancer breast cell lines by optical methods

Khaksar Jalali, B.*[1,2], Salmani Shik, S.[1,3], Shahi, Sh[2,4]

[1]*Department of physics, Kharazmi University, University Sq., Shahid Beheshti Street, Karaj, Iran*
[2]*Laser and Biophotonics in Biotechnologies Research Center, Isfahan (Khorasgan) branch, Islamic Azad University, University Blvd. Arqavanieh. Jey Street. Isfahan, Iran*
[3]*Applied Sciences Research Center, Kharazmi University, University Sq., Shahid Beheshti Street, Karaj, Iran*
[4]*Department of Biomedical Engineering, Isfahan (Khorasgan) branch, Islamic Azad University, University Blvd. Arqavanieh. Jey Street. Isfahan, Iran*
bahar.khaksar6969@gmail.com, salmani@khu.ac.ir, shahilaser@khuisf.ac.ir

In this study, optical properties of normal and cancer breast cell lines have been reported. Growth and proliferation both normal cell lines (MCF10A) and cancer cell lines (MCF7) are formed on transparent and fresh cell culture, then fixed on sterilized lamellar substrate by paraformaldehyde. Prepared bio-layers are arranged on two optical setups. The absorption coefficient (α) and nonlinear refractive index (n_2) of all normal cell lines (MCF10A) and cancer cell lines (MCF7) samples are measured. Results show that not only the linear absorption coefficient of cancer cells (MCF7) is more than normal cells (MCF10A), but also the magnitude of nonlinear refractive index for cancer cells. But there is a main difference between their sign of nonlinear refractive index. Therefore, considering the obvious difference between normal and cancer cells based on optical behavior and the unique biological-optical characteristics of each cell line, optical technique can be used to evaluate normal and cancer breast cells in future

S18

Growth and laser properties of $Tm^{3+}:KY(WO_4)_2$ crystals

Guretskii, S.A.*[1], Trukhanova, K.L.[1], Kravtsov, A.V.[1], Gorbachenya, K.N.[2], Kisel, V.E.[2], Karpinsky, D.V.[1], Ozen, Y.[3], Erenler, B.[3], Ozcelik, S.[3], Kuleshov, N.V.[2]

[1]*Scientific and Practical Materials Research Center NAS Belarus, P.Brovki st., 19, Minsk, Belarus*
[2]*Center for Optical Materials and Technologies, Belarusian National Technical University, Nezavisimosty Ave., 65, Minsk, Belarus*
[3]*Photonics Application & Research Center, Gazi University, Ankara, Turkey*
crystal2@physics.by

The factors affecting the growth and crystallization of Tm-doped $KY(WO_4)_2$ single crystal are studied; the synthesis parameters used to improve a quality of the single crystals are discussed. The laser properties of the grown $Tm^{3+}:KY(WO_4)_2$ crystals were investigated. A maximum CW output power of about 0.65 W with a slope efficiency of 55 % was obtained at the wavelength of 1940 nm. In a passively Q-switched regime of operation laser pulses with energy of 40 μJ and duration of 10 ns were obtained at a repetition rate of 2.8 kHz at the incident pump power of 2.2 W.

Keywords: potassium yttrium tungstate crystals, phase diagram, metastable zone, controlled growth, absorption and luminescence spectra

S19

A New Three-Dimensional PCB Design

Canyurt, K.[1], Asar T.[2,3,*]

[1]Department of Physics, Graduate School of Natural and Applied Sciences, Gazi University, 06500 Ankara, TÜRKİYE
[2]Department of Physics, Faculty of Science, Gazi University, 06500 Ankara, TÜRKİYE
[3]Photonics Application and Research Center, Gazi University, 06500 Ankara, TÜRKİYE
*trkasar@gazi.edu.tr

The first patent of the Printed Circuit Board (PCB), which means creating an electrical path on an insulated surface and combining circuit elements, was received in England in 1903 by the German inventor Albert Hanson [1]. In the following years, the need for PCBs increased rapidly [1,2].

Generally, PCBs are designed and manufactured as two-dimensional (2D) planar, one or more layers. In this study, three-dimensional (3D) spherical PCB design was used in order to solve the problems of planar 2D design of PCB and to make electronic tools more useful and thus save more space. With the 3D PCB prototypes to be produced in accordance with the design, the wiring harness on electronic devices such as computers will be terminated, and it will be possible to turn any insulating surface on the device into a PCB instead of creating an external board surface. Thus, with this design, it may be possible to say that electronic devices can become more aesthetic, take up less space and consume less electricity.

Reference:

[1] Hamed Shamkhalichenar, Collin J. Bueche and Jin-Woo Choi, “Printed Circuit Board (PCB) Technology for Electrochemical Sensors and Sensing Platforms”, Biosensors, 10, 159 (2020).
[2] Swarup Bhunia, Mark Tehranipoor, “Printed Circuit Board (PCB): Design and Test”, Hardware Security Book, Pages: 81-105 (2019).

S20

The effect of temperature on refractive indices in two high birefringence liquid crystals using the wedge-cell technique

Farezi, N.*[1], Koshsima, H.[2], Zakerhamidi, M.S.[3], Ranjkesh, A.[4], Yoon, T.H.[5]

[1] *Research Institute for Applied Physics and Astronomy, University of Tabriz, Tabriz, Iran*
[2] *Research Institute for Applied Physics and Astronomy, University of Tabriz, Tabriz, Iran*
[3] *Research Institute for Applied Physics and Astronomy, University of Tabriz, Tabriz, Iran*
[4] *Condensed Matter Department, J. Stefan Institute, Jamova 39, Ljubljana, Slovenia*
[5] *Department of Electronic Engineering, Pusan National University, Busan 46241, Republic of Korea*
n_farezi@tabrizu.ac.ir, khoshsima@tabrizu.ac.ir, zakerhamidi@tabrizu.ac.ir,
amid.ranjkesh@ijs.si, *thyoon@pusan.ac.kr*

The effect of temperature on refractive indices for two high birefringence and high clearing temperature liquid crystals (1734A, $T_{NI} = 119$ ℃ and 1791, $T_{NI} = 109$ ℃) was studied experimentally using the thin prism technique. The He- Ne lasers by 632.8 nm lines were used to measure the refractive indices n_o and n_e. A thermometer with a hole drilled in it was used to control the temperature then laser light could pass through it. By using the thin prism technique, we report the variation in refractive indices of these two liquid crystals as a function of temperature. The measured refractive indices were used to calculate the liquid crystals' birefringence. A modified four-parameter model was taken, which is based on Vuk's equation. It describes the effect of temperature on the refractive indices. The modified Vuks equation was also used to fit the variation in refractive indices and birefringence. The results show that the theoretical and experimental values are in good agreement.

S21

Studying the effects of indistinguishable photonic gases on dynamics of multimodal quantum optomechanical systems

Safarinia, N.*[1], Saeidian, S.[2], Asadian, A.[3]

[1]*Department of Physics, Institute for Advanced Studies in Basic Sciences (IASBS), Zanjan 45137-66731, Iran,*
[2]*Department of Physics, Institute for Advanced Studies in Basic Sciences (IASBS), Zanjan 45137-66731, Iran,*
[3]*Department of Physics, Institute for Advanced Studies in Basic Sciences (IASBS), Zanjan 45137-66731, Iran,*
nader_safari@iasbs.ac.ir, saeidian@iasbs.ac.ir, ali.asadian@iasbs.ac.ir

Indistinguishability of objects plays a vital role in natural phenomena. We will explore the effect of indistinguishability on various quantities related to an optomechanical piston. Consider a movable membrane in the middle of a cavity. This membrane which behaves like a 50/50 beam splitter, is exposed to photonic gases with different polarizations. Due to the HOM effect, photon bunching on either side of the cavity occurs in some exceptional cases.

It is easy to observe the signature of photon bunching in different quantities. We present a novel correlation matrix (C_2) to rapidly find the dynamics of any second-order quantity related to this complex multimodal quantum optomechanical system. This method benefits from low memory and computational cost and high efficiency. It also enables us to detect the HOM dip in the second-order correlation function (g^2).

In addition, by extending this closed quantum optomechanical setup to an open system in contact with hot baths, one can easily explore the consequences of breaking PT-Symmetry. We are able to derive the result of the paper, “Observation of PT-symmetric Quantum Interference,” published in the Nature Photonics Journal, only by adding some terms to the differential equation governing C_2.

Finally, we address this question; to what extent does photon distinguishability effects the transfer of energy through this setup, from one side of the cavity to the other? We explore the obstacles on our way to fully detecting the effects of photon bunching on energy transfer.

S22

Simulation of optical coherence tomography in MATLAB by using angular spectrum propagation and Fresnel equations for multilayer samples

Heidary, K.*[1], Ebrahimzadeh, A.[1], Akhlaghi, A. E.[1,2]

[1]Department of Physics, Institute for Advanced Studies in Basic Sciences, P.O. Box 45195-1159, Zanjan, Iran,
[2]Optics Research Center, Institute for Advanced Studies in Basic Sciences, P.O. Box 45137-66731, Zanjan, Iran,
**kamal.heidary@iasbs.ac.ir, e.a.akhlaghi@iasbs.ac.ir*

Optical Coherence Tomography (OCT) is a 3D imaging method based on measuring the interference of a low coherence light source and is widely used for biomedical applications. using numerical methods and simulating OCT and applying the real effects like vibration and dispersion makes it possible to optimize the analyzed OCT signal and improve the analyzing parameters.

In this study, we present a simulation package for generating a virtual laboratory for Fourier domain optical coherence tomography (FD-OCT). We developed an adaptive virtual lab to apply arbitrary samples, errors, and noises and control the features of the light source and the spectrometer as the detector. The package is based on the angular spectrum method for propagating the light and Fresnel equations to calculate reflection and transition fields in MATLAB programing language. Also, the vibration noise and dispersion of the sample can be applied and the entrance angle of the light can be controlled. We simulated and analyzed a single OCT signal from a human eye for a model. We used a gaussian distribution for the beam's intensity and shape of the light source's spectrum. The center wavelength of the light source is considered 850 nanometers with a bandwidth of 40 nanometers. An uncertainty of 50 micrometers for the sample position has been applied and Gaussian noise has been added to the interference signal. Also, the beam reflections into the layers of the sample have been thought up to three times. The model and result of the simulation have been shown in Fig.1. Figure1(a) shows the assumed human eye's model with its layer. The output interference spectrum is demonstrated in Fig.1 (b) and the resulted OCT signal is shown in Fig.1 (c). By determining the point spread function of the system and applying by deconvolution method the improved OCT signal was obtained (Fig1. (d)).

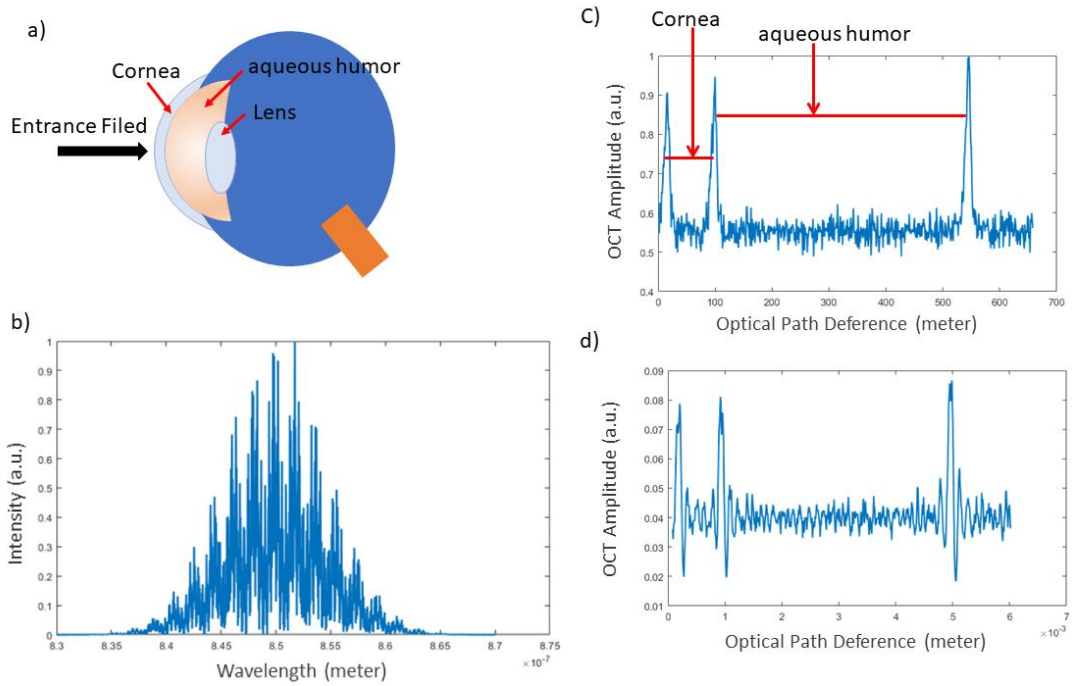

Fig.1: (a) The assumed human eye's model in the simulation; (b) The simulated interference spectrum; (c) The resulting OCT signal; (d) The deconvolved OCT signal.

S23

Using Mirau microscope to nanoscale calibrate piezoelectric actuators

Khanjanji, M.*[1], Jafari Siavashani, M.[2], Ahadi Akhlaghi, E.[1,3]

[1]*Department of Physics, Institute for Advanced Studies in Basic Sciences (IASBS), Zanjan, 45137-66731, Iran.*
[2]*Morteza Jafari Siavashani, Department of Physics, Sharif University of Technology, Azadi Street, Tehran 11365-9161, Iran.*
[3]*Optics Research Center, Institute for Advanced Studies in Basic Sciences (IASBS), Zanjan, 45137-66731, Iran.*
mohammadkhanjani@iasbs.ac.ir, m.siavashani@iasbs.ac.ir, e.a.akhlaghi@iasbs.ac.ir

In the science of measurement, and especially in many microscopic methods, it is necessary and useful to be able to make precise displacements of the nanometer order. A piezoelectric transducer (PZT) is a device that can make nanometer and micrometer displacements based on the amount of potential difference applied to it. However, they suffer from nonlinear behavior (Fig. 1(a)). Strain gauges (SG) are commonly used to determine the real-time length change of a PZT actuator by measuring changes in their electrical resistance. Therefore, a precise system is needed to determine the nonlinear behavior of the output of the SG due to the change in PZT length, and finally to have an accurate linear output of the displacement. For this purpose, we used a Mirau interference microscope to determine the exact PZT length variation (of the nanometer order) so that we could calibrate the output resistance behavior of the SG based on the displacement rate (Fig. 1(b)). By placing a mirror as an object on the PZT, interference intensity changes can be recorded as a function of the PZT length variation. The interferogram analysis results in the phase difference which is directly related to the optical path difference. Therefore, the exact amount of PZT length variation is obtained (Figs. 1(c) and 1(d)). Finally, with the output values of the SG and the PZT length variation, we calibrated the length variations according to the output values of the SG.

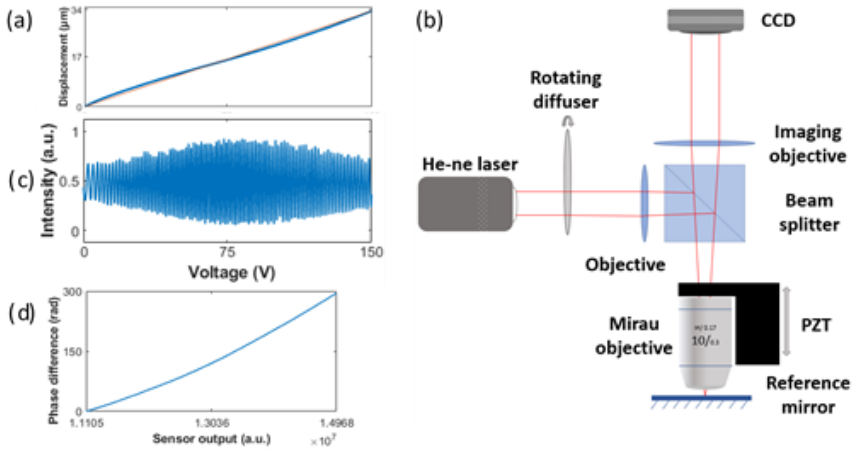

Fig1. (a) Nonlinearity behavior of PZT. (b) Schematic of Mirau interferometer microscope used for scanning displacements (c) Intensity changes based on the increasing potential difference. (d) Phase differences based on sensor output.

S24

Simultaneous thickness and group index measurement of multilayer thin films with spectral-domain optical coherence tomography

Omidi, P.[1], Ebrahimzadeh Kouyakhi, A.[2*], Heydari, K.[2], Akhlaghi, A.E.[2,3]

[1]*Department of Experimental Ophthalmology, Saarland University, Homburg/Saar, Germany*
[2]*Department Physics, Institute for Advanced Studies in Basic Sciences (IASBS), Zanjan, 45137-66731, Iran*
[3]*Optics Research Center, Institute for Advanced Studies in Basic Sciences (IASBS), Zanjan, 45137-66731, Iran*
*pooria.omidi@uks.eu, *aliebrahimzadeh@iasbs.ac.ir, e.a.akhlaghi@iasbs.ac.ir*

Measurement of geometrical thickness and the refractive index (RI) of different samples is always a challenge in research and industry. RI is one of the substantial physical properties that are significant for optical design and metrology. It can be changed by exterior conditions such as electric and magnetic fields, tension, temperature and etc. This gives rise to a variety of methods that can measure these physical quantities with the help of measuring RI. Therefore, measuring RI and physical thickness of various samples such as thin films, glass plates, and living tissues is always consequential. Numerous methods like interferometry, diffractometry, reflectometry, confocal microscopy, and optical coherence tomography (OCT) are developed in order to measure RI and physical thickness. Each of these approaches has a particular resolution and penetration depth that prove superiority for specific applications. However, simultaneous measurement of RI and physical thickness is stealing a challenge in optical metrology [1-3]

In this report, we present a simple and cost-effective method based on spectral-domain optical coherence tomography to determine the group refractive index and the geometrical thickness of multilayer transparent thin films simultaneously. The diversity of this method is the usage of Snell's law and the location of the sample in the setup. The average optical path difference of thin films changes when the sample rotates slightly in the sample arm of the OCT system [4]. The sample rotates about an axis perpendicular to the beam propagation path at specific angles and more information about the sample is obtained. RI and geometrical thickness of each layer can be determined by solving the system of equations on OCT theory.

This method has been used to measure a sample stack of Polydimethylsiloxane polymer (PDMS), SU-8 photoresist and cover glass. Figure 1 shows the data acquisition results from this three-layer sample in which the rotation effect is also demonstrated. In Fig. 1(a) the interference spectrum is shown and in Fig. 1(b) the optical path differences at 0-, 10- and 20-degrees rotations are presented. The results show that the axial resolution in the thickness measurement is about 2 μm, and the uncertainty is in the second decimal place for refractive index values.

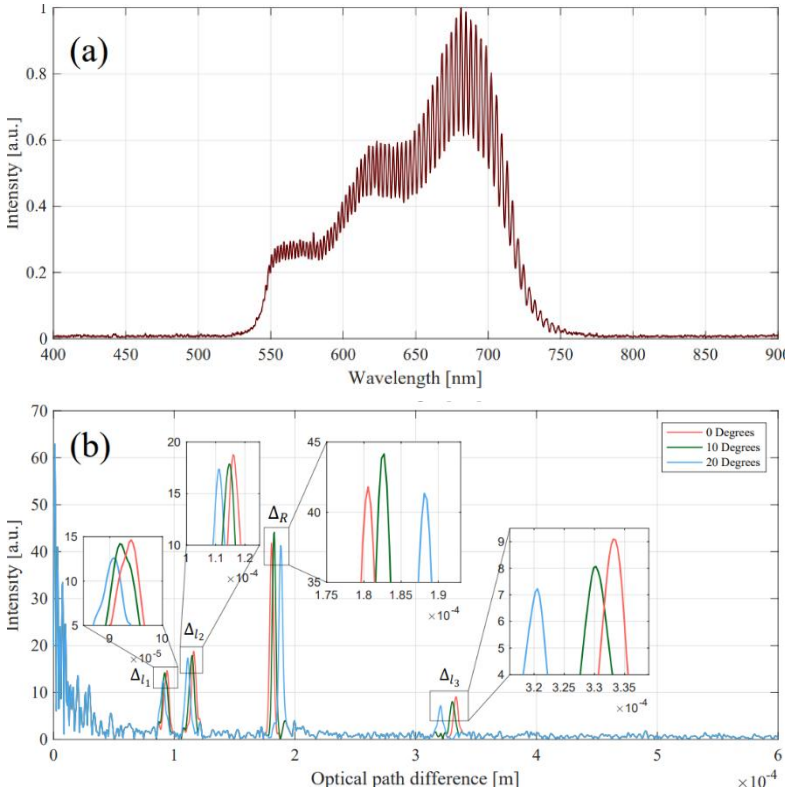

Fig 1. The data acquisition results from this three-layer sample (Polydimethylsiloxane polymer (PDMS), SU-8 photoresist and cover glass) in which the rotation effect is also seen. (a) Interference spectrum obtained from three-layered sample of SU-8 on PDMS on cover glass. (b) Optical path difference obtained in 0, 10 and 20 degrees.

References:

[1] D. Pristinski, V. Kozlovskaya, and S. A. Sukhishvili, “Determination of film thickness and refractive index in one measurement of phase modulated ellipsometry,” JOSA A 23, 2639–2644 (2006).

[2]J. Kattner and H. Hoffmann, “Simultaneous determination of thicknesses and refractive indices of ultrathin films by multiple incidence medium ellipsometry,” The J. Phys. Chem. B 106, 9723–9729 (2002).

[3] F. L. McCrackin, E. Passaglia, R. R. Stromberg, and H. L. Steinberg, “Measurement of the thickness and refractive index of very thin films and the optical properties of surfaces by ellipsometry,” J. Res. Nat. Bur. Sec. A 67 (1963).

[4] Bae, Jaeseok, et al. "Total physical thickness measurement of a multi-layered wafer using a spectral-domain interferometer with an optical comb." *Optics Express* 25.11 (2017): 12689-12697.

S25

Acoustic trapping of large micro-particles

Rameh, M.*[1], Akhlaghi, E.A. [1, 2], Hajizadeh, F.[1]

[1]*Department of Physics, Institute for Advanced Studies in Basic Sciences (IASBS), Zanjan, 45137-66731, Iran.*
[2]*Optics Research Center, Institute for Advanced Studies in Basic Sciences (IASBS), Zanjan, 45137-66731, Iran.*
m.rameh@iasbs.ac.ir, e.a.akhlaghi@iasbs.ac.ir, hajizade@iasbs.ac.ir

The study of living organisms has always been of interest. To this end, trapping and controlling individual organisms of different sizes has received much attention and applications in recent decades. A well-known non-contact method for microscopic manipulation is optical tweezers. However, recent studies have shown that the trapping potential can be expanded by using high-frequency standing sound waves, called acoustic tweezers. Acoustic tweezers are biocompatible and can trap larger particles compared to the optical tweezers while the heat-damaging effect is much less.

In this study, we characterize acoustic traps produced by a homemade acoustic device [1]. The acoustic device contains an aluminum holder with two piezo transducers placed opposite each other to transform acoustic waves inside a liquid chamber under the microscope. The interface of traveling sound waves leads to a standing wave pattern in which particles are confined and trapped in pressure nodal lines. By adjusting the frequency, amplitude, and relative phase difference of two waves, the position of the traps could be shifted or their stiffness can be adjusted. The samples used here are colloidal solutions of polystyrene beads with diameters of 40 μm and 80 μm that were diluted in different mixtures of water and glycerol. “Fig.1” shows acoustic trapping of 40 μm particles at 11 nodal lines. Our results show that by fine-tuning the parameters of traveling waves, the acoustic trapping of desired particles at the desired position could be achieved.

Keywords: optical tweezers, acoustic tweezers, manipulation, micro-particles

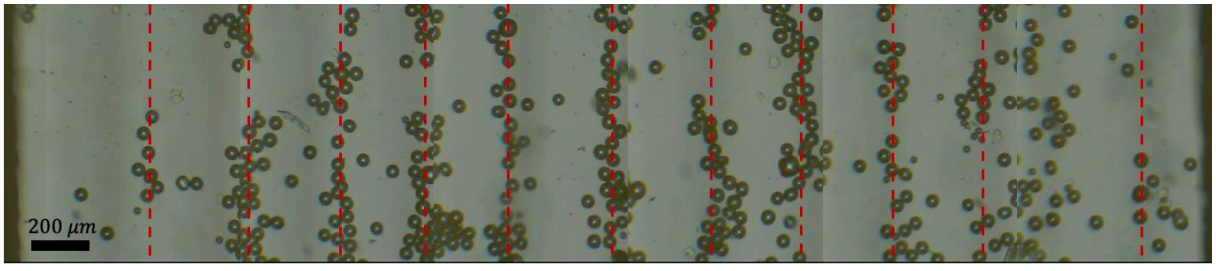

Figure 1. The 40 μm particles are trapped in the nodal lines in acoustic chamber.

References:
[1] Løvmo, M. K., Pressl, B., Thalhammer, G., & Ritsch-Marte, M. (2021). Controlled orientation and sustained rotation of biological samples in a sono-optical microfluidic device. *Lab on a Chip*, *21*(8), 1563-1578.

S26

Fabrication and characterization of ZnO p-n homojunction by spin coating method

Kilic, M.*, Ozdal, T., Kavak, H.

Cukurova University (Cukurova Univ, Dept Phys, TR-01330 Adana, Turkey)
**merhankilic@gmail.com*

Zinc oxide (ZnO) thin films are environmentally friendly and low-cost semiconductors and have various applications. Overall cost of the homostructures they form can also be reduced via economic fabrication methods. ZnO p-n homojunction films can be deposit under normal laboratory conditions on glass substrates by deposition K doped p type ZnO layer on In doped n type ZnO layer via spin coating. However, main problems of the low-cost methods are growth of stable n and p type ZnO films. Moreover, it is still worth applying low-cost spin coating methods due to their efficient thin film growth potential. Herein, we applied one-step spin coating method to prepare ZnO thin films. The structural, morphological, optical and electrical measurements show that n-type ZnO and p-type ZnO thin films were successfully deposited. Although the current of the homojunction device prepared is low, the methods here we apply and the conditions have the potential to fabricate a diode with reasonable rectifying behavior. The current and thus diode properties will increase by improving interfaces by chemical methods and more effective annealing.

References:

[1] Amirhossein Rakhsha, Hossein Abdizadeh, Erfan Pourshaban, Mohammad Reza Golobostanfarda, Maziar Montazerian, Valmor Roberto Mastelar, Controlling the performance of one-dimensional homojunction UVdetectors based on ZnO nanoneedles, Sensors and Actuators A 331 (2021) 112916.
[2] M. Shaheera, K.G. Girija, Manmeet Kaur, V. Geetha, A.K. Debnath, R.K. Vatsa, K. P. Muthe, S.C. Gadkari, Characterization and device application of indium doped ZnO homojunction prepared by RF magnetron sputtering, Optical Materials 101 (2020) 109723.
[3] R. Krithiga, S. Sankar, G. Subhashree, Room temperature diluted magnetism in Li, Na and K co-doped ZnO synthesized by solution combustion method, Superlattices and Microstructures 75 (2014) 621–633.

S27

PbSe quantum-dot doped borosilicate glasses as saturable absorbers

Erenler, B.*[1,2], Özen, Y.[1,3], Karpinsky, D.V[4] and Özçelik S.[1,2]

[1]*Photonics Application and Research Center, Gazi University, 06500 Ankara, Turkey,*
[2]*Department of Photonics, Gazi University 06500, Ankara,*
[3]*Department of Physics, Gazi University 06500, Ankara, Turkey,*
[4]*Scientific and Practical Materials Research Center NAS Belarus, P.Brovki st., 19, Minsk, Belarus*
**berkcan.erenler@gazi.edu.tr; yozen@gazi.edu.tr; crystal2@physics.by, sozcelik@gazi.edu.tr*

Glasses doped with PbSe quantum dots (QDs) have received increasing attention recently owing to their large Bohr radii and broadband near-infrared (NIR) emission. Due to the quantum confinement effect, the photoluminescence (PL) of PbSe QDs spans the entire NIR range depending on quantum dot size [1-3]. The result of stable and tunable emission of PbSe quantum dots makes them excellent candidates for applications in telecommunications, biological imaging and solar cells [4]. In this study, QDs doped glasses were produced by sol-gel method in many stages. The produced PbSe QDs doped borosilicate glasses were characterized by x-ray diffraction (XRD) and Photoluminescence spectroscopy. The optical and structural properties of that doped glasses were investigated. It was determined that the films were the diffraction peaks observed in the orientation of (200) from the XRD pattern. In the results obtained from photoluminescence spectroscopy, a peak was obtained at a wavelength of 1.4 μm and the width of the PL band was found to be around 100 nm.

Acknowledgements:
This work was supported by the Presidency of Strategy and Budget (Turkey) under project numbers of 2019K12-149045 and it is performed in the framework of the bilateral project supported by NAS of Belarus and Tubitak (project number 120N014) and RFBR (grant # F21MS-035).

Reference:

[1] C. Cheng, N.S. Hu, X.Y. Cheng, Experimental realization of a PbSe quantum dot doped fiber amplifier with ultra-bandwidth characteristic, Opt. Commun. 382 (2017) 470e476.
[2] S.D. Park, D. Baranov, J. Ryu, B. Cho, A. Halder, S. Seifert, S. Vajda, D.M. Jonas, Bandgap inhomogeneity of a PbSe quantum dot ensemble from twodimensional spectroscopy and comparison to size inhomogeneity from electron microscopy, Nano Lett. 17 (2) (2017) 762e771.
[3] C. Cheng, F. Yuan, X.Y. Cheng, Study of an unsaturated PbSe QD-doped fiber laser by numerical simulation and experiment, IEEE J. Quantum Elect. 50 (11) (2014) 882e889.
[4] Tan, T. T., Selvan, S. T., Zhao, L., Gao, S., & Ying, J. Y. (2007). Size control, shape evolution, and silica coating of near-infrared-emitting PbSe quantum dots. Chemistry of Materials, 19(13), 3112-3117.

S28

Developing interdigital electrodes for electro-optical applications with aerosol jet printing technique

Serbest, B.*[1,2], Poyraz, M.E. [1,2], Balcı, E.[1,3], Ataşer, T.[1], Sönmez, Akın N.[1,2], Özçelik S.[1,2]

[1]Gazi University, Photonics Application and Research Center, Ankara, Turkey
[2]Gazi University, Department of Photonics, Faculty of Applied Sciences, Ankara, Turkey
[3]Hacı Bayram Veli University, Department of Physics, Faculty of Science and Letters, Ankara, Turkey
**berkserbest@gmail.com*

Aerosol Jet Printing (AJP) is emerging technology for manufacturing printed electronics due to its high process speed, and low material consumption. In addition, this technique is not require vacuum and masking [1-3]. Moreover, this technique allows to printing lines or curves with different inks on various substrates. Gold, silver, copper, polyamide, UV acrylics, organic semiconductors, enzymes and proteins can be selected to main substance of inks for developing different applications, including; active and passive electronic components, actuators, sensors with this technique. Process parameters like sheath gas flow, atomizer flow, ink temperature and printing speed affect the printing quality. Therefore, system must be optimized for printing high electrical conductive electrodes [4-5]. Width, thickness and geometry of interdigital electrodes highly affect the device efficiency. For example, to product high efficiency solar panel needs to qualified metallization process and this technique could allow this [6]. In this study, interdigital electrodes in different geometry were developed and printed on various substrates. Electrodes were printed through ultrasonic atomizer header to flexible (Polyimide, PET) and non-flexible (Si, Ge and glass) substrates. The widths, thicknesses and electrical resistances of these printed electrodes were measured and compared with each other. The range of physical measurement of the printed electrodes was measured as 15-80 μm for line width, 1-2 μm for thickness and 0.5-0.9 ohm for electrical resistance.

Acknowledgements:
This work was supported by SBB (TR) under the project numbers of 2016K121220.

References:
[1] Secor, Ethan B. "Principles of aerosol jet printing." Flexible and Printed Electronics 3.3 035002, 2018.
Agarwala, Shweta, Guo Liang Goh, and Wai Yee Yeong. "Optimizing aerosol jet printing process of silver ink for printed electronics." IOP Conference Series: Materials Science and Engineering. Vol. 191. No. 1. IOP Publishing, 2017.
[2] Gupta, Anubha A., et al. "Aerosol Jet Printing for printed electronics rapid prototyping." 2016 IEEE International Symposium on Circuits and systems (ISCAS). IEEE, 2016.
[3] Skarżyński, Kacper, et al. "Highly conductive electronics circuits from aerosol jet printed silver inks." Scientific Reports 11.1, 2021.

[4] Salary, Roozbeh Ross, et al. "A state-of-the-art review on aerosol jet printing (AJP) additive manufacturing process." International Manufacturing Science and Engineering Conference. Vol. 58745. American Society of Mechanical Engineers, 2019.
[5] A. Mette, P. L. Richter, M Hörteis, S. W. Glunz, “Metal Aerosol Jet Printing for Solar Cell Metallization”, Progress In Photovoltaics, 15, 621-627, 2007.

S29

Acousto-optic control of a laser beam profile in a DIRCM laser laboratory setup

Keskin, M.Z.*[1,2], Figen, Z.G.[2] and Özdür, İ.T.[1]

[1]*Department of Electrical and Electronics Engineering, TOBB University of Economics and Technology, 06560, Söğütözü, Ankara, TURKEY*
[2]*TÜBİTAK BİLGEM/İLTAREN, Şehit Yzb. İlhan Tan Kışlası, 06800, Ümitköy, Ankara, TURKEY*
**mehmetziyakeskin@etu.edu.tr, ziya.keskin@tubitak.gov.tr*

Directed Infrared Counter Measure (DIRCM) systems are utilized on air and other platforms for countermeasuring infrared (IR) heat-seeking missiles. DIRCM laser laboratory setups are used to mimic the DIRCM system and seeker engagement scenarios in isolated laboratory environments. Typically, in these setups, the output beam of a mid-infrared (Mid-IR) laser source is modulated in time using an acousto-optic modulator (AOM), which usually does not change the initial beam profile. Following the AOM in the optical path, within a distance of few meters, the laser beam is expanded and collimated using optics to have almost a uniform intensity profile at the target aperture. The whole process results in the simulation of the engagement of a countermeasure laser with an IR heat-seeking missile on an optical table. In order to expand and collimate the output laser beam, large aperture parabolic mirrors, aspheric or diffractive optical systems are often employed [1]. AOM devices, together with their common usage of modulation in time, can also be used to transform a given laser beam profile into various other beam profiles [2]. As distinct from using bulk optics for shaping the laser beam, an AOM device uses radio frequency (RF) signal. Normally, a single frequency RF signal exciting the medium creates the moving sinusoidal gratings, resulting in the diffraction of the laser into a single order. However, when the RF signal consists of multiple frequency components, diffraction occurs into multiple orders and various beam profiles can be obtained at the output. Usually, this method performs well in short distances and for output beam widths that are close to input ones. In this study, we analyze the usage of an AOM device in order to have an expanded beam profile (with a beam diameter of minimum 30mm) having a uniform intensity distribution at few meters away from the laser source. With the use of an AOM device for beam shaping, we aim to alleviate the need of costly and complex optical setups. The analysis is made in two dimensions using a numerical simulation software, which employs the finite element method with appropriate boundary conditions.

References:

[1] A. Başaran and Z.G. Figen, Proc. SPIE 11161, Technologies for Optical Countermeasures XVI, 111610M (2019).
[2] S. N. Antonov and A. L. Filatov, Technical Physics, Vol. 63 (2018).

S30

Sapphire single crystal growth with kyropoulos technique

Korkmaz, B.[1,2,*], Gümrükçü, A.E.[1], Akpınar, Ö.[1,3], İdare, B.[1,2], Akın Sönmez, N.[1,2], Özçelik, S.[1,2]

[1]Gazi University, Photonics Application and Research Center, Ankara, Turkey
[2]Gazi University, Faculty of Applied Science, Department of Photonics, Ankara, Turkey
[3]Gazi University, Faculty of Science, Department of Physics, Ankara, Turkey
**burakkorkmaztr@gmail.com*

Sapphire crystal has high hardness, very good tensile strength, thermal conductivity, electrical insulation, abrasion resistance and thermal shock resistance. Its excellent chemical, optical and mechanical properties make it a suitable substrate material for LED, HEMT, FET applications. Sapphire is an oxide crystal with a high melting temperature at 2050 C. Sapphire has a high refractive index covering the UV, visible and IR regions. It also has a transmittance of 0.14 - 6.0 μm wide. Alumina (Al_2O_3) raw material can be used as powder, broken crystal, and polycrystalline ingot to grow sapphire crystal. To produce sapphire crystal to be used in optical systems, Alumina raw material must be of high purity (≥99.996%) and high density. The Kyropoulos technique has been preferred because it has been designed to produce high quality large sized bulk crystals with low dislocation density. In this study, sapphire crystals weighing 100 kg and 33 kg were grown successfully with this technique. Thereafter, that crystals were drilled on C-plane and sliced 4.5 mm thick. The structural, optical, and mechanical properties of this part were examined. The structural properties of these parts were examined with the HR-XRD system, their optical properties with UV-Vis Spectrometer and FTIR Spectrometer, and their mechanical properties with a hardness tester. As a result, the properties of the produced crystals were found to be compatible with the literature.

Acknowledgements:
This work was supported by SBB (TR) under the project numbers of 2016K121220.

S31

Improving power conversion efficiency by Light-Assisted annealing of triple cation perovskite layer in solar cell applications

Turgut, S.B., Gultekin, B.

Solar Energy Institute, Ege University, 35100, Izmir/Turkey

Perovskite solar cells (PSCs) have achieved significant lab-scale efficiencies raised from 3.8% to 25.5% in the last decade. Perovskite film quality, morphology, and crystallinity are deeply dependent to the annealing type, temperature and time. Here, a light-assisted annealing (LA) method have chosen for the formation of relatively larger and uniform grains of triple perovskite crystals with less nano-cracks in a custom designed LA system with a halogen lamb. This method has the potential to reduce the annealing process time and energy consumption for mass production of perovskite solar cells (PSCs) instead of conventional thermal annealing method. In this study, a series of perovskite films are prepared by LA method with various annealing time (1, 3, 5, 10, 15 min) to determine the optimum conditions. In order to investigate the effect of the LA process on the structure and morphology of perovskite crystals, X-ray diffraction (XRD), atomic force microscopy (AFM), scanning electron microscopy (SEM), and UV–Vis absorption spectroscopy techniques have been carried out. According to the photovoltaic characterization results, power conversion efficiency (PCE) of 17.86 % is achieved with a LA device annealed for 5 min (5-min-LA), while that of 16.74% is obtained with the standard device annealed on a hotplate for 60 min (60-min-TA).

S32

Dependence of the optical properties of composites based on GO/PVA on the annealing temperature and filler concentration

Baghirov, M.A.*, Muradov, M.B., Mammadyarova, S.J., Eyvazova, G.M.

Nanoresearch Laboratory/Baku State University/Baku, Azerbaijan/
bmbaghir@gmail.com, mbmuradov@gmail.com, sevinc.memmedyarova@inbox.ru, eygoncha@gmail.com

Recently, extensive research has been conducted on the development of graphene oxide (GO), GO-based materials and new types of composites based on them. These types of materials have a wide range of applications in various industry fields. They are used in energy storage devices, in the development of supercapacitors, in creating various types of sensors, in the process of photocatalysis, and etc. Such kind of materials have a wide range of applications. The ability to manage their physical properties through modification allows them to expand their application area. Thus, depending on the degree of reduction, it is possible to control the band gap of GO in the range of 0.02-2.2 eV. One of the most widely used materials is GO/PVA-based composites. These types of composites are perspective materials in the manufacture of supercapacitor batteries. Therefore, the stability of these materials to various influences, the dependence of their optical, electrical and other properties on the temperature is of great interest.

In this study, GO was obtained by Hummer's method. The obtained sample was filtered through filter paper, washed several times with HCl (30%) and distilled water. GO dried at room temperature and then was added to distilled water. The solution was exposed to ultrasound for 1 hour and then centrifuged. The precipitation was dried at room temperature. GO with different concentrations (1%, 2%, 3%, and 5%) was mixed with PVA and dried at room temperature. The obtained GO/PVA-based composite was subjected to thermal treatment at different temperatures (25ºC, 40ºC, 70ºC and 110ºC). Absorption and transmission spectra of samples were recorded with the Specord 250 Plus device in the wavelength range of 190 nm-1100 nm. According to Tauc's law, graphs were plotted and the temperature and concentration dependence of the band gap (Eg) was determined. The band gap value of the samples decreases with the increasing annealing temperature of samples. When samples are annealed at 110 ºC, the change in the band gap for a GO with a 3% concentration is 0.15 eV, whereas for a GO with a 5% concentration is 0.5 eV. Most likely, this is due to changes in particle size as a result of coalescence processes. An increase in concentration to 3% initially increases the value of the band gap (2.55 eV). The next increase in the concentration of GO nanoparticles (5%) leads to a decrease in the band gap (1.80 eV). This is due to a decrease in the distance between the particles and an increase in the probability of aggregation processes.

S33

Encoding information into the classical non-separability of light

Singh, K.*[1], Nape, I.[1,2], Dudley, A.[1], Forbes, A.[1]

[1]School of Physics, University of the Witwatersrand, Private Bag 3, Johannesburg 2050, South Africa
[2]Department of Physics, University of Ottawa, Advanced Research Complex, 25 Templeton, Ottawa, Ontario, Canada K1N 6N5
**keshaanSingh@gmail.com*

Vector states of light have non-separable spatial and polarization degrees-of-freedom. This intriguing property can be quantified and is invariant to general unitary transformations, most notably pure phase aberrations such as those induced by propagation through atmospheric turbulence. Free space communication using structured light aims to increase data transfer rates by encoding simultaneous signals in superpositions of spatial modes which carry independent data streams. The efficacy of these systems is severely impeded by atmospheric turbulence due to the induced modal crosstalk. We propose a method of encoding information into a basis formed by the discretized non-separability of classical vector beams. We show how the discretization into n elements will results in the ability to encode d = ln(n)/ ln(2) simultaneous data streams. We demonstrate the effectiveness of the proposed idea in a dynamic experiment while highlighting the benefits and limitations. We believe this will be of interest to the optical communication community.

S34

Low symmetry photonic crystal cavity phase properties

Oguz, H.*[1], Karakılınç, Ö. Ö.[2], Adak, M.[1], Berberoğlu, H.[3],Ozdemir Kart, S.[1]

*[1]*Department of Physics, Pamukkale University, Denizli, Turkey.*
[2]*Department of Electrical-Electronics Engineering, Pamukkale University, Denizli, Turkey.*
[3]*Department of Physics, Hacı Bayram Veli University, Ankara, Turkey.*
hasanoguz@gmail.com, okarakilinc@pau.edu.tr, madak@pau.edu.tr,
halil.berberoglu@hbv.edu.tr, ozsev@pau.edu.tr.

In this study, phase shift properties of a photonic crystal (PhC) waveguide with a low symmetry cavity structure that exhibits ultra slow light characteristic modes are investigated. Phase shift behavior is explored semi-analytically by applying harmonic inversion with filter diagonalization method to the contemporary coupled-mode theory. It is well known that low group velocity PhC waveguide structures have great potentials for fine-tuning phase characteristics which can be easily controlled by structural parameters without adding length to any given structure. Thus, we have observed from our simulations based on Finite Difference Time Domain (FDTD) method that low symmetry coupled cavity structure may yield an opportunity for engineering of precise phase properties depending on the number of cavities, the distance between them, cavity and auxiliary radii, and the angle of auxiliary rods. We focus on band gap guided modes matching with resonant modes of cavity in our calculations. Therefore we are aimed to investigate the effects of the structural parameters of cavity and auxiliary rods on the phase characteristics for the modes chosen. In conclusion, we show that PhC structure may have well defined phase behavior by fine tuning the parameters of cavity and auxiliary rods.

S35

The study of diffraction polarization of fork grating printed on dye-doped liquid crystal cell

Soleimani, P*[1,2], Khoshsima, H[1,2], Yeganeh, M[3]

[1]*Research Institute for Applied Physics and Astronomy, University of Tabriz, Tabriz, Iran*
[2]*Faculty of Physics, University of Tabriz, Tabriz, Iran*
[3]*Department of Physics, Institute for Advanced Studies in Basic Sciences (IASBS), Zanjan, Iran*
p_soleimani@tabrizu.ac.ir, khoshsima@tabrizu.ac.ir, moyeganeh@iasbs.ac.ir

We proposed a dye-doped liquid crystal (DDLC) planar cell which is printed onto its fork grating. Based on experimental evidence, it is used for designed polarization gratings. Furthermore, it can be generated by planar cells without any external voltage, nor even an external magnetic field. however, it characterizes the transmitted field of polarization. The far-field diffraction properties of the m_th order of polarized fork grating are studied at a 194cm distance. It is capable of producing a selective number of diffraction orders with linearly polarized light. It plays an essential role in many optical systems to generate and detect polarized light in a controlled technical. There are some cases in which different states of polarization need to be controlled with polarization state generators. when it is illuminated with an arbitrary state of polarization, except zeroth diffraction, the output beam has linear polarization. Finally, we use a planar DDLC cell to generate the polarized fork gratings.

S36

Wavelength depending measurements of the optical anisotropic properties of 5CB liquid crystal

Özden, Pınar

Mugla Sitki Kocman University, Department of Physics, Mugla, Turkey
pozden@mu.edu.tr

Liquid crystals (LCs) are intermediate state of matter which exhibit both rheologic behavior likewise isotropic liquids and molecular order likewise solid crystals at specific temperature interval. This temperature interval is specified as mesophase range. Depending on molecular shape and compound, LCs take place in various mesophases. There is a mesophase, which is named as nematic (N), that shows a weak orientational molecular order. The molecules which are rod-like shape line up along a direction on average. Since the LCs give good response to external stimuli e.g. electric field, they can make a large application such as display, bio-sensor, gas sensor technologies etc.

The members of 4-n-alkyl-cyanobiphenyl (nCB) liquid crystal homologous series are quite important materials for both fundamental science and display technology owing to working capabilities of some members at room temperature. 4-Cyano-4'-pentylbiphenyl (5CB), which is a nematic LC and the member of nCB homologues, has five carbon atoms in its alkyl chain and its mesophase range involves at temperatures between 24.0 and 35.3 ^{o}C.

In this study, some thermo-physical properties of 5CB are investigated into depending on the wavelength of applied light. The temperature features of average refractive index, ordinary refractive index and extraordinary index are presented. Moreover, the change in birefringence and anisotropic polarization parameters depending on temperature, which can be acquired from anisotropic refractive indices, are measured under 465 nm, 525 nm and 625 nm wavelength lights. In addition, the thermo-morphological properties of 5CB are examined by presenting textures obtained under polarizing microscope.

S37

Investigation of optical characteristics of In_2S_3 thin films by spectroscopic ellipsometry and spectrophotometry methods

Staskov, N.I.[1], Gremenok, V.F.[2], Chudakov, E. A.[1]*, Akcay, N.[3,4] and Ozcelik, S.[3,5]

[1]A.A. Kuleshov Mogilev State University, 212022, Mogilev, Kosmonavtov str. 1, Republic of Belarus
[2]State Scientific and Production Association "Scientific-Practical Materials Research Centre of the National Academy of Sciences of Belarus", 220072, Minsk, P. Brovka str. 19, Republic of Belarus
[3]Gazi University, Photonics Application & Research Centre, 06500, Ankara, Turkey
[4]Department of Mechanical Engineering, Faculty of Engineering, Baskent University, 06790, Ankara, Turkey,
[5]Department of Photonics, Faculty of Applied Sciences, Gazi University, 06500, Ankara, Turkey
ni_staskov@mail.ru, gremenok@physics.by, neslihanakcay@baskent.edu.tr, sozcelik@gazi.edu.tr

In_2S_3 films (d_f~100 nm) were deposited on soda-lime glass (SLG) substrates (D=1.2 mm) by RF magnetron sputtering method at 150°C and annealed at 350°C and 450°C. The optical properties of the films were studied by spectroscopic ellipsometry (SE, UVISEL2 HORIBA, θ=60°, 65°, 70°), transmission spectrophotometry (T, θ=0°, Perkin Elmer Lambda 2S UV-Vis), reflection spectrophotometry R and T (SRT, θ=10°, PHOTON RT, EssentOptics, Belarus). The film characteristics d_f, n_f, k_f and E_g were calculated using the DeltaPsi2 program for SE using the parameters of the Tauc-Lorenz (TL) dispersion formula with one oscillator. This formula ensured the agreement between the calculated and measured SE spectra when using the three-layer model of films with Bruggeman layers. We took into account the absorption of light by the substrate in the region from 345 nm to 850 nm (E_{gs}=(3.60±0.02) eV). From T (θ=0°) k_{fT} was calculated. For this we used d_f and n_f from SE. The absorption coefficients α_f and α_{fT} were determined from k_f and k_{fT}. To calculate α_{fRT} using the formula from [1], SRT (θ=10°) and d_f (SE) were used. The spectra of k_{fRT} were calculated from the α_{fRT} spectra. The k_{fT} and k_{fRT} spectra have minima whose wavelength decreases with increasing temperature. E_g of the films can be determined by the Tauc formula only for m=0.5. The value of d_f is independent of the film annealing temperature. With an increase in the annealing temperature, E_g increases from 1.81 eV to 2.03 eV and the refractive indices increase from 2.307 to 2.423 (λ = 632.8 nm). Based on the Lorentz-Lorentz formula, the increase in the refractive index was explained by an increase in the density of the films. We assume that the supramolecular structure of the films is amorphous-crystalline with a low content of the crystalline part. An increase in n in the transparency region of the films with an increase in the annealing temperature is due to an increase in the density in the amorphous part of the films.

Acknowledgments:
This work was financially supported by the State Program of Scientific Research of the Republic of Belarus 1.15 "Photonics and Electronics for Innovations", this work was

supported by the Belarusian State Programme for Research «Physical Material Science, New Materials and Technologies» and TUBITAK with the grant № 118F009.

References:

[1] W.Q. Hong, Extraction of extinction coefficient of weak absorbing thin films from special absorption, J. Phys. D: Appl. Phys. 22 (1989) 1384-1385.

S38

Ti doped sapphire crystal growth

Akpinar, O.*[1,2], Gumrukcu, A.E.[1], Korkmaz, B.[1,3], Akin Sonmez, N.[1,3], Ozturk, M.K.[1,2], Özçelik, S.[1,3]

[1]Gazi University, Photonics Research and Application Center, Ankara, Turkey
[2]Gazi University, Faculty of Science, Department of Physics, Ankara, Turkey
[3]Gazi University, Faculty of Applied Science, Department of Photonics, Ankara, Turkey
**omerakpinar9@gmail.com*

The single Crystal growth process with titanium (Ti) doped sapphire bulk crystal was carried out with the Kyropoulos (KY) technique in the Photonics Application and Research Center. The stages of this grown crystal are given in detail below:
After cleaning the insulation materials, 15 kg of alumina (Al_2O_3) and 30 gr Ti consumables were loaded into the molybdenum (Mo) crucible. After loading, the guide was attached to the Crystal molybdenum holder. After the cover part was closed, the inside of the system was placed under vacuum. In order to start the crystal growth process, the targeted power value was gradually increased to realize the melting phase. Before the first contact of the guide crystal with the melt, the melt surface condition was checked. After the conditions were met, the seeding stage was started. In order to establish a thermodynamic equilibrium between the melt surface and the guide crystal, the guide crystal was gradually lowered onto the melt surface. At a given moment, the solid was brought into contact with the liquid. In order to minimize defects caused by thermal shock caused by solid-to-liquid contact, a neck region of approximately 10 cm in length was obtained under high tensile speed. Optimal adjustments after the neck stage resulted in a voluminous single Crystal with a fixed body diameter of 13 cm and a body length of 35 cm.

Acknowledgements:
This work was supported by SBB (TR) under the project numbers of 2016K121220.

S39

Evaluation of optical properties of hexagonal and circular solid core photonic crystal fibers for various structural design parameters

Yuksel, Z. M.[*1], Berberoğlu, H.[2], Ozdemir Kart, S.[1], Karakılınç, Ö. Ö.[3], Adak, M.[1]

[*1]*Department of Physics, Pamukkale University, Denizli, Turkey.*
[2]Department of Physics, Ankara Hacı Bayram Veli University, Ankara, Turkey.
[3]*Department of Electrical-Electronics Engineering, Pamukkale University, Denizli, Turkey.*
zekeriyamehmet.yuksel@gmail.com, halil.berberoglu@hbv.edu.tr*, ozsev@pau.edu.tr, okarakilinc@pau.edu.tr, madak@pau.edu.tr.*

Photonic crystal fibers (PCFs) have periodic optical structures in the wavelength scale which enable unprecedented control over the propagation of light. Light propagation in PCFs with a lower refractive index due to air holes in the cladding region is far superior to that in conventional fibers. In this study, the structural and optical properties of fused silica-based index guided solid core IG-PCF (Part No: NL-2.3-790-02) produced by NKT photonics [1] have been characterized by the computational methods. The cladding of this PCF is originally designed in the form of a hexagonal structure with six rings around the core radius of only 2.4 microns (PCF-1). Moreover, we designed PCF with the same structure except it has a circular shape instead of hexagonal (PCF-2). These PCFs are designated by some structural parameters, namely pitch which is the distance between the neighboring air holes (Λ), the diameter of the circular air holes (d), the side of hexagonal holes (S) and the diameter of the solid core (Dc) as shown in Figure 1. We have solved the electromagnetic Maxwell's equations as a function of frequency on the cross-sectional mesh of the fiber by utilizing the Finite-Difference Eigenmode (FDE) solver as implemented in Lumerical Mode Solutions software [2] to identify the structural and optical properties of our proposed PCFs. After the effective index neff and mode profiles of the structure are revealed from the simulations in the frequency domain, we have predicted some optical properties, such as zero-dispersion wavelength, nonlinear coefficient, effective nonlinear area for different structural parameters. It can be reported that as the structural parameters of both PCF structures decreases, zero-dispersion wavelength, and effective nonlinear area reduces, while the nonlinear coefficient increases.

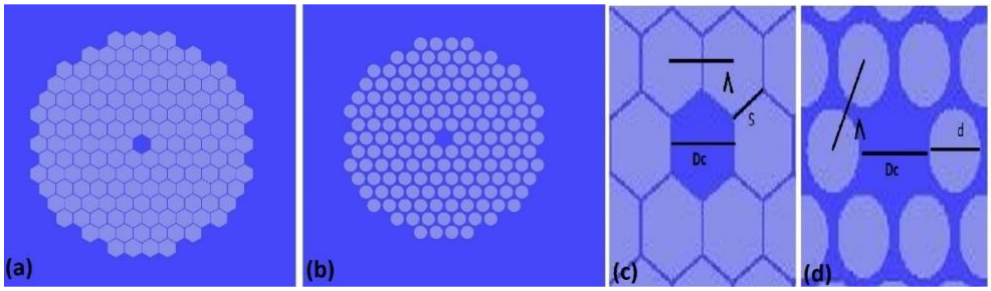

Fig. 1. Schematic cross-sectional view of (a) PCF-1 and (b) PCF-2. Structure parameters of (c) PCF-1 and (d) PCF-2.

Reference:

[1] https://www.nktphotonics.com/
[2] https://www.lumerical.com/products/mode

S40

Future trends of EO/IR systems for airborne ISR systems

Artan, Göktuğ Gencehan

Teops, Arp Kule Business Center, Ankara, Turkey
goktug@teops.com.tr

Rapid developments in infrared (IR) and electro-optical (EO) systems are crucial to further enhance the intelligence, surveillance, and reconnaissance (ISR) capabilities of platforms. The operational conditions of these platforms are getting harsher each day and new technologies must be adapted into these EO/IR systems swiftly to keep up with these challenges. While the performance requirements are increasing, the size, weight, and power (SWaP) constraints are becoming more stringent, especially in airborne platforms such as UAVs. Land systems and naval platforms don't typically use EO/IR systems for the purpose of ISR, but regularly for situational awareness and self-defense. Airborne systems are where EO/IR systems are most used for ISR purposes. Especially with UAVs becoming cost effective and being deployed on longer missions EO/IR systems have become a vital part of UAVs. In both land and naval platforms these EO/IR systems are mostly placed upon a pan-tilt stage; however, on airborne platforms, the EO/IR systems are packaged in a tight gimbal where SWaP is a real issue. Advancements in infrared detector technology such as smaller detector pitch and high operating temperature (HOT) detectors are paving way for compact imagers with high resolution. Folding the optical path using mirrors in continuous zoom systems is a way to reduce the size of the objective which often takes a lot of space. Novel actuation methods have been gradually utilized in these systems. Incorporating all these new technologies and designs is a good way to meet the emerging challenges of EO/IR systems for the purpose of ISR.

Keywords: EO/IR Systems, ISR Platforms, Imaging systems, Gimbal Technologies

S41

Effect of sputtering conditions on the physical quality of sub-10 nm Ag films prepared by DC magnetron sputtering

Gümrükçü, A.E.[1], Akın Sönmez, N.[1,2], Azizian-Kalandaragh, Y.[1,2], Özçelik, S.[1,2]

[1]Gazi University, Photonics Application and Research Center, Ankara, Turkey
[2]Gazi University, Faculty of Applied Science, Department of Photonics, Ankara, Turkey

In this work, the magnetron sputtering method was utilized to systematically investigate the influence of deposition conditions on the structural, optical, and electrical properties of sub-10 nm ultrathin Ag films that have the chance to be used in Low-E applications. Firstly, Ag films were sputtered on AZO/Al_2O_3/Glass structure at different argon gas flow rates and sputtering power in order to optimize conditions. Afterwards, lower thickness Ag thin films were prepared under the determined coating conditions. Ag thin films with a thickness of 5 nm and film continuity were obtained. The transmittance values, surface resistances, morphologies and wettability values of the prepared thin films were analyzed. Continuous and conductive 5 nm Ag thin films which have a surface resistance of 6.36 Ω/sq, and the transmittance of 71% at 550 nm were achieved. Finally, the low emissivity value of this structure was obtained for the NIR region. Ag/AZO/Al_2O_3/Glass (5 nm/10 nm/25 nm) films has the low-emissivity value as 0.0793, in NIR region (780-2500 nm).

Keywords: Silver ultrathin film, magnetron sputtering, wettability measurement, Low-E glass

Acknowledgements:
This work was supported by SBB (TR) under the project numbers of 2016K121220.

S42

Development of the near infrared absorbing LaB_6 optical filter

Güloglu Bülbül, B.*[1,2], Özen, Y.[1,3], Sayraç, M.[4] and Özcelik, S.[1,2,5]

[1]*Photonics Application and Research Center, Gazi University, Ankara, Turkey*
[2] *Department of Photonics Science and Engineering, Institute of Science, Gazi University, Ankara, Turkey*
[3] *Department of Physics, Science Faculty, Gazi University, Ankara, Turkey*
[4]*Nanotechnology Engineering, Faculty of Engineering, Cumhuriyet University, Sivas, Turkey*
[5]*Department of Photonics, Applied Science Faculty, Gazi University, Ankara, Turkey*
[*]*busragguloglu@gmail.com; sozcelik@gazi.edu.tr*

The development of inorganic materials that absorb near infrared (NIR) radiation with a wavelength of 1064 nm is important for many optical applications [1]. Lanthanum hexaboride (LaB6) is a very interesting material due to its absorption valley centered around a wavelength of about 900nm-1000 nm. This valley is redshifted by doping with rare earth elements [2]. In this study, LaB_6 thin films are coated on glass and PET substrates with sol-gel spin coating technique. First of all $La(OH)_3$ material with powder form was obtained by sol-gel process using lanthanum nitrate, sodium hydroxide, and tergitol as precursors. Structural and optical analyzes of the obtained material were made and it was concluded that it was compatible with the literature. The LaB6 powders were synthesis with mixing $La(OH)_3$ powders with Lanthanum nitrate hexahydrate $La(NO_3)_3{\cdot}6\ H_2O$ at suitable conditions. The XRD, FT-IR measurements of the obtained LaB_6 thin films coated on the substrates by spin coating using LaB_6 powder solution in ethanol and ethylene glycol solvent. Developed films with a thickness of 110 nm were characterized by using XRD and FTIR techniques. It was determined that the optical absorption around 1000 nm and Vis transmittance of the films having a cubic structure (lattice constant 4.19A) were 60% and 70%, respectively.

Acknowledgement:
This work was supported by the Presidency of Strategy and Budget (Turkey) and TUBİTAK under project numbers of 2019K12-149045 and 120F322, respectively.

References:

[1] Mattox, T., Coffman, D., Roh, I., Sims, C., Urban, J. (2018). “Moving the Plasmon of LaB6 from IR to Near-IR via Eu-Doping”, Materials, 11, 226.
[2] Yu, Y., Wang, S., Li, W. 2018. “Fabrication and characterization of ternary La1-xCexB6 by a novel molten salt synthesis route” J. Am. Ceram. Soc., 101, 4498-4502.

S43

2D heterostructures formed by graphene-like ZnO and MgO for novel optoelectronic applications

Seyedmohammadzadeh, M.*, Oğuz, G.

Department of Physics, Bilkent University, Ankara 06800, Turkey
**mahsa@bilkent.edu.tr*

Two-dimensional (2D) van der Waals heterostructures (vdWHs) are an emerging class of 2D materials. Due to their intriguing properties arising from the different functionalities of each layer, they have been considered revolutionary in nanodevice engineering. Alongside vdWHs, recently observed bonded bilayer heterostructures (BBHs) possess distinctive properties. In BBHs, the properties of both layers are changing, which is not so noticeable in vdWHs [1]. Hence BBHs create a novel platform for controlling the physical properties of 2D materials.

We performed a systematic study of 2D heterostructures formed by graphene-like ZnO and MgO by investigating the thermodynamic, mechanical, and dynamical stability of four different stackings. A previous study on the electronic properties of one of the possible stacking of 2D ZnO/MgO vdWHs has shown that MgO can increase the photocurrent by reducing parasitic absorption losses and unwanted backscattering processes [2]. Our results reveal that all of the considered structures are thermodynamically and mechanically stable. Interestingly a BBH formed by AB stacking created by placing the Mg atom on top of the O atom of the ZnO layer is also dynamically stable at zero Kelvin. In the predicted dynamically stable structure, the MgO layer forms the valance band, whereas the conduction band is dominated by the Z atom of the ZnO layer. Furthermore, we examined the electronic and optical properties of the ZnO/MgO heterostructures utilizing GW approximation and solving the Bethe-Salpeter equation. Our results indicate that strong excitonic effects reduce the optical band gap to the visible light spectrum range. These results show that this new 2D form of ZnO/MgO opens an avenue for novel optoelectronic device applications.

Reference:

[1] Chen, Y., Gong, P., Ren, Y., Hu, L., Zhang, H., & Wang, J. et al. (2021). Interlayer Quasi-Bonding Interactions in 2D Layered Materials: A Classification According to the Occupancy of Involved Energy Bands. The Journal Of Physical Chemistry Letters, 12(50), 11998-12004.
[2] Ekuma, C., Najmaei, S., & Dubey, M. (2019). Surface passivated and encapsulated ZnO atomic layers by high-κ ultrathin MgO layers. Nanoscale, 11(26), 12502-12506.

S44

Investigation of the effect of annealing on the structural and optical properties of RF sputtered WO_3 nanostructure for memristor applications

Efkere, H.İ.*[1,3], Gumrukcu, A.E.[3], Ozen, Y[2,3]., Kınacı, B.[3], Aydın, S.S.[3,4], Ates, H.[1], and Ozcelik, S.[3,4]

[1]*Department of Metallurgical and Materials Engineering, Faculty of Technology, Gazi University, 06500, Ankara, Turkey*
[2]*Department of Physics, Faculty of Sciences, Gazi University, 06500, Ankara, Turkey*
[3]*Photonics Research and Application Center, Gazi University, 06500, Ankara, Turkey*
[4]*Department of Photonics, Faculty of Applied Sciences, Gazi University, 06500, Ankara, Turkey*
**i.efkere@gazi.edu.tr*

Advances in complementary metal oxide semiconductor (CMOS) and flash memory technologies have greatly impacted the world over the past few decades. Parameters such as reducing material sizes, developing devices that can operate with lower energy, increasing data transfer speed, reaching smaller volumes in data storage and reaching larger capacities can be counted as the driving force of these revolutionary changes in electronic technology. In this context, in this study, studies have been carried out to develop data storage and synaptic imitation amounts and memristor devices that have come to the fore in recent years. The metal oxide material we have chosen to prepare the samples whose memristive properties will be examined is WO_3. The samples were produced by RF magnetron sputtering technique at room temperature and then annealed in a CTA furnace between 300 and 700 ^oC. Then, structural and optical analyzes of the samples were carried out. From the results obtained, the memristive properties and upper contacts of the samples to be examined were taken and I-V measurements were made.

Acknowledgements:
This work was supported by SBB (TR) under the project numbers of 2016K121220.

S45

About statistical patterns of exoplanets

*Tuzelbay, M.Y

Physics and Astronomy, Al-Farabi Kazakh National University, Kokziek Mikro bölgesi, 21, 050028/A20A5C3, Almatı, Kazakistan
malika-97.11@mail.ru

Exoplanets are called planets outside the Solar system (from others-Greek. ἔξω - — outside, outside") [1]. The discovery, study of the characteristics and replenishment of the catalog of exoplanets is undoubtedly one of the most relevant areas of modern astronomy. To date (02/15/2022), according to the NASA Exoplanet Archive catalog, 4933 exoplanets have been confirmed and 5243 planets are candidates for exoplanets. [2]. The total number of exoplanets in the Milky Way galaxy is estimated at at least 100 billion, of which there may be from 5 to 20 billion Earth-like planets. The search and exploration of exoplanets is part of the overall problem of the search for extraterrestrial life.

As a result of the dynamic evolution of exoplanets, there are a number of regular stages that can have a universal character. To date, a generally accepted and consistent theory of the formation of planetary systems and multiple star systems has not been created. In this regard, the identification of general statistical patterns is certainly relevant, since it contributes to a deeper understanding of the origin and evolution of planetary systems.

The paper collects and analyzes data on the characteristics of exoplanets from the catalogues of exoplanets [3-7]. The reliability of the presented data was assessed. To obtain the mass functions of planetary bodies, data from confirmed exoplanets with reliably determined masses were used, respectively, planets with only a lower mass limit and planets with a projective mass msin(i) were excluded from the list of exoplanets. The analysis and approximations of the obtained functions of the masses of planetary bodies are carried out.

References:

[1] Armitage, P., Livio, M., Lubow, S., & Pringle, J. 2002, MNRAS, 334, 248
[2] Eggenberger, A., Udry, S., & Mayor, M. 2003, A&A, submitted (Paper III)
[3] Ford, E., Rasio, F., & Yu, K. 2003, in Scientific Frontiers in Research on Extrasolar Planets, ed. D. Deming, & S. Seager, ASP Conf. Ser., in press
[4] Kley, W. 2001, in The Formation of Binary Stars, ed. H. Zinnecker, & R. Mathieu, IAU Symp.
[5] Lin, D., Bodenheimer, P., & Richardson, D. 1996, Nature
[6] Marcy, G., Butler, R., Vogt, S., et al. 2001, ApJ,
[7] Trilling, D., Lunine, J., & Benz, W. 2002, A&A

S46

Fabrication and characterization of MoS_2/Si heterojunction structure

Donmez Kaya, M.*[1], Ozcelik, S.[1,2]

[1]*Gazi University, Photonics Application and Research Center, 06500 Ankara, Turkey*
[2]*Gazi University, Department of Photonics, 06500 Ankara, Turkey*
**meltmdn@gmail.com, meltem.kaya1@gazi.edu.tr*

Molybdenum disulfide (MoS_2), which is an interesting and promising material among the transition metal dichalcogenides (TMDs) family, is an exciting and emerging material in nature due to its unique electronic and optical properties in all aspects, including structure and abundance. With these interesting properties, MoS_2 has potential applications in various fields such as solar cells, energy storage devices, transistors, sensing devices. Moreover, since the light absorption of MoS_2 extends from the visible to the near-infrared spectral region (350-950 nm), there has been a lot of work recently in the development of optoelectronic devices such as photodetectors [1]. Many researchers have reported that the performance of MoS_2-based heterojunction devices is strongly influenced by the thickness of the thin film, and the light absorption of the MoS_2 film increases remarkably with the use of large film thickness [2]. In this study, it was aimed to obtain the n-MoS_2/p-Si heterojunction using 100 nm thick MoS_2 thin film and to increase the operating performance of the produced device for near-infrared photodetector applications. In line with this goal, MoS_2 thin film coating process was carried out at 600 °C on p-Si and corning glass substrates with RF magnetron sputtering system. Structural, morphological and optical analyzes of the obtained films were performed. Then, the Au/n-MoS_2/p-Si heterojunction structure was fabricated and its optoelectronic properties were investigated using the I–V system. As a result of the research, it was observed that the n-MoS_2/p-Si heterojunction, which was determined to have high quality with its high rectification performance and a small ideality factor of 1.98, exhibited sensitivity to light at a wavelength of 780 nm. It was determined that the MoS_2/Si heterostructure with its near-infrared response has significant potential for optoelectronic applications.

Acknowledgement:
This work was supported by SBB - Strategy and Budget Presidency (TR) under project number of 2019K12-149045.

References:
[1] P. Xiao, J. Mao, K. Ding, W. Luo, W. Hu, X. Zhang, J. Jie, “Solution-processed 3D RGO–MoS2/pyramid Si heterojunction for ultrahigh detectivity and ultra-broadband photodetection”, Advanced Materials, 30, 1801729 (2018).
[2] L. Wang, J. Jie, Z. Shao, Q. Zhang, X. Zhang, Y. Wang, S.T. Lee, “MoS_2/Si heterojunction with vertically standing layered structure for ultrafast, high-detectivity, self-driven visible–near infrared photodetectors”, Advanced Functional Materials, 25, 2910-2919 (2015).

S47

Role of UV absorbers on the IR-LD spectra of liquid crystal network polymer

Alipanah, Zh.*[1], Ranjkesh, A.[2], Zakerhamidi, M. S.[1,3]

[1]*Faculty of Physics, University of Tabriz, Tabriz, Iran*
[2]*Condensed Matter Department, J. Stefan Institute, Jamova 39, Ljubljana, Slovenia*
[3]*Photonics Center of Excellence, University of Tabriz, Tabriz, Iran*
**zh.alipanah@tabrizu.ac.ir*

Responding to external stimuli is a trait observed in all living organisms. This fundamental property has been adopted by modern artificial materials, kicking off the field of stimuli–responsive systems. Liquid crystal networks (LCNs) are appealing members of this system family, which is important in research and technology. As a result, conducting studies to characterize them is quite valuable. The study of the IR-LD spectra of these materials is important to characterize these materials as accurately as possible due to the need to gather high-precision information in regard to the functional groups. The influence of molecular orientation, which can be controlled by applying surface orientation, on the order of functional groups in the RM82 structure was examined using the IR-LD spectra of LCN polymer based on reactive mesogen RM82 containing UV absorber from the Tinuvin group. RM82 makes up a considerable portion of the constituent in polymer network, while Tinuvin only makes up a minor percentage of the constituents. The results indicate that molecular orientation has a direct effect on the IR-LD spectrum, which gives significant information about structural order. This allows for the careful selection of the type of structure for the preparation of the LCN polymer based on the planned application.

S48

Dependence of film thicknesses on the XRD, AFM and Transmittance Properties of NiO_x

Hopoğlu, H. [*,1,2], Kaya, D.[3], Akyol, M.[4], Demir, İ.[2,5], Altuntaş, İ.[2,5], Ekicibil, A.[6], Şenadım Tüzemen, E.[1,2]

[1] *Department of Physics, Sivas Cumhuriyet University, 58140 Sivas, Turkey*
[2] *Nanophotonics Research and Application Center, Sivas Cumhuriyet University, 58140 Sivas, Turkey*
[3]*Department of Electronics and Automation, Vocational School of Adana, Cukurova University, 01160, Adana, Turkey*
[4]*Department of Materials Science and Engineering, Faculty of Engineering, Adana Alparslan Turkes Science and Technology University, 01250, Adana, Turkey*
[5]*Department of Nanotechnology Engineering, Sivas Cumhuriyet University, 58140 Sivas, Turkey*
[6]*Department of Physics, Faculty of Art and Sciences, Cukurova University, 01330, Adana, Turkey*
[*]*20199251008@cumhuriyet.edu.tr*

NiO thin films exhibit wide band gaps, good electrical conductivity, transparency in the visible light [1]. In this study, NiO_x thin films having various thicknesses were grown on glass substrates by RF magnetron sputtering deposition system at room temperature. XRD data revealed fcc structure with a space group of $Fm\bar{3}m$. X-ray diffraction peaks indicate that while there was only NiO (111) orientation at 100 nm, other characteristic NiO (200) and (220) peaks were appeared with the increasing of NiO thickness. The peak intensities increased with the NiO thickness that indicates the better crystallization at thicker NiO samples. Atomic force microscopy images revealed that the surface of films varies depending on the thickness. Optical parameters such as optical transmittance and energy band gap have been studied and discussed. As expected, the transmittance of the films decreases with increasing film thickness [2]. The decrease in transmittance is thought to be due to the free carrier absorption, which increases carrier density in thicker films. It is seen that the absorption edge shifts to a longer wavelength with increasing thickness. There are shifts in the band gap as the thickness changes and it can be explained by the Burstein-Moss shift [3]. The direct energy band gap decreases from 3.74 to 3.70 eV as the film thickness increases from 200 nm to 300 nm. This situation can be explained by the structural feature of the film.

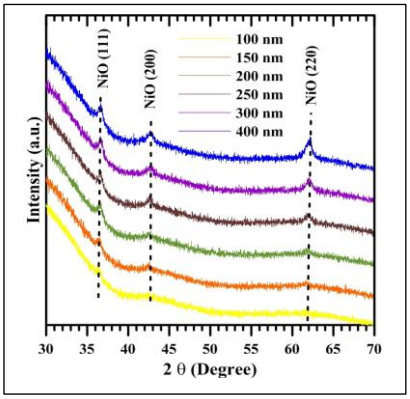

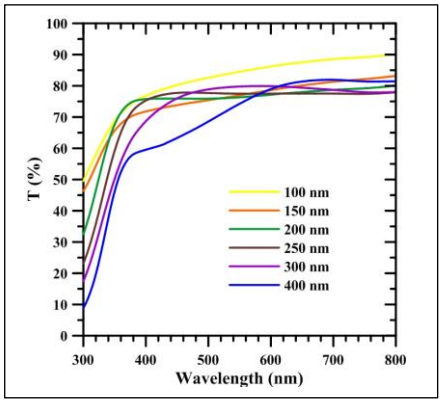

Keywords: NiO_x, magnetron sputtering, optical properties. XRD, AFM

Acknowledgement:
This work is supported by the Scientific Research Project Fund of Sivas Cumhuriyet University under the project number F-2021-640 and Cukurova University, Adana, Turkey, under Scientific Research Funding Grand Numbers: FAY-2020-12933.

Reference:
[1] Anas A. Ahmed, Mutharasu Devarajan, Naveed Afzal, Fabrication and characterization of high performance MSM UVphotodetector based on NiO film, Sensors and Actuators A, 262 78–86 (2017).
[2] F. Saadati, A.-R. Grayeli, H. Savaloni, Dependence of the optical properties of NiO thin films on film thickness and nano-structure, Journal of Theoretical and Applied Physics, 4-1, 22-26 (2010).
[3] Ebru ŞenadımTüzemen, Sıtkı Eker, Hamide Kavak, Ramazan Esen, Dependence of film thickness on the structural and optical properties of ZnO thin films, Applied Surface Science, 255, 6195-6200 (2009).

S49

Production and characterization of TiO_xN_y thin films for stent applications by co-sputtering system with confocal geometry method

Özkök, Y.[*1,2], Sönmez, N.A.[1,3], Akman, B.[1], Çakmak, M.[1,3], Özçelik, S.[1,3]

[1]*Gazi University, Photonics Application and Research Center, Ankara*
[2]*Gazi University, Department of Physics, Ankara*
[3]*Gazi University, Department of Photonics, Ankara*
[*]*yelizozkok@gmail.com, sozcelik@gazi.edu.tr*

In the treatment of vascular occlusion with coronary artery disease, it is aimed to restore normal blood flow by placing stents in the narrowed vessel [1]. Various inorganic materials are available for improving the surface properties of the implant material in medical applications. During the production of stent coatings, possible inorganic materials include nitrides, oxides, carbide and silicide, hydroxyapatite-based materials, noble metals, diamond and diamond-like carbon [2]. As an alternative to bare metal stents (BMS) and drug-eluting stents (DES), Titanium Oxynitride (TiO_xN_y) coated stents, called new generation biologically active stents (BAS), have been developed [3]. TiO_xN_y coated stents show good results in mass loss, restenosis and target vascularization, as well as reduce fibrinogen binding and platelet adhesion. It is also known to reduce migration, toxicity and inflammation of nickel, chromium, molybdenum or other metals from the stainless steel surface. In these coatings, titanium improves biocompatibility, is inert and has excellent corrosion resistance, titanium oxide improves stent compatibility with blood and living cells, while the presence of nitrogen in the structure reduces platelet adhesion and fibrinogen binding [1]. In this study, we designed our own stent using the SOLIDWORKS program. Before the TiO_xN_y coating was applied on the stent, the calibration samples of the co-sputtering system with the confocal geometry method were grown. 316L stainless steel, soda lime glass (SLG) and pure silicon were chosen as substrates. Titanium nitride (TiN) was used as the target material. The coatings carried out at room temperature had an argon ratio of 100% and an argon pressure of 3mTorr. XPS analyzes of TiO_xN_y thin films coated on silicon and stainless steel substrates were performed. In the analysis results obtained for silicon, the O1s ratio was 33.27, the C1s ratio was 41.50, the N1s ratio was 11.99, and the Ti2p ratio was 13.24. The Ti2p peak at 456.465 eV represents the TiO_xN_y thin film. In the analysis results obtained for stainless steel, the O1s ratio was 36.45, the C1s ratio was 28.67, the N1s ratio was 18.39, and the Ti2p ratio was 16.48. The Ti2p peak at 455,833 eV belongs to the TiO_xN_y thin film. AFM analysis of thin films grown on stainless steel and silicon substrates was performed. For stainless steel, 2d and 3d images were obtained in a 20x20 μm^2 scan area. The RMS value was found to be 37.71 nm. For silicon, 2d and 3d images were obtained in 3x3 μm^2 scanning area. The RMS value was found to be 1.07 nm. In addition, the distribution of atomic species (Ti, N, O, Si) was observed with the secondary ion mass spectrometry (SIMS) depth profile and the target thickness value of approximately 230 nm was observed.

Keywords: Thin film, TiO_xN_y, co-sputtering system with confocal geometry

Acknowledgment:
This study was supported by the Presidency Strategy and Budget Department with the project numbered 2019K12-149045.

References:
[1] Beshchasna, N., Ho, A. Y. K., Saqib, M., Kraśkiewicz, H., Wasyluk, Ł., Kuzmin, O., Duta, O.C., Ficai, D., Trusca, R. D., Ficai, A., Pichugin, V. F., Opitz, J., Andronescu, E. (2019). Surface evaluation of titanium oxynitride coatings used for developing layered cardiovascular stents. Materials Science & Engineering, C 99, 405-416.
[2] Beshchasna, N., Saqib, M., Kraskiewicz, H., Wasyluk, Ł., Kuzmin, O., Duta, O. C., Ficai, D., Ghizdavet, Z., Marin A., Ficai A., Sun Z., Pichugin V. F., Opitz J., & Andronescu, E. (2020). Recent advances in manufacturing innovative stents. Pharmaceutics, 12(4), 349.
[3] Gotman, I., Gutmanas, E.Y. (2014). Titanium nitride-based coatings on implantable medical devices. Advanced Biomaterials and Devices in Medicine, 1, 53-73.

S50

Tunning and enhancing the electroluminescence properties of blue polymer light emitting diode by incorporation of perylene diimide derivatives

Bozkus, V.[1*], Aksoy, E.[1,2], Varlikli, C.[1]

[1]Department of Photonics, Izmir Institute of Technology, Urla, 35430 Izmir, Turkey*
email: volkanbozkus@iyte.edu.tr
[2]Project and Technology Office, Rectorate, Bartin University, 74100, Bartin, Turkey
eaksoy@bartin.edu.tr, cananvarlikli@iyte.edu.tr

Organic light emitting diodes (OLEDs) studies have accelerated in the last decade as a result of which it is used in smartphone screens, lighting, TVs and wearable devices found in the market[1]. The blue part of the spectrum is most important in almost all applications such as RGB screens and solid-state lighting. Due to its wide band gap, blue emitters have a high charge generation barrier which causes a charge imbalance in the active layer[2]. For these reasons, the efficiency of the fabricated devices mostly depends on the efficiency of blue emission.

Here we report, enhanced blue OLED by doping red emitting functional and non-functional PDIs, PDIref and PDI1, to blue emitter of ADS231BE (poly[9,9-di-(2-ethylhexyl)-fluorenyl-2,7-diyl]). All fabricated device has a structure of ITO/PEDOT:PSS/PVK(or PVK:mCP)/Active layer/Cs_2CO_3/Al where poly(3,4-ethylenedioxythiophene):poly(styrene sulfonate) used as a hole injection layer. ADS, ADS:PDIref(0.1wt%) and ADS:PDI1(0.1wt.%) configuration is used at active layer. Two different hole transport layer material of PVK with a hole mobility of μ^h: $2.5x10^{-6}$ $cm^2V^{-1}s^{-1}$ [4] and PVK:mCP(1,3-Di(9H-carbazol-9-yl)benzene, (3:1wt.%) with a hole mobility of μ^h:$1x10^{-3}$ $cm^2V^{-1}s^{-1}$ were used. PDIref and PDI1 are used to enhance the device performance. We obtained an enhanced blue emission with a brightness of around six times higher and quadrupled efficiency.

Acknowledgements:
We acknowledge the project support fund of the Scientific Research Council of Turkey (TUBITAK) (Project Number: 119F031).

References:
[1] Huang, Y., Hsiang, E. L., Deng, M. Y. & Wu, S. T. Mini-LED, Micro-LED and OLED displays: present status and future perspectives. *Light Sci. Appl.* 9, (2020).
[2] Fan, S., Sun, M., Wang, J., Yang, W. & Cao, Y. Efficient white-light-emitting diodes based on polyfluorene doped with fluorescent chromophores. *Appl. Phys. Lett.* 91, 2005–2008 (2007).
[3] Aksoy, E., Danos, A., Li, C., Monkman, A. P. & Varlikli, C. Silylethynyl Substitution for Preventing Aggregate Formation in Perylene Diimides. *J. Phys. Chem. C* 125, 13041–13049 (2021).
[4] Lee, D. H., Liu, Y. P., Lee, K. H., Chae, H. & Cho, S. M. Effect of hole transporting materials in phosphorescent white polymer light-emitting diodes. *Org. Electron.* 11, 427–433 (2010).

S51

Influence of environment to optical properties of CdS nanoparticles

Gahramanli, L.R.*[1], Muradov, M.B.[1], Eyvazova, G.M.[1], Balayeva, O.O[2].

[1] *Nano Research Center, Baku State University, Z.Khalilov str. 33, Azerbaijan,*
[2] *Faculty of Chemistry Baku State University, Z.Khalilov str. 33, Azerbaijan.*
qahramanli.lala@mail.ru

Semiconductor nanomaterials have attached much interest due to interesting physical and chemical properties. One of the important combination of II-VI group materials - CdS have great application field such as solar cells, light-emitting diodes LEDs, electronic, optoelectronic, and quantum size effect semiconductor devices [1-3], photocatalysts [4] and electrochemical cells [5]. Cadmium sulfide (CdS) is an important direct intermediate bandgap (2.42 eV at 300 K) with excellent thermal and chemical stability and strong optical absorption and is used in solar cells, photodetectors, light emitting diodes, and lasers.

The solution concentration can effect on the optical properties of formed nanoparticles due to different physical interaction. While, in this paper, the effect of different electrolyte concentrations on the optical properties of formed CdS nanoparticles by sonochemical method. In this purpose, CdS nanoparticles placed in 4 concentrations (0.01M; 0.1M; 1M; and 2M) of different electrolyte solution such as Cadmium nitrate tetrahydrate ($Cd(NO_3)_2 \cdot 4H_2O$), cadmium acetate dihydrate ($Cd(CH_3COO)_2 \cdot 2H_2O$) and sodium chloride (NaCl).

In the nanoparticles, covered by electrolyte solution occur different interactions with charge carriers: electron-ion, dipole-electron, ion-ion, ion-dipole, dipole-dipole, etc.

Ion-electron interaction:

$$\omega\,(r_e, R_i) = -\frac{Ze^2}{|r_e - R_i|} \qquad (1)$$

where, $\omega\,(r_e, R_i)$ is potential of the electron–ion interaction. R_i- coordinate of ions, r_e – coordinate of electrons in nanoparticles. Z –valence of ion, e – electron charge.
Dipole-dipole interaction:

$$W = \frac{(P_1 P_2)r^2 - 3(P_1 r)(P_2 r)}{r^5} \qquad (2)$$

In Fig. 1, the absorption spectra of different concentrated electrolyte solution before and after the addition of CdS nanoparticles are shown.

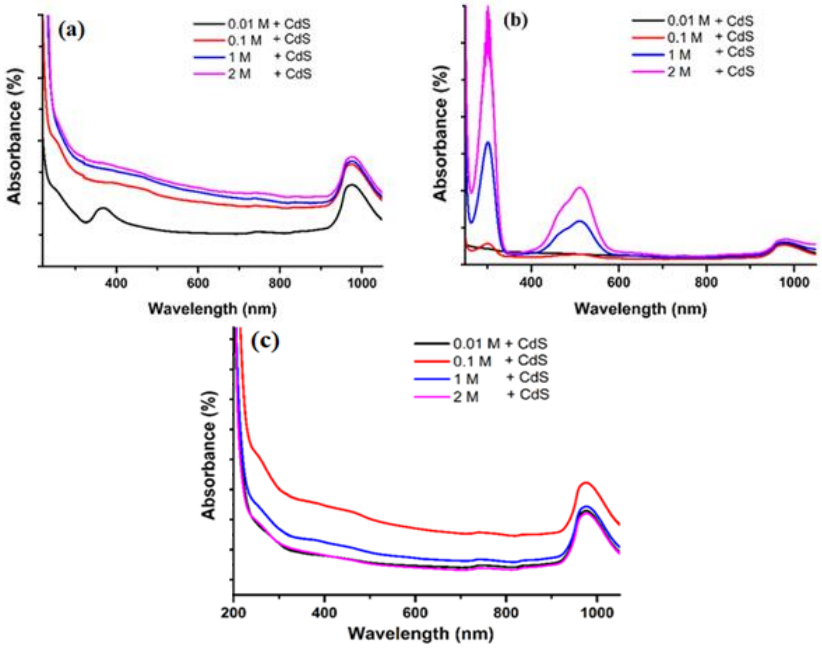

Fig. 1. The absorbance spectra of different concentration of electrolyte solution after added CdS nanoparticles: a) cadmium acetate; b) cadmium nitrate; c) sodium chloride.

As can be seen from the absorbance spectrum, the band gap of nanoparticles strongly depends on the nature of the environment. Adding CdS into electrolyte solution the band gap decreased by increasing the concentration of electrolyte solution.

Reference:

[1] J. Yao, G. Zhao, D. Wang, G. Han, Solvothermal synthesis and characterization of CdS nanowires/PVA composite films, Mater. Lett. 59 (2005) 3652- 3655.
[2] A. Kharazmi, E. Saion, N. Faraji, N. Soltani, A. Dehzangi, Optical Properties of CdS/PVA Nanocomposite Films Synthesized using the Gamma-Irradiation-Induced Method, Chin. Phys. Lett. 30 (2013) 057803.
[3] V. Bala, M. Sharma, S.K. Tripathi, R. Kumar, Investigations of Al:CdS/PVA nanocomposites: A joint theoretical and experimental approach, Mater. Chem. Phys. 146 (2014) 523-530.
[4] P. Deepak, S. Sarita, R. Bhim, Synthesis, characterization and photocatalytic application of bovine serum albumin capped cadmium sulphide nanopartilces, Chalcogenide Letters 8 (2011) 396 – 404.
[5] A. Hagfeldt, M. Gratzel, Light-Induced Redox Reactions in Nanocrystalline Systems, Chem. Rev. 95 (1995) 49-68.

FULL TEXTS

FT1

Reflection Shift Characterization of Plasmonic Core/Shell Metasurfaces

Zoghi, M.

School of Engineering Science, University of Tehran, 16 Azar, Enqelab Square, Tehran, Iran
maryam.zoghi@ut.ac.ir

A metasurface is composed of two-dimensional subwavelength periodic array. Their functionalities and performance are dominated by the resonant optical plasmonic nanoparticles or high-refractive index dielectric nanoparticles. Metasurfaces are able to modulate the amplitude, phase and polarization of incident light. Reflected light from a surface exhibits a deviation from the rules governed by geometric optics and displaces in directions parallel and perpendicular to plane of incidence. Using generalized sheet transition conditions, we study GH reflection shift in a metasurface composed of spherical core/shell nanoparticles in a square array. A detailed analysis reveals that large reflection shifts are achievable in both visible and ultraviolet ranges due to plasmonic resonance of metallic shell. A comparison of cores with different metal oxides and shells of two noble metals is also carried out to get an inclusive characterization. The results could be useful in sensitive beam deflection measurements like in AFM or reflective UV sensors.

Keywords: Metasurface, Core-Shell Nanoparticles, Reflection Shift, Plasmonics

Introduction

Metasurfaces are special class of two-dimensional metamaterials composed of periodic or specially arranged metal/dielectric structures whose thickness and periodicity are small compared to the wavelength in the surrounding media. These materials can couple to the electric and magnetic fields of incident light and demonstrate effective properties that are not usually found in nature [1]. Surfaces can also be designed to have sharp phase changes which effect the reflection of an optical beam. Many of the first applications of metasurfaces demonstrate subdiffraction lensing [2], spectroscopy [3], monochromatic holography [4], color holography [5], polarization converters [6], vortex plates [7], invisibility cloaks [8] and polarization-selective elements [9].

A beam reflected off an interface experiences spatial and angular shifts depending on the polarization and the beam profile [10]. The displacements are the well-known Goos-Hanchen (GH) shift in the plane of incidence and the Imbert-Fedorov (IF) shift normal to the plane of incidence. Beam shifts have received much attention because of their potential applications in the design of optical devices, such as optical waveguide switch, optical sensors as well as precision metrology and spin photonics. Over the last few years, the reports on Goos-Hanchen effect in specifc metamaterial interfaces have included ferromagnetic materials, linear metasurfaces, gradient metasurfaces and patterned surfaces. Recently, it has been shown that a metasurface of plasmonic core-shell nanoparticles is capable of possessing tunable high reflectivity

at plasmonic resonances that can act as wavelength-selective surface with multiple stopbands. Here, we study reflection shifts in a metasurface comprising of zinc oxide/gold core-shell nanoparticles by modeling the interaction of metasurface with an incident light wave. We use generalized sheet transition conditions to obtain reflection coefficients for a TM wave and the amounts of GH shifts are then calculated for various geometrical parameters of the surface. Also a comparison of cores with different metal oxides and shells of two noble metals is carried out to get an inclusive characterization.

Theory

Reflection Shifts of the Surface

When light with the angle θ incidents from air onto a plane surface, the reflection coefficients are described with the magnitudes R_m and the phase shifts φ_m as $r_m = R_m e^{i\varphi_m}$, where $m \in \{TE.TM\}$ pertaining to TE and TM polarizations. Considering a linearly polarized beam with in-phase transverse electric field components, the explicit expression of the unitless spatial and angular shifts are [11]:

$$k\Delta_{GH} = \Omega_{TM}\frac{\partial\varphi_{TM}}{\partial\theta} + \Omega_{TE}\frac{\partial\varphi_{TE}}{\partial\theta}. \qquad (1-1)$$

$$\Theta_{GH} = -\left(\Omega_{TM}\frac{\partial LnR_{TM}}{\partial\theta} + \Omega_{TE}\frac{\partial LnR_{TE}}{\partial\theta}\right) \qquad (1-2)$$

where $\Omega_m = \frac{{a_m}^2{R_m}^2}{{a_{TE}}^2{R_{TE}}^2+{a_{TM}}^2{R_{TM}}^2}$, a_m are the electric field components for parallel and perpendicular directions and *k* is the vacuum wave number. Fig.1 indicates (in-plane) GH and (out-of-plane) IF shifts including spatial (Δ) and angular (Θ) parts.

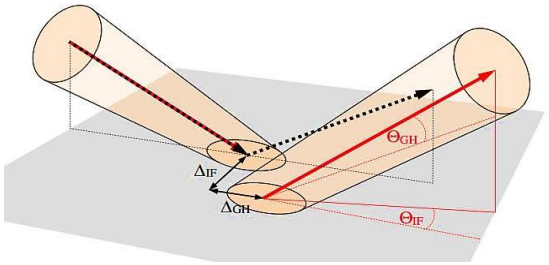

Fig.2 GH and IF shifts in a plane reflecting interface.

Metasurface of Core-Shell Nanoparticles

Nanoparticles (NPs) with core-shell structure have attracted intensive scientific and technical interests due to their potential applications in catalysis, drug delivery, microelectronics, sensor, and many other emerging nanotechnologies. The important feature of this type of nano-structures is the possibility of controlling their optical and spectral properties by varying the size of the core and/or the thickness of the shell. NPs coated with a noble metal exhibit strong coupling between the plasmon resonance of the metal and the quantum size effect of the NPs that give rise to new properties. In particular, core/shell nanostructure composites with metal-oxide core and metallic shell have several unique optical, photocatalytic, and electronic properties neither shown by the bare metal nor by metal-oxide nanostructures.

Consider a spherical core/shell composite consisting of a semiconductor core of dielectric function (DF) ε_c and radius r_1 and a metallic shell of DF ε_s and outer radius r_2. The permittivity of plasmonic shell ε_s is described by Drude model

$$\varepsilon_s(\omega) = \varepsilon_0 - \frac{{\omega_p}^2}{\omega^2 + i\,\omega\Gamma} \tag{2}$$

where ε_0 represents the contribution from interband transitions and ω_p is the bulk plasma frequency. The damping frequency Γ includes bulk frequency and a term due to particle size:

$$\Gamma = \Gamma_{\text{bulk}} + \frac{AV_F}{l_e} \tag{3}$$

Where A is a model-dependent constant whose values have been theoretically justified from 0.1 to 2 [55]. V_F is the Fermi velocity and l_e indicates the electrons effective mean free path. For a spherical NP of core radius r_1 and core/shell radius r_2, the mean free path is given by

$$l_e = \frac{r_2}{2}\left[(1-\beta^{\frac{1}{3}})(1-\beta^{\frac{2}{3}})\right]^{\frac{1}{3}} \tag{4}$$

where $\beta = (\frac{r_1}{r_2})^3$. A metasurface manipulates light using a 2D array of optical scatterers with a subwavelength distance between the scatterers. We consider a metasurface composed of plasmonic core–shell NPs arranged in a square lattice of period *P*. A schematic of core-shell nanoparticles and the of metasurface are illustrated in Fig.2.

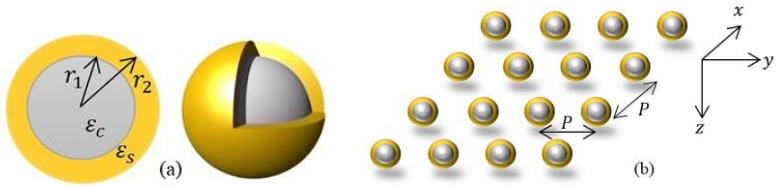

Fig.2 (a) Two and three dimensional schematics of a core-shell nanoparticle; (b) A metasurface of spherical core-shell nanoparticles arranged in a square lattice with periodicity P.

The behavior of a metasurface can be characterized by the dyadic surface electric and magnetic susceptibilities, denoted by $\overleftrightarrow{\chi}_{ES}$ and $\overleftrightarrow{\chi}_{MS}$, interpreted as effective electric and magnetic polarizability densities per unit area respectively. We assume that the surface susceptibility tensors are diagonal:

$$\overleftrightarrow{\chi}_{ES} = \chi_{ES}^{xx}\,\hat{\boldsymbol{x}}\hat{\boldsymbol{x}} + \chi_{ES}^{yy}\,\hat{\boldsymbol{y}}\hat{\boldsymbol{y}} + \chi_{ES}^{zz}\,\hat{\boldsymbol{z}}\hat{\boldsymbol{z}} \tag{5}$$

$$\overleftrightarrow{\chi}_{MS} = \chi_{MS}^{xx}\,\hat{\boldsymbol{x}}\hat{\boldsymbol{x}} + \chi_{MS}^{yy}\,\hat{\boldsymbol{y}}\hat{\boldsymbol{y}} + \chi_{MS}^{zz}\,\hat{\boldsymbol{z}}\hat{\boldsymbol{z}} \tag{6}$$

Boundary conditions link the electric and magnetic fields on opposite sides of a metafilm consisting of a distribution of isolated small scatterers (the so-called cermet topology). Assuming a monochromatic wave with angular frequency ω and time dependence as $e^{i\omega t}$, the generalized sheet transition conditions (GSTCs) are [12]

$$\hat{\boldsymbol{z}} \times \boldsymbol{H}\big|_{z=0^-}^{z=0^+} = i\omega\varepsilon\overleftrightarrow{\chi}_{ES}\,.\,\boldsymbol{E}_{t.av}\big|_{z=0} - \hat{\boldsymbol{z}} \times \boldsymbol{\nabla}_t\left(\chi_{MS}^{zz} H_{z.av})\right|_{z=0} \tag{7-1}$$

$$\boldsymbol{E}\big|_{z=0^-}^{z=0^+} \times \hat{\boldsymbol{z}} = i\omega\mu\overleftrightarrow{\chi}_{MS}\,.\,\boldsymbol{H}_{t.av}\big|_{z=0} + \hat{\boldsymbol{z}} \times \boldsymbol{\nabla}_t\left(\chi_{ES}^{zz} H_{z.av})\right|_{z=0} \tag{7-2}$$

Here z is the direction perpendicular to the surface containing the nanoparticle scatterers, taken to be the plane $z = 0$. The subscript "av" represents the average of the field quantity on either side of the metafilm and subscript "t" denotes the two directions (x and y) tangential to that surface. The electric and magnetic surface susceptibility dyadics can be approximated by means of a sparse application formula [12]. For the electric and magnetic surface susceptibilities, we have

$$\chi_{ES}^{i} = \frac{N\langle\alpha_{ES\,i}\rangle}{1 - j\frac{N\langle\alpha_{ES\,i}\rangle}{4d}} \quad . \quad \chi_{MS}^{i} = \frac{-N\langle\alpha_{MS\ i}\rangle}{1 - m\frac{N\langle\alpha_{MS\,i}\rangle}{4d}} \tag{8}$$

Where $i \in \{xx\,.yy.zz\}$, $j = \begin{cases} +1 & for\ xx.yy \\ -1 & for\ zz \end{cases}$ $and\ m = \begin{cases} -1 & for\ xx.yy \\ +1 & for\ zz \end{cases}$. Here, α_E and α_M are the electric and magnetic polarizabilities of an individual core-shell nanoparticle, $N(=P^{-2})$ denotes the average number of particles per unit area, and $< >$ denotes an average over scatterers [12]. The quantity d is related to the dipole interaction of the scatterers and for a periodic distribution of scatterers in a square array of period P, it was first calculated by Maslovski et al. [13] as $d \approx 0.6956\,P$. The problem of scattering of electromagnetic waves by core–shell spherical structures can be solved by Mie theory [14]. Considering an x-polarized incident plane wave propagating along the z direction with wave vector k, the scattered field by a spherical scatterer located at the origin can be expressed in terms of the vector spherical wave functions

$$E_{sca} = E_0 \sum_{n=1}^{\infty} \frac{i^n(2n+1)}{n(n+1)} \left[i\,a_n N_{0n1}^{(3)}(kr.\theta.\phi) - b_n M_{0n1}^{(3)}(kr.\theta.\phi) \right] \tag{9}$$

where $N_{0n1}^{(3)}$ and $M_{0n1}^{(3)}$ are the same as in [14] and a_n and b_n are Mie scattering coefficients corresponding to TM and TE fields respectively. For simplicity, we assume our materials are magnetically inert $\mu = \mu_c = \mu_s = 1$, which is true for most materials at optical wavelengths [59]. Meanwhile, the scatterers are considered small enough compared to the incident wavelength so we can closely approximate the scattering behaviour by only considering the dipolar term $(n = 1)$. Under such conditions, the scattering is dominated by TM fields, which implies $b_n \approx 0$ [15]. The electric and magnetic polarizabilities of spherical particles have been derived in terms of a_1 and b_n as

$$\alpha_E = -\frac{6\pi i a_1}{k^3} \quad . \quad \alpha_M = -\frac{6\pi i b_1}{k^3} \tag{10}$$

For nonmagnetic media, $b_1 \approx 0$ and the magnetic polarizability is negligible as well. We use a simpler expression that is derived based on quasi-static approximation [14]

$$\alpha_E = 4\pi {r_2}^3 \frac{(\varepsilon_s - \varepsilon)(\varepsilon_s - \varepsilon) + \beta(\varepsilon_c - \varepsilon_s)(\varepsilon + 2\varepsilon_s)}{(\varepsilon_s + 2\varepsilon)(\varepsilon_c + 2\varepsilon_s) + \beta(2\varepsilon_s - 2\varepsilon)(\varepsilon_c - \varepsilon_s)} \tag{11}$$

where ε denotes the permittivity of the surrounding medium.

For oblique TM plane waves with angle of incidence θ on a nonmagnetic metasurface, the reflection coefficients are given by [16]

$$r_{TM} = \frac{i\,\frac{k_0}{2\cos\theta}(\chi_{ES}^{xx}cos^2\theta - \chi_{ES}^{zz}sin^2\theta)}{D_2} \tag{12-1}$$

$$D_2 = 1 - \left(\frac{k_0}{2}\right)^2 \chi_{ES}^{xx}\chi_{ES}^{zz}\, sin^2\theta + i\,\frac{k_0}{2\cos\theta}(\chi_{ES}^{xx}cos^2\theta + \chi_{ES}^{zz}sin^2\theta) \qquad (12-2)$$

Once we have characterized the reflectivity of our metasurface, the reflection shifts can be obtained subsequently.

Results and Discussion

A series of numerical calculations were performed to investigate the reflection shift of TM wave from the metasurface based on (1-1). The metasurface contains spherical ZnO/Au core-shell nanoparticles. Zinc-oxide (ZnO) is a direct band gap semiconducting material which has wide band gap (3.37 eV), high exciton binding energy (~60 meV) at room temperature, and high dielectric constant [17]. Besides, noble metals like Ag and Au are preferred as a shell material because of their high chemical stability, bio-affinity, and strong absorption of light. The parameters used for gold are $\varepsilon_0 = 9.9$, $\omega_p = 13 \times 10^{15}\ Hz$, $\gamma_{\text{bulk}} = 1.1 \times 10^{14}\ Hz$, $V_F = 1.4 \times 10^6\ ms^{-1}$, A = 2 while setting $\varepsilon_c = 8.5$ for ZnO core. The surrounding medium is taken to be air with $\varepsilon = 1$. The IF shifts are zero for TM and TE waves and our analysis focuses on GH spatial shift solely. Fig.3 shows the results for the spatial GH reflection shifts of metasurface plotted in terms of wavelength of light λ , angle of radiation θ and the lattice constant P.

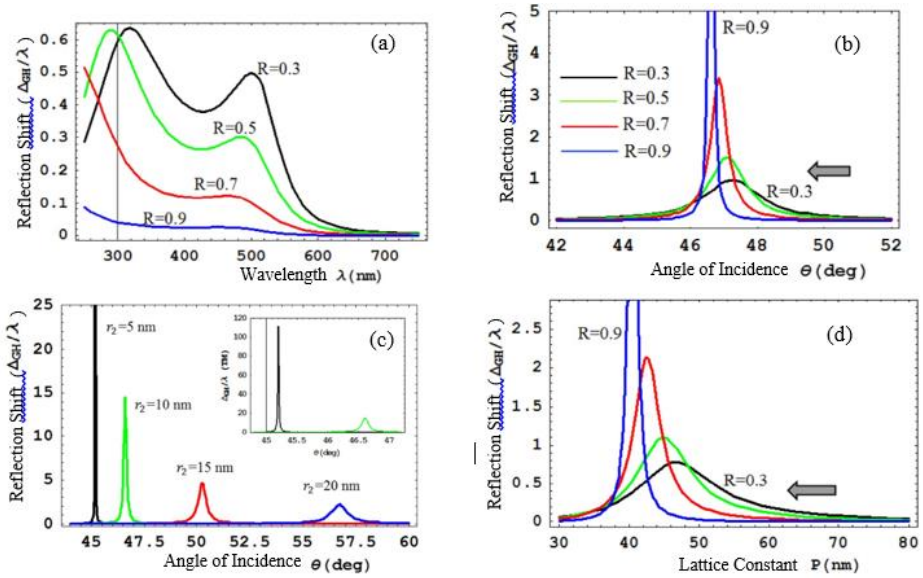

Fig.3 GH spatial shifts from ZnO/Au core-shell metasurface versus (a) wavelength, (b) and (c) angle of radiation, (d) lattice constant.

In Fig.3(a) the size of target nanoparticles is 10 nm with periodicity 50 nm at different core to shell ratios R. Angles of incidence are chosen to give larger shift. Fig.3 (b) is depicted for λ = 320 nm, r_2 = 10 nm, P = 50 nm and R = 0.3, 0.5, 0.7, 0.9. Fig.3 (c) shows the result for different values of particles' size; λ = 320 nm, R = 0.9, P = 50 nm, r_2 = 5,10,15, 20 nm. The inset is a close-up view of GH shift for r_2 = 5, 10 nm. Fig.3 (d) indicates how the reflection shifts are impressed by periodicity when the wavelength of light and size of nanoparticles are fixed (λ = 320 nm, r_2 = 10 nm).

We compared the reflection shift response of our metasurface when the metal dioxide core is chosen from widely available dielectric materials ZnO, SiO_2 and Al_2O_3 and also for the plasmonic shells of Ag and Au in Fig.(4).

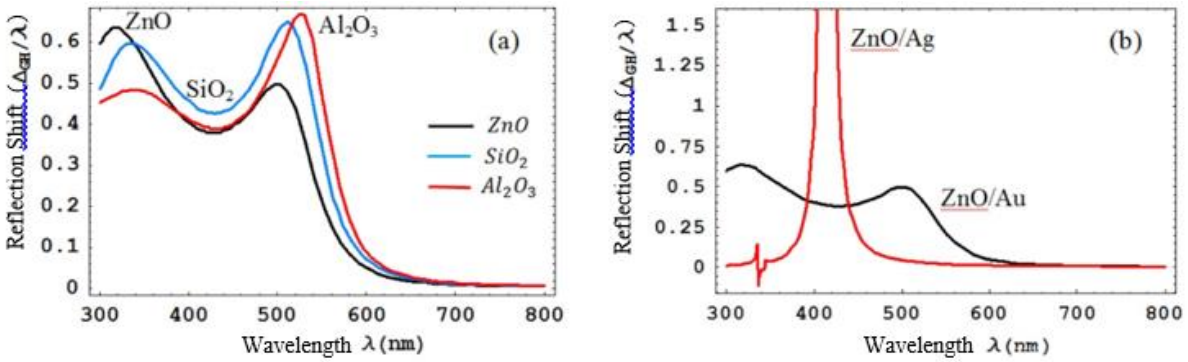

Fig.4 Spatial GH shift as a function of wavelength for a TM wave at θ = 48°, r_2 = 10 nm, R = 0.3, P = 50 nm. (a) Different cores of ZnO, SiO_2 and Al_2O_3 with Au shell. (b) ZnO core with different shells of Ag and Au.

According to Fig.4 (a) it is possible to enhance/weaken the peak value of the maximum achievable reflection shift, over visible or UV wavelength interval with a simultaneous red/blue shift by changing refractive index of the core (typical values of refractive indices for SiO2, Al2O3 and ZnO within 550–850 nm are 1.45, 1.76 and 2.00 respectively). Compared to gold, a silver shell exhibits one notable peak at about 420 nm (Fig.4 (b)). Its high value is a consequence of weaker losses in silver.

Conclusion

We modeled the interaction of metasurface with an incident light wave using generalized sheet transition conditions. The reflection shift of TM wave from core-shell metasurfaces exhibits two peaks which are attributed to the surface plasmon resonance of the metal shell at the interfaces with the core and the air. Remarkable enhance in reflection shift is feasible by accurate tuning of periodicity and core to shell ratio in small particles. Sharp high peaks especially arose in ultraviolet region that serve beneficially in UV reflective sensors. This research is carried out for suspended particles. However, it is stated that pinning the nanoparticles to a dielectric half-space substrate has very little effect on the trend of scattering response [18,19]. These findings may provide important guidelines for the design and fabrication of efficient metasurfaces applied in novel optical devices.

References

[1] A. Li, S. Singh, D. Sievenpiper, Metasurfaces and their applications, Nanophotonics 7 (6) (2018) pp. 989–10110.
[2] M. Khorasaninejad, W.T. Chen, R.C. Devlin, J. Oh, A.Y. Zhu, F. Capasso, Metalenses at visible wavelengths: diffraction-limited focusing and subwavelength resolution imaging, Science 352 (2016) pp.1190–1194.
[3] Z. Li, E. Palacios, S. Butun, K. Aydin, Visible-frequency metasurfaces for broadband anomalous reflection and high-efficiency spectrum splitting, Nano Lett. 15 (2015) pp. 1615–1621.
[4] W. Ye, F. Zeuner, X. Li, et al., Spin and wavelength multiplexed nonlinear metasurface holography, Nature Commun. 7 (2016) 11930.
[5] S. Choudhury, U. Guler, A. Shaltout, V.M. Shalaev, A.V. Kildishev, A. Boltasseva, Pancharatnam-berry phase manipulating metasurface for visible color hologram based on low loss silver thin film, Adv. Opt. Mater. 5 (2017) 1700196.

[6] F. Ding, Z. Wang, S. He, V.M. Shalaev, A.V. Kildishev, Broadband high-efficiency half-wave plate: a supercell-based plasmonic metasurface approach, ACS Nano 9 (2015) pp. 4111–4119.
[7] F. Yue, D. Wen, J. Xin, B.D. Gerardot, J. Li, X. Chen, Vector vortex beam generation with a single plasmonic metasurface, ACS Photonics 3 (2016)1558–1563.
[8] X. Ni, Z.J. Wong, M. Mrejen, Y. Wang, X. Zhang, An ultrathin invisibility skin cloak for visible light, Science 349 (2015) pp.1310–1314.
[9] J. Kim, S. Choudhury, C. DeVault, et al., Controlling the polarization state of light with plasmonic metal oxide metasurface, ACS Nano 10 (2016) pp.9326–9333.
[10] M. Born, E. Wolf, Principles of Optics, 7th edn., Pergamon, London, 2005.
[11] M. Ornigotti, A. Aiello, Goos–Hänchen and Imbert–Fedorov shifts for bounded wavepackets of light, J. Opt. 15 (2013) 014004.
[12] C.L. Holloway, A. Dienstfrey, E.F. Kuester, J.F. O'Hara, A.K. Azad, A.J. Taylor, A discussion on the interpretation and characterization of metafilms/metasurfaces: the two-dimensional equivalent of metamaterials, Metamaterials 3 (2009) pp.100–112.
[13] S.I. Maslovski, S.A. Tretyakov, Full-wave interaction field in two dimensional arrays of dipole scatterers, Int. J. Electron. Commun. 53 (1999) 135–139.
[14] C.F. Bohren, D.R. Huffman, Absorption and Scattering of Light by Small Particles, Wiley-VCH, 2004.
[15] A. Alù, N. Engheta, Achieving transparency with plasmonic and metamaterial coatings, Phys. Rev. E 72 (2005) 016623.
[16] C.L. Holloway, E.F. Kuester, J. Gordon, J. O'Hara, J. Booth, D.R. Smith, An overview of the theory and applications of metasurfaces: the two-dimensional equivalents of metamaterials, IEEE Antennas Propag. Mag. 54 (2) (2012) pp.10–35.
[17] P. Rong, Sh. Ren, Q. Yu, Fabrications and applications of ZnO nanomaterials in flexible functional devices -A review, Crit. Rev. Anal. Chem. 49 (2019) 4, http://dx.doi.org/10.1080/10408347.2018.1531691.
[18] S. Farazi, F.A. Namin, D.H. Werner, Tunable multiband metasurfaces based on plasmonic core–shell nanoparticles, J. Opt. Soc. Amer. B 35 (4) (2018) pp. 658-666.
[19] M. Zoghi, Goos–Hanchen shift in a metasurface of core–shell nanoparticles, Opt. Commun., 475 (2020) 126265.

FT2

Growth and Laser Properties of Tm^{3+}:$KY(WO_4)_2$ Crystals

Guretskii, S.A.*[1], Trukhanova, K.L.[1], Kravtsov, A.V.[1], Gorbachenya, K.N.[2], Kisel V.E.[2], Karpinsky, D.V.[1], Ozen, Y.[3], Erenler, B.[3], Ozcelik, S.[3], Kuleshov, N.V.[2]

[1]*Scientific and Practical Materials Research Center NAS Belarus, P.Brovki st., 19, Minsk, Belarus*
[2]*Center for Optical Materials and Technologies, Belarusian National Technical University, Nezavisimosty Ave., 65, Minsk, Belarus*
[3]*Photonics Application & Research Center, Gazi University, Ankara, Turkey*
crystal2@physics.by

The factors affecting the growth and crystallization of Tm-doped $KY(WO_4)_2$ single crystal are studied; the synthesis parameters used to improve a quality of the single crystals are discussed. The laser properties of the grown Tm^{3+}:$KY(WO_4)_2$ crystals were investigated. A maximum CW output power of about 0.65 W with a slope efficiency of 55 % was obtained at the wavelength of 1940 nm. In a passively Q-switched regime of operation laser pulses with energy of 40 μJ and duration of 10 ns were obtained at a repetition rate of 2.8 kHz at the incident pump power of 2.2 W.

Keywords: potassium yttrium tungstate crystals, phase diagram, metastable zone, controlled growth, absorption and luminescence spectra

Introduction

The growth of a-$KY(WO_4)_2$:Tm^{+3} (KYW) single crystals by the modified Czochralski method is a complex physicochemical process in which heat and mass transfer play an extremely important, often decisive role. When growing single crystals, it is necessary to observe strictly specified thermal conditions, it is necessary to maintain constant temperature gradients at the growth front and high thermal stability of the process at a level of several tenths of a degree. In addition, it is necessary to create a concentration gradient that ensures the diffusion of the dissolved substance in the direction of the growth surface on the seed crystal. The concentration gradient is created using the temperature difference between the zone of superheated solution-melt and the zone of crystallization. Crystal growth was carried out using the dynamic growth mode and selection of the required temperature gradient at the crystallization front. These factors fully provide the necessary process of crystal nutrition at various stages of growth [1].

Diode-pumped thulium lasers operating in the spectral range near 2 μm are attractive for applications in different areas: surgery, since their radiation is strongly absorbed by water, range determining, and environmental atmosphere monitoring due to the presence of absorption lines of a number of chemical compounds (benzol, ethanol, etc.) in the spectral region around 2 μm. The Tm:KYW crystals attract attention due to relatively high absorption and emission cross-section, broad emission bands, and the possibility to grow highly activated crystals.

Experiment

The laboratory model of the setup for growing crystals by the modified Czochralski method was equipped with a shaft two-zone furnace-crystallizer with a frame heater. With the help of two-zone heaters, the vertical temperature gradient was changed to increase the efficiency of convection mixing and prevent parasitization of the near-bottom region of the solution-melt [2]. The temperature axial gradient above the surface of the solution-melt was formed by changing the thickness and profile of the upper part of the crystallizer. Heat removal from the melt surface can be controlled both by changing the temperature distribution on the bottom and side heaters, and by changing the thickness of the thermal insulation in the upper part of the furnace - crystallizer. It should be noted that the optimal axial temperature gradient in the crucible, at which there is no bottom contamination during the synthesis relative to the surface of the solution-melt, (″O″) should have the following form (Table 1).

Table I. Axial distance between the crystal seed and the solution-melt surface

Bottom	-20 mm	-10 mm	-5 mm	Surface	+5 mm	+10 mm
+7,5 – 8,3°	+4,6 – 5,3°	+3,7 – 4,2°	+3,2 – 3,6°	0	4,0 – 4,6°	-4,8 – 5,5°

To study the temperature-concentration parameters of the synthesis of KYW single crystals by the modified Czochralski method, we used melt solutions based on the solvent $K_2W_2O_7$. Crystal growth was carried out using the dynamic growth mode and the selection of the optimal temperature gradient at the crystallization front. These factors fully provide the necessary process of crystal nutrition at various stages of growth [3].

Crucibles with a diameter of 80–100 mm were used. The temperature range of cultivation is in the range of 900-980 ^{0}C. The height of the solution-melt varied within 50–70 mm. The seed element in the form of a cylinder 8 mm and 8-12 mm long is oriented along the [010] axis with an accuracy of ≤ 0.5'. All components of the solution-melt immediately before weighing were annealed at a temperature of 200-250 ^{0}C for 1.0-1.5 hours. The solution-melt intended for crystallization was heated in a crucible to a temperature of 1030 – 1040 ^{0}C at a rate of 100-200 ^{0}C/h and it was homogenized for 12 hours. Stirring with a platinum stirrer is used to ensure complete homogenization of the melt solution. Then, instead of a stirrer, a crystal holder with a single-crystal seed is installed. The single-crystal seed was slowly lowered until its lower part touched the surface of the solution-melt, which is 4-5 ^{0}C higher than the saturation temperature, which is in the temperature range 980÷985 ^{0}C. In order to solve the problem of mechanical mass transfer of dissolved KYW from peripheral, locally supersaturated zones of the melt solution, at the stage of seed crystal growth, the crystal rotation speeds were set at 100–120 rpm with a gradual decrease to 25–40 rpm by the end of synthesis as the size of the growing crystal increased [4]. The rate of temperature decrease to the saturation temperature is 25-300 sec/h, then to the temperature of the beginning of growth below the saturation temperature by 0.8-1.2 ^{0}C. The rate of descent slows down to 2-30 sec/h. After the growth start temperature is reached, the crystal elongation rate is set within 0.5–0.8 mm/day. At the same time, the solution-melt temperature is reduced at rates from 0.05 ^{0}C/h at the beginning of synthesis to 0.4 ^{0}C/h at the end. The process of growing a KYW crystal lasts 20-25 days. The height

of the crystal is determined by the height of the extract and the size of the part of the crystal that has grown under the surface of the melt solution. During this time, the temperature of the solution-melt decreases by 60-80 ^{0}C. After reaching the lower limit of the growth temperature, the KYW crystal was detached from the surface of the solution-melt, while the stretching and rotation were stopped. Then the furnace-crystallizer was cooled to room temperature at a rate of 25-30 ^{0}C/h.

The experimental laser setup is presented in the Figure 1. The near hemispherical laser cavity consisted of a curved output coupler (OC) and a plane high reflector was used. The cavity length was about 24 mm. A laser crystal was Ng-cut Tm(3 %):KYW with the thickness of 2.8 mm and antireflection coatings on it's working sides. The temperature of active element (AE) was kept at 14 °C by means of copper slab and thermoelectrical cooling of the elements with a water-cooled heatsink. A 3-W continuous-wave fiber-coupled diode laser (λ = 802 nm, Ø = 100 μm, N.A. = 0.15) was used for a longitudinal pumping of the active element. A pump beam was focused into a 200 μm spot inside the laser crystal. The cavity length was adjusted to get TEM_{00} transversal mode diameter at the active element close to the pump beam waist considering induced thermal lensing effects. A set of output couplers with different transmissions (Toc) was used during continuous-wave laser experiments.

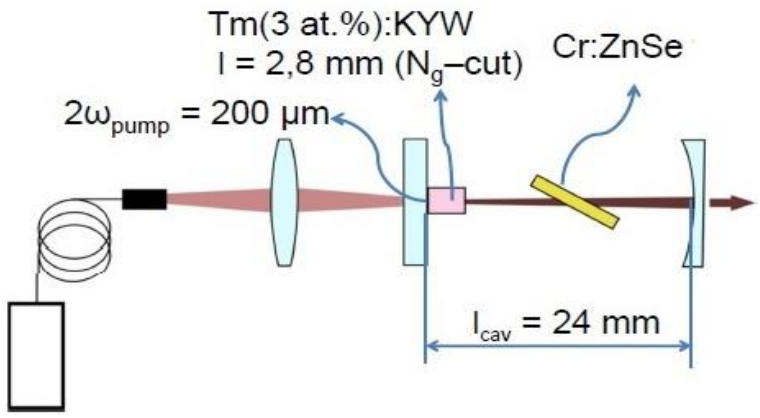

Figure 1 – Experimental laser setup

Results and discussion

Initially, laser experiments were carried out in the continuous-wave regime of operation. The maximum output power of 645 mW at 1940 nm was measured with an output coupler transmission of 3 %. A slope efficiency of 55 % with respect to the absorbed pump power was obtained. Laser emission was linearly polarized along N_m axis. Input-output diagrams for the CW Tm: KYW laser are shown in the Figure 2.

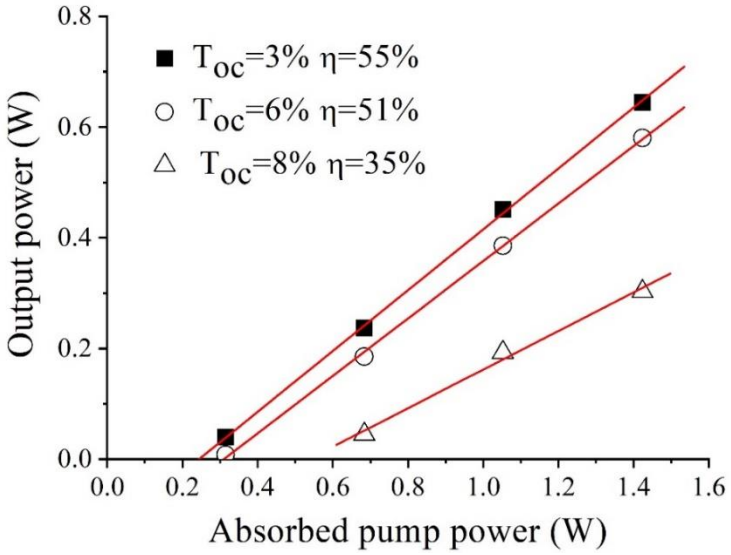

Figure 2 Input-output diagrams of the continuous-wave Tm: KYW laser

The Q-switch laser experiments were performed taking into account comparatively low light induced damage threshold of the Cr^{3+} :ZnSe saturable absorbers (≈ 2.5 J/cm^2). The saturable absorber was inserted into the cavity between active medium and OC at Brewster angle. Two SAs with initial transmissions of 95 % and 90 % were used. Laser pulses with energy of about 26 μJ and repetition rate of 6 kHz corresponding to 156 mW of average output power at 1910 nm were obtained at 2.2 W of incident pump power for the SA with the initial transmission of 95 % nm and OC with transmission of 6 %. With the increase of incident pump power from the threshold to its maximal value the pulse energy and repetition rate varied from 20 to 26 μJ and 0.2 to 6 kHz, respectively. The dependence of pulse duration and repetition rate on incident pump power is shown in the Figure 3. The increase of pulse energy with incident pump power can be explained by changing in the TEM_{00} mode size due to thermal effects in the gain medium. The spatial profile of the output beam was TEM_{00} mode with $M^2 < 1.2$ at maximal incident pump power (inset in the Figure 3).

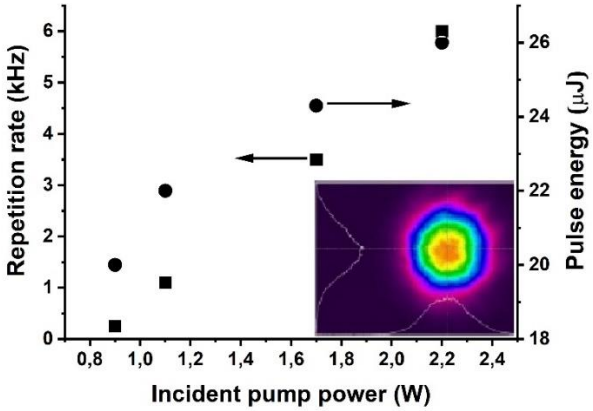

Figure 3 Dependence of laser pulse characteristics on incident pump power for saturable absorber with initial transmission of 95%

The shortest laser pulse duration was measured to be 14 ns. The oscilloscope traces of single pulse with the duration of 14 ns and output pulse train with maximal repetition

rate of 6 kHz are presented in the Figure 4. It should be mentioned that maximum pulse repetition rate was limited by the laser-induced damage threshold of the SA.

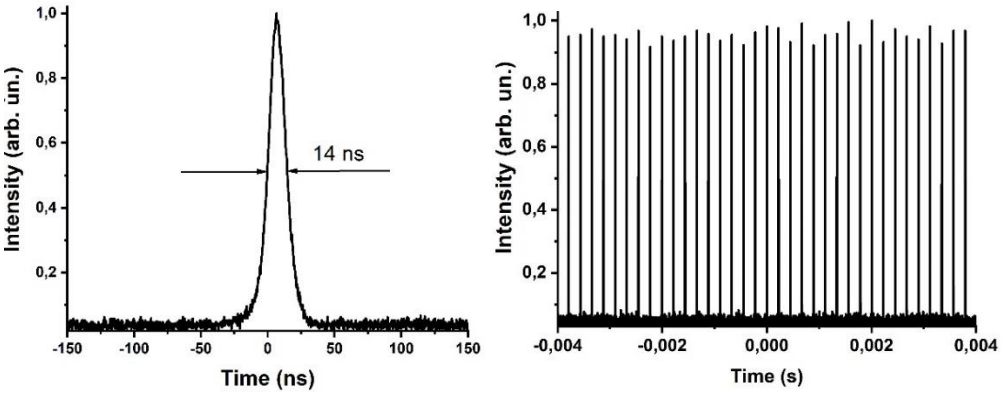

a b

Figure 4 Oscilloscope traces: *a* – single pulse with the duration of 14 ns; *b* – output pulse train maximal repetition rate of 6 kHz

Conclusion

High quality $KY(WO_4)_2:Tm^{+3}$ single crystals were grown by the modified Czochralski method. The values of the growth parameters (thermal expansion coefficient, crystal's rotation speed etc.) notably affecting the crystal quality were determined and discussed focusing on their impact on the crystallization front and the structural defects.

A maximum CW output power of about 0.65 W with a slope efficiency of 55 % was obtained at the wavelength of 1940 nm. In a passively Q-switched regime of operation laser pulses with energy of 40 μJ and duration of 10 ns were obtained at a repetition rate of 2.8 kHz at the incident pump power of 2.2 W. Based on the obtained results, it can be concluded that Tm:KYW crystals are promising active media for lasers emitting in the spectral range near 2 μm for the usage in surgery and range finding.

Acknowledgements

This research is performed in the framework of the bilateral project supported by NAS of Belarus and Tubitak (project number 120N014) and RFBR (grant # F21MS-035).

References:

[1] Timofeeva V.A. Growth of crystals from solution-melts - M.: Nauka, 1978, 265.
[2] Ostrach S. Influence of hydrodynamics on crystal growth. Freeman lecture. Theoretical foundations, 1983, vol. 105, No. 1.
[3] Bagdasarov H.S. High-temperature crystallization from the melt. - M.: Fizmatlit, 2004, 159.
[4] .A. Guretskii, E.L. Trukhanova, A.V. Kravtsov, N.V. Gusakova, K.N. Gorbachenya, V.E. Kisel, A.S. Yasukevich, R. Lisiecki, A. Lukowiak, D.V. Karpinsky, S. Ozcelik, N.V. Kuleshov, Features of growing $Tm^{3+}:KY(WO_4)_2$ single crystals and their optical properties S Actual problems of solid state physics: proc. book IX Intern. Scient. Conf., (Minsk, November 22-26, 2021). 2 b. B. 1 / SSPA Scientific-Practical Materials Research Centre of NAS of Belarus; edit. board: V.M. Fedosyuk (chairman) [et al.]. – Minsk: Publisher A. Varaksin, 2021. – P. 81-84.

AUTHOR INDEX

Author's Name	Abstract No
Abdelmoula N.	S12
Adak, M.	S34, S39
Ahadi-Akhlaghi, E.	IS9, S23
Akcay, N.	S37
Akhlaghi, A. E.	S22, S24, S25
Akman, B.	S49
Akpınar, Ö.	S30, S38
Aksoy, E.	S50
Akyol, M.	S48
Alipanah, Z.	S47
Altuntaş İ.	S48
Amenitsch, H.	IS3, S15
Artan, G. G.	S40
Asadian, A.	S21
Asar, T.	S2, S19
Ataşer, T.	S28
Ates, H.	S44
Aydın, S. S.	S44
Aygün, M.	IS16
Azizian-Kalandaragh, Y.	S41
Baghdedi, D.	S12
Baghirov, M. A.	S32
Balayeva, O. O.	S5, S51
Balcı, E.	S28
Balcı, S.	IS14
Baltakesmez, B. A.	IS16
Baz, Z.	S16
Bek, A.	IS8
Berberoğlu, H.	S34, S39,
Bernstorff, S.	S15
Bharti, A.	IS3, S15
Booth, M. J.	IS1
Bozkus V.	S50
Buono, W. T.	S14
Canyurt, K	S19
Chudakov, E. A.	S37
Coşkun, A.	IS16
Cox, M.	S8
Çakmak, B.	IS16
Çakmak, M.	S49
Çelik, K.	IS16
Demir, H. V.	P5
Demir, İ.	S48
Demircioğlu, Z.	S1
Donmez Kaya, M.	S46
Dudley, A. L.	IS5, S3, S11, S33
Ebrahimzadeh Kouyakhi, A.	S22, S24,
Efkere, H. İ.	S44
Ekicibil A.	S48
Erenler, B.	S18, S27,
Eyvazova, G. M.	S5, S32, S51
Farezi, N.	S20
Figen, Z. G.	S29

Author's Name	Abstract No
Forbes, A.	P2, S3, S8, S9 S10, S11, S13, S14, S33
Gahramanli, L. R.	S51
Gremenok, V. F.	S37
Golshahi, S.	IS15
Gorbachenya, K. N.	S18
Gultekin, B.	S31
Guretskii, S. A.	S18
Güloglu Bülbül, B.	S42
Gümrükçü, A. E.	S30, S38, S41, S44
Gür E.	S12
Hailstone, M.	IS1
Hajizadeh, F.	S25
Heidary, K.	S22, S24
Hopoğlu, H.	S48
Hu, Q.	IS1
Işık, M. A.	IS16
Işık, M. B.	S2
İdare, B.	S30
Jafari Siavashani, M.	S23
Karakılınç, Ö. Ö.	S34, S39
Karpinsky, D. V.	S18, S27
Kavak, H.	S26
Kaya, D.	S48
Keskin, M. Z.	S29
Khaksar Jalali, B.	S17
Khalesifard, H.	IS2
Khanjanji M.	S23
Khoshsima, H.	S35
Kınacı, B.	S44
Kilic, M.	S26
Kiraz, A.	P7
Kisel, V. E.	S18
Klug, A.	S9
Konrad, T.	S8
Korkmaz, B.	S30, S38
Koshsima, H.	S20
Kravtsov, A. V.	S18
Kudrynskyi, Z.	IS11
Kuleshov, N.V.	S18
Leuchs, G.	P1
Mammadyarova, S. J.	S5, S32
Mamuk, A. E.	S6
Muradov, M. B.	IS13, S32, S51
Marmiroli, B.	IS3, S15,
Mello, K. R.	S13
Miri, M.	IS10
Mohapi, L. P.	S3
Moodley, C.	S10
Muradov, M. B.	S5
Nape, I.	S8, S33
Nasser, H.	S1
Oguz, H.	S34
Oğuz, G.	S43

Author's Name	Abstract No
Omidi, P.	S24
Ornelas, P.	S13
Ozcelik, S.	S18, S27, S28, S30, S37, S38, S41, S42, S44, S46, S49
Ozdal, T.	S26
Ozdemir Kart, S.	S34, S39
Ozen, Y.	S18, S27, S42, S44
Ozturk, M. K.	S38
Özden, P.	S36
Özdür, İ. T.	S29
Özerbaş, Z. E.	IS16
Özkök, Y.	S49
Peters, C.	S9
Phala, A. M.	S11
Poyraz, M. E.	S28
Rameh, M.	S25
Ranjkesh, A.	S20, S47
Razeghi, M.	P3
Robert, F. C.	P4
Roux, F. S.	S8
Rubinsztein-Dunlop, H.	P6
Saeidian, S.	S21
Safarinia, N.	S21
Salmani, Shik, S.	S17
Sánchez-Soto, L. L.	IS4
Sartori, B.	IS3
Sayraç, M.	S42
Sephton, B.	S8
Seravalli, L.	IS7
Serbest, B.	S28
Seyedmohammadzadeh, M.	S43
Shahi, S.	S17
Singh, K.	S13, s33
Soleimani, P.	S35
Somhorst, F.	S7
Sönmez Akın, N.	S28, S30, S38, S41, S49
Staskov, N. I.	S37
Steinlechner, F.	S8
Şenadım Tüzemen, E.	S12, S48
Torres, J.P.	S8
Trukhanova, K. L.	S18
Tuchin, V. V.	IS12
Turan, R.	S1
Turchet, A.	IS3
Turgut, G.	IS16
Turgut, S. B.	S31
Tuzelbay M. Y	S45
Vallés, A.	S8
Varlikli, C.	S50
Volyar, A. V.	IS6
Wang, J.	IS1
Wincott, M.	IS1
Yeganeh, M.	S35

Author's Name	Abstract No
Yoon, T. H.	S20
Yuksel, Z. M.	S39
Zakerhamidi, M. S.	S20, S47
Zoghi, M.	S4